Conformational Characteristics of Radiation-Modified Polysilanes in Their Self-Assemblies

Hidenori TANAKA

2012

Contents

Chapter 3

Synthesis of pH-Responsive Polysilane with Polyelectrolyte Side Chains through γ-ray-Induced Graft Polymerization

Part II

Chapter 4

Conformational Transition of the Core Chain in Radiation-Modified Polysilane Micelles Formed in Selective Solvents

Chapter 5

Core Phase Transition of Radiation-Modified Polysilane Micelles As Revealed from Their Thermochromism

Part III

Chapter 6

Effect of the Graft Chain Length and Density on the Morphology of Radiation-Modified Polysilane Monolayers at the Air/Water Interface

Chapter 7

Orientation of Radiation-Modified Polysilane in Monolayers at the Air/Water Interface As Revealed from Its Optical Property

Chapter 1

General Introduction

1.1. Background and Motivation

Nanoscience and nanotechnology have been attracting growing interest since they are expected to bring innovations in various fields such as electronics, environmental and medical technologies.[1] Nanostructures show unique properties that bulk correspondent materials do not have, and accordingly fabrications of nanostructured membranes, templates for nanoparticle synthesis, high-density information storage and so forth are attempted.[2-4] Two approaches, top-down and bottom-up, have been taken to prepare such nanostructures.[5,6] A typical top-down approach is lithography with light, electrons and ions.[7,8] Nanostructures can be formed by lithography on an industrial scale. However, the interest in the bottom-up approach by utilizing self-assembly of molecules has grown rapidly because the self-assembly is a powerful tool that enables the preparation of nanostructures often not accessible by the top-down approach.[9-14]

Molecular self-assembly is spontaneous association of molecules into structurally well-defined aggregates by noncovalent interactions.[15] It is well known that block and graft copolymers consisting of incompatible polymer chains self-assemble to form nanostructures.[16,17] In selective solvents composed of good solvents for one block and poor for the other, block and graft copolymers self-assemble and form micelles in which insoluble and soluble blocks constitute micellar cores and coronas, respectively.[18-23] The typical size of polymeric micelles is in the range from several

tens to hundreds of nanometers.[24] One of the most useful properties of micelles is their ability to enhance the aqueous solubility of hydrophobic substances.[25] The enhancement arises from the fact that micellar cores can serve as a compatible environment for the water insoluble molecules. Owing to such an unique property, micelles are expected to be used as nanocarriers for small compounds and applied to drug delivery systems.[26,27] The Langmuir-Blodgett (LB) technique is also one of the promising approaches to prepare well-defined structures in nano-scale.[28-31] In LB methods, monolayers spread at the air/water interface are transferred onto a solid substrate and multilayers are obtained by the successive deposition of monolayers. The LB technique is widely used to fabricate ultra-thin films for biosensors, gas sensors and electronic devices.[32-44]

There are many studies on micelles and LB films formed with polysilane-based block copolymers.[45-54] Since polysilane has unique properties such as high hole drift mobility, photoconductivity and non-linear optical effect,[55-63] application of polysilane to electronic and optical devices is expected.[64-66] Because the properties of polysilane are derived from delocalized electrons along the silicon backbone,[67-69] it is very significant to understand and control the conformation of polysilane chains in the nano devices.

This thesis focuses on the conformational characteristics of polysilane-based graft copolymers in their self-assemblies. In order to reveal the conformation of polysilane chains in micelles, monolayers and LB films, the author mainly took advantage of UV absorption of polysilane because the absorption band changes depending on the conformation of its backbone. The author prepared polysilane-based graft copolymers by γ-ray-induced graft polymerization. The

synthesis of polysilane-based graft copolymers is hard because polysilane synthesized by a common method generally does not have functional groups. However, γ-ray-induced grafting enables the modification of polymers without functional groups. In this thesis, synthetic methods and characterization of radiation-modified polysilanes is also discussed.

1.1.1. Polysilane

Polysilanes are high polymers which have the silicon backbone with a variety of organic side chains.[67-69] The first polysilane, poly(diphenylsilane), was prepared by Kipping in 1924 by condensation of diphenyldichlorosilane with sodium metal.[70] 25 years later, poly(dimethylsilane) was prepared by a similar synthetic route.[71] Because of difficulty with characterization and processing of these polysilanes, study on polysilane was not interesting scientifically and industrially. Since the use of polysilane for the generation of β-silicon carbide fibers was described by Yajima et al. in 1975,[72-74] however, polysilanes with processibility have been synthesized and studies on these materials have attracted much attention.

In the synthesis of polysilane, the Wurtz-type coupling of dichlorosilane is commonly employed.[68] This reaction is usually carried out at elevated temperature in a solvent such as toluene or xylene using an alkali metal. Sodium is usually utilized as an alkali metal. Owing to vigorous reaction conditions, side chains of polysilane are limited to alkyl- and aryl-substituted derivatives.

Polysilane shows strong UV absorption derived from the excitation of σ electrons delocalized along its silicon backbone and the absorption peak appears in the range from 300 to 350 nm.[67] The absorption of polysilane depends somewhat on the

degree of polymerization. The absorption peak and the molar absorption coefficient increase initially with increasing degree of polymerization and approach a limiting value around a degree of polymerization of 40-50.[75] The UV absorption of polysilane depends also on the conformation of its backbone and thermochromism has been the subject of numerous experimental and theoretical studies.[76-83] For example, solutions of poly(di-*n*-hexylsilane) at room temperature shows a broad absorption around 320 nm. With decreasing temperature to –50 °C, the absorption band decreases in intensity and a new absorption band grows in around 357 nm.[76,84,85] This is because polysilane chains easily take energetically stable conformations at lower temperatures, which are favorable for the delocalization of σ electrons. As a result, the absorption band shows red-shift with decreasing temperature.

In this study, PMPrS is utilized as a base polymer for the following reasons: (1) good solubility in common organic solvents, (2) the simplest side-chain structure among soluble polysilanes, and (3) relatively smaller molecular weight distribution.[68]

1.1.2. Radiation-Induced Graft Polymerization

Radiation-induced graft polymerization has been studied since 1950s.[86,87] This method can combine incompatible polymer chains and introduce new properties to original polymers.[88] Taking advantage of this characteristic, radiation-induced grating is utilized to modify polymer properties such as wettability, adhesion, printability and so forth.[89] Radiation-induced grating has been a subject of an intensive research especially in the industrial world because it can initiate

polymerization in various states such as solution, emulsion and solid, and also it can simplify production process and reduce the cost of production.[90,91]

Several types of ionizing radiation are available for radiation-induced graft polymerization: electromagnetic radiation such as γ-rays and X-ray, particle radiation such as electrons and swift heavy ions.[92] However, γ-rays and electrons are commonly utilized. As γ-irradiation source, ^{60}Co and ^{137}Cs are usually utilized. On the other hand, electrons are obtained from accelerators. Effects and roles of γ-rays in radiation-induced grafting are basically equal to those of electrons.

In radiation-induced graft polymerization, reactive sites on polymer chains are generated by irradiation and the sites react with monomers.[92] This reaction is usually performed by two methods: simultaneous grafting and pre-irradiation grafting. In simultaneous grafting, polymers are irradiated in the presence of monomers. The reaction mechanism is shown in Scheme 1.1. Simultaneous grafting is a simple technique, but a lot of homopolymers originated from the monomers are generated. Accordingly, various conditions have been studied to suppress the generation of homopolymers.[93]

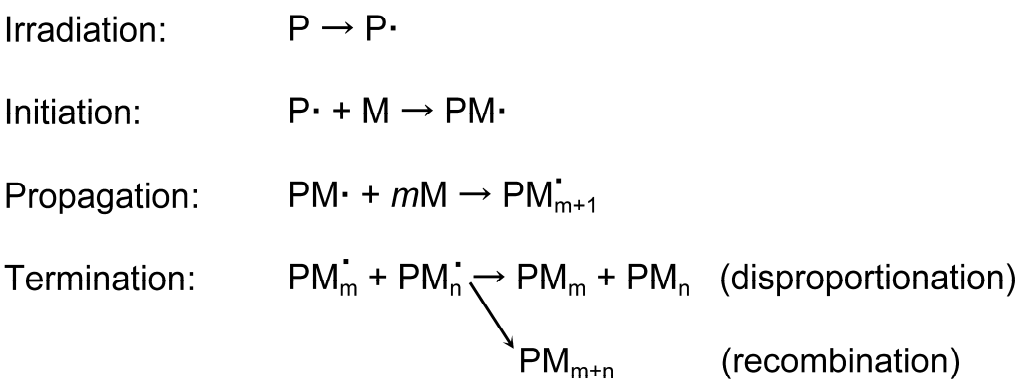

Scheme 1.1. Mechanism of simultaneous grafting.

In pre-irradiation grafting, polymers are solely irradiated without monomers. If polymers are irradiated in air, generated radicals react with oxygen to form peroxides. The peroxides initiate polymerization of monomers by thermal decomposition. The reaction mechanism is shown in Scheme 1.2.

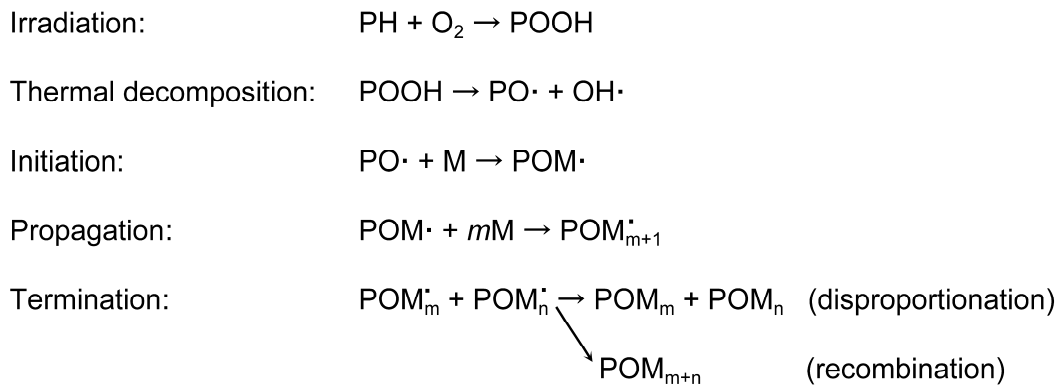

Scheme 1.2. Mechanism of pre-irradiation grafting in air.

On the other hand, if polymers are irradiated under vacuum or inert atmosphere, generated radicals on polymer chains initiate polymerization as shown in Scheme 1.3.

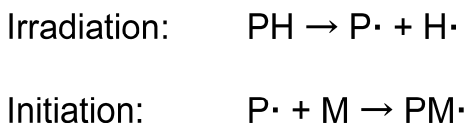

Scheme 1.3. Mechanism of pre-irradiation grafting under vacuum or inert atmosphere.

It is difficult to decide which one of simultaneous and pre-irradiation grafting is superior. However, pre-irradiation grafting has attracted greater attention because it can suppress the generation of homopolymers.[94]

1.1.3. Polymeric Micelles

In selective solvents composed of good solvents for one block and poor for the other, block and graft copolymers associate reversibly to form micelles, in which cores are formed by insoluble blocks and shells by soluble blocks.[25] Micelles are generally spherical with narrow size distribution, but shapes and size distribution vary with the change of conditions.

The micellization in organic media is an enthalpic driven process.[95-97] The standard Gibbs energy change of micellization is expressed by $\Delta G° = \Delta H° - T\Delta S°$, where $\Delta H°$ is the standard enthalpy change and $\Delta S°$ the entropy change. Both $\Delta H°$ and $\Delta S°$ are negative. The negative value of $\Delta S°$, which is unfavorable to micellization, arises from the constraint of copolymers in micelles. On the other hand, the negative value of $\Delta H°$ arises from the exthothermic energy which results from the replacement of polymer/solvent interactions by polymer/polymer and solvent/solvent interactions. However, this situation in organic media is opposite to that in aqueous media.[16,25,97,98] The value of $\Delta H°$ is positive because the transfer of unimers into micelles is endothermic process, whereas $\Delta S°$ has a positive value. The presence of hydrophobic chains in water causes a significant decrease in the water entropy because the degree of structuring of water molecules is increased. The structure of water molecules is recovered and water entropy increases as hydrophobic chains aggregate, which overcomes the loss of entropy owing to the

aggregation of hydrophobic chains.

Micellar systems are usually produced by the following two procedures.[99] In the first method, copolymers are dissolved in a common solvent which is good for each block, and then a selective precipitant of one of blocks is gradually added. As alternative to the addition of the precipitant, the dialysis technique is also often utilized. In the second method, a solid sample of copolymers are directly dissolved in a selective solvent. However, it is pointed out that micelle formation by direct dissolution is not suitable because generated micelles inherit the morphology of the bulk sample.[25]

1.1.4. Langmuir-Blodgett Films

The LB technique, first introduced by Langmuir and applied by Blodgett, is a useful approach for the preparation ultra-thin organic films with well-defined structures.[29,100-103] Amphiphilic molecules are adsorbed at the air/water interface owing to the balance of hydrophilic and hydrophobic groups of them.[29] The resulting film is one molecule in thickness and called a monolayer. Monolayer-forming molecules are applied on the water subphase by first dissolving them in a volatile solvent. And then, the surface pressure of the monolayer is controlled so that the organic film is in a condensed and stable state. Figure 1.1 displays the commonest form of LB film deposition. As the hydrophilic substrate is raised through the water, the first monolayer is transferred. Subsequently, a monolayer is deposited on each traversal of the monolayer/air interface. As shown in Figure 1.1e, molecules are stacked in a head-to-head and tail-to-tail pattern. This deposition mode is called Y-type.

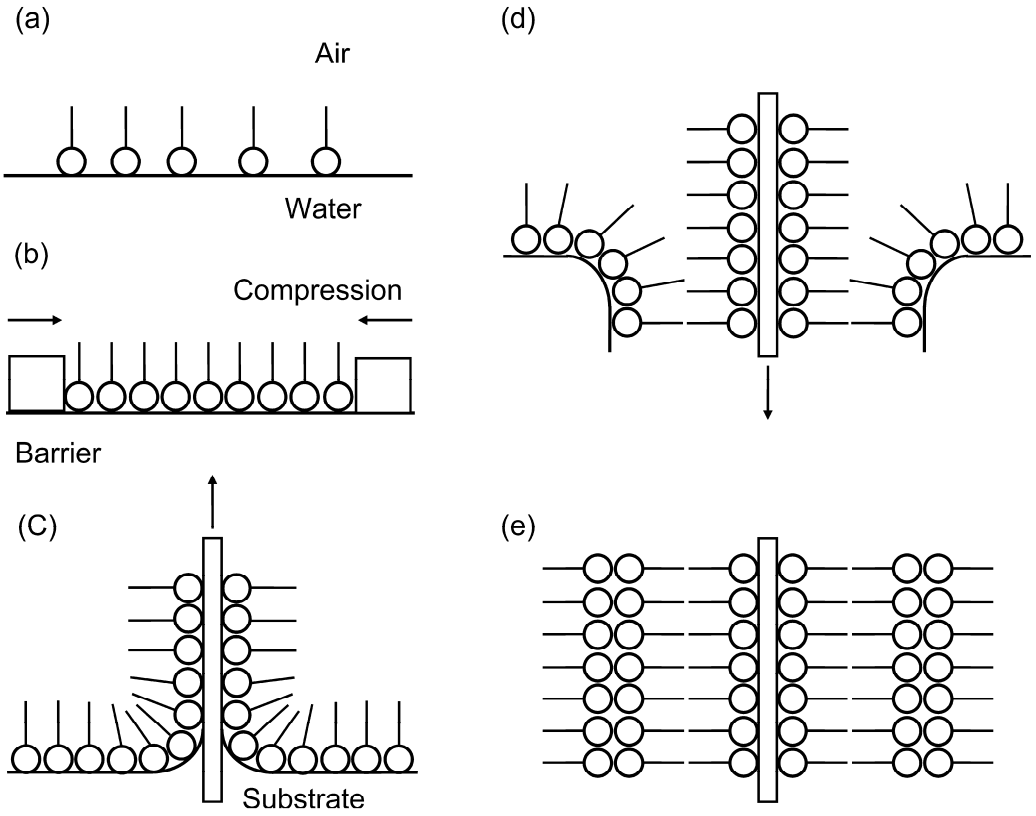

Figure 1.1. Langmuir-Blodgett film deposition.

The quality of LB films are dependent on the character of source materials. LB films prepared from low molecular weight amphiphilic compounds usually have poor stability to mechanical and thermal treatments. Because LB films made of amphiphilic polymers can overcome these defects, they have been extensively studied.

1.2. Outline of This Thesis

This thesis is composed of seven chapters. The first chapter describes the background and motivation, in which the key concepts of polysilane, radiation-induced graft polymerization, micelle formation and LB films are explained. The following six chapters are divided into three parts. Part I (Chapter 2 and 3) takes up the synthesis and characterization of radiation-modified polysilane.

In Chapter 2, γ-ray-induced graft polymerization of amphiphilic monomers onto poly(methyl-*n*-propylsilane) (PMPrS) is performed. Irradiation conditions for the preparation of radiation-modified PMPrS is investigated by changing total absorption dose, dose rate and concentrations of grafting monomers. The structures of obtained radiation-modified PMPrS are examined by ^{1}H NMR measurements.

In Chapter 3, the synthesis of pH-responsive PMPrS through γ-ray-induced graft polymerization is described. Irradiation conditions for the synthesis of PMPrS with polyelectrolyte graft chains are investigated. The pH responsiveness for an obtained graft copolymer is examined mainly by observing interfacial behavior of its monolayer at the air/water interface.

Part II (Chapter 4 and 5) deals with the micelles formed with radiation-modified PMPrS.

In Chapter 4, the micelle formation of radiation-modified PMPrS is investigated in selective solvents composed of good and poor solvents for the PMPrS main chain. Conformational transition of PMPrS chains in the micelle core is closely examined by analyzing UV absorption spectra. The overall process of micelle formation is also discussed.

In Chapter 5, core phase transition of radiation-modified PMPrS micelles in

selective solvents is described. The conformational transition of PMPrS core chains induced by a temperature change is examined by UV absorption spectroscopy. Light scattering measurements and a fluorescent method are also employed for clarifying the physical state of the micelles in the solution.

Part III (Chapter 6 and 7) describes monolayers at the air/water interface and LB films formed with radiation-modified PMPrS.

In Chapter 6, the effect of structures of radiation-modified PMPrS on the morphology of their monolayers at the air/water interface is surveyed. The surface pressure-area isotherms of radiation-modified PMPrS at the air/water interface are examined to clarify interfacial behavior of its monolayers, and then AFM observation for the monolayers transferred onto solid substrates is performed to obtain detailed information about the morphology of the monolayers. In addition, the deposition of LB films of radiation-modified PMPrS is demonstrated.

In Chapter 7, the relationship between the orientation and the conformation of polysilane main chains in both monolayers at the air/water interface and LB films of radiation-modified PMPrS is investigated by the close analysis of polarized UV absorption spectra of the monolayers and LB films.

References

1. Lazzari, M.; Liu, G.; Lecommandoux, S., Eds. *Block Copolymers in Nanoscience;* WILLEY-VCH, Weinheim, 2006.
2. Park, C.; Yoon, J.; Thomas, E. L. *Polymer* **2003**, *44*, 6725.
3. Hamley, I. W. *Nanotechnology* **2003**, *14*, R39.
4. Lazzary, M.; Lopez-Quintela, M. A. *Adv. Mater.* **2003**, *15*, 1583.
5. Mijatovic, C.; Eijkel, J. C. T.; van den Berg, A. *Lab Chip* **2005**, *5*, 492.
6. Zhihong, N. *Nature Materials* **2008**, *7*, 277.
7. Kim, C. N.; Kang, E. R.; Lee, H. *Synthetic metals* **1997**, *85*, 1407.
8. Zhang, W.; Potts, A.; Bagnall, D. M.; Davidson, B. R. *Thin Solid Films* **2007**, *515*, 3714.
9. Tolles, W. M. *MRS Bull.* **2000**, *25*, 36.
10. Boncheva, M.; Whitesides, G. M. *MRS Bull.* **2005**, *30*, 736.
11. Lazzari, M.; Rodriguez-Abreu, C.; Rivas, J.; Lopez-Quintela, M. A. *J. Nanosci. Nanotechnol.* **2006**, *6*, 892.
12. Seto, C. T.; Whitesides, G. M. *J. Am. Chem. Soc.* **1990**, *112*, 6409.
13. Manka, J. S.; Lawrence, D. S. *J. Am. Chem. Soc.* **1990**, *112*, 2440.
14. Koert, U.; Harding, M. M.; Lehn, J.-M. *Nature* **1990**, *346*, 339.
15. Whitesides, G. M.; Mathias, J. P.; Seto, C. T. *Science* **1991**, *254*, 1312.
16. Alexandridis, P.; Lindman, B. *Amphiphilic Block Copolymers: Self-Assembly and Application*; Elsevier, Amsterdam, 2000.
17. Lehn, J. M. *Science* **2002**, *295*, 2400.
18. Cameron, N. S.; Corbierre, M. K.; Eisenberg, A. *Can. J. Chem.* **1999**, *77*, 1311.
19. Ding, J. F.; Liu, G. J.; Yang, M. L. *Polymer* **1997**, *38*, 5497.

20. Tuzar, Z.; Kratochivil, P. *Adv. In Colloid and Interface Science* **1976**, *6*, 201.
21. Riess, P. B. G.; Hurtrez, G. *Encyclopedia of Polymer Science and Engineering: volume 2;* Wiley, New York, 1985.
22. Gast, A. P. *Scientific Methods for the Study of Polymer Colloids and Their Applications;* Kluwer, Boston, 1990.
23. Halperin, A.; Tirrell, M.; Lodge, T. P. *Adv. Poly. Sci.* **1992**, *100*, 31.
24. Miyata, K.; Christie, R. J.; Kataoka, K. *React. Funct. Polym.* **2011**, *71*, 227.
25. Webber, S. E., Munk, P., Tuzar, Z., Eds. *Solvents and Self-Organization of Polymers;* Kluwer, The Netherlands, 1996.
26. Kataoka, K.; Harada, A.; Kulkarni, P. N. *Methods Enzymol.* **1983**, *93*, 280.
27. Goldin, A.; Rahman, A.; Casazza, A. M.; Guiliani, F.; DiMarco, A.; Kaplan, N. O.; Schein, P. S. *Anthracyclines: Current Status and Future Developments*; Mathe, G., Maral, R., Dejager, R., Eds.; Masson, New York, 1983.
28. Robert, G.., Ed *Langmuir-Blodgett Films;* Plenum, New York, 1990.
29. Petty, M. C. *Langmuir-Blodgett films: AN INTRODUCTION;* Cambridge University Press, Cambridge, 1996.
30. Ulman, A. *An Introduction to ULTRATHIN ORGANIC FILMS From Langmuir-Blodgett to Self-Assembly;* Academic Press, San Diego (1991).
31. Schwartz, D. K. *Surf. Sci. Rep.* **1997**, *27*, 241.
32. Badr, H. A. I.; Meyerhoff, E.M. *J. Am. Chem. Soc.* **2005**, *127*, 5318.
33. Mayes, A. G.; Blyth, J.; Millington, R. B.; Lowe, C. R. *Anal. Chem.* **2002**, *74*, 3649.
34. Umezawa, Y.; Roki, H. *Anal. Chem.* **2004**, 321A.
35. Liu, M.; Ushida, K.; Kira, A.; Nakahara, H. *J. Phys. Chem. B* **1997**, *101*, 1101.

36. Henrichs, S.; Collier, C. P.; Saykally, R. J.; Shen, Y. R.; Heath, J. R. *J. Am. Chem. Soc.* **2003**, *122*, 4077.
37. Petty, M. C. *Thin Solid Film* **1992**, *210−211*, 417.
38. Hamley, I. W. *Angew. Chem., Int. Ed.* **2003**, *42*, 1692.
39. Fujiki, M.; Tabei, H. *Langmuir* **1988**, *4*, 320.
40. Valli, L. *Adv. Colloid Interface Sci.* **2005**, *116*, 13.
41. Barlow, W. A. *Langmuir-Blodgett Films;* Elsevier, Amsterdam, 1980.
42. Lvov, Y.; Decher, G.; Möhwald, H. *Langmuir* **1993**, *9*, 481
43. Moriizumi, T. *Thin Solid Films* **1998**, *160*, 413.
44. Ferreira, M.; Riul, A., Jr.; Wohnrath, K.; Fonseca, F. J.; Oliveira, O. N.; Mattoso, L. H. C. *Anal. Chem.* **2003**, *75*, 953.
45. Sanji, T.; Kitayama, F.; Sakurai, H. *Macromolecules* **1999**, *32*, 5718.
46. Sanji, T.; Nakatsuka, Y.; Ohnishi, S.; Sakurai, H. *Macromolecules* **2000**, *33*, 8524.
47. Embs, F. W.; Wegner, G.; Neher, D.; Albouy, P.; Miller, R. D.; Willson, C. G.; Schrepp, W. *Macromolecules* **1991**, *24*, 5068.
48. Yoshida, H.; Kani, R.; Hayase, S.; Horie, K. *J. Phys. Chem.* **1993**, *97*, 5370.
49. Kani, R.; Nakano, Y.; Majima, Y.; Hayase, S.; Yuan, C. H.; West, R. *Macromolecules* **1994**, *27*, 1911.
50. Kani, R.; Yoshida, H.; Nakano, Y.; Marui, S.; Mori, Y.; Kawata, Y.; Hayase, S. *Langmuir* **1993**, *9*, 3045.
51. Seki, T.; Tanigaki, N.; Yase, K.; Kaito, A.; Tamaki, T.; Ueno, K.; Tanaka, Y. *Macromolecules* **1995**, *28*, 5609.
52. Yoshida, M.; Nakanishi, F.; Seki, T.; Sakamoto, K.; Sakurai, H. *Macromolecules*

1997, *30*, 1860.

53. Tachibana, H.; Kishida, H.; Tokura, Y. *Langmuir* **2001**, *17*, 437.
54. Fujino, M. *Chem. Phys. Lett.* **1987**, *136*, 451.
55. Kepler, R. G.; Zeigler, J.M.; Harrah, L. A.; Kurtz, S. R. *Phys. Rev.* **1987**, *B35*, 2818.
56. Stolka, M.; Yuh, H. J.; McGrane, K.; Pai, D. M. *J. Polym. Sci., Polym. Chem.* **1987**, *25*, 823.
57. Abkowitz, M. A.; Knier, F. E.; Yuh, H. J.; Weagley, R.J.; Stolka, M. *Solid State Commun.* **1987**, *62*, 547.
58. Yuan, C. H.; Hoshino, S.; Toyoda, S.; Suzuki, H.; Fujiki, M.; Matsumoto, N. *Appl. Phys. Lett.* **1997**, *71*, 3326.
59. Suzuki, H.; Hoshino, S.; Furukawa, K.; Ebata, K.; Yuan, C. H.; Bleyl, I. *Polym. Adv. Technol.* **2000**, *11*, 460.
60. Samuel, L. M.; Sanda, P. N.; Miller, R. D. *Chem. Phys. Lett.* **1989**, *159*, 227.
61. Yokoyama, K.; Yokoyama, M. *Chem. Lett.* **1989**, 1005.
62. Mitter-Neher, S.; Neher, D.; Stegeman, G. I.; Embs, F. W.; Wegner, G. *Chem. Phys.* **1992**, *161*, 289.
63. Kajar, F.; Messier, J.; Rosilio, C. *J. Appl. Phys.* **1986**, *60*, 3040.
64. Nagano, S.; Seki, T.; Ichimura, K. *Langmuir* **2001**, *17*, 2199.
65. Nagano, S.; Seki, T. *J. Am. Chem. Soc.* **2002**, *124*, 2074.
66. Fujiki, M.; Koe, J. R.; Terao, K.; Sato, T.; Teramoto, A.; Watanabe, J. *Polym. J.* **2003**, *35*, 297.
67. West, R. *J. Organomet. Chem.* **1986**, *300*, 327.
68. Miller, R. D.; Michl, J. *Chem. Rev.* **1989**, *89*, 1359.

69. West, R. Polysilanes and Related Polymers. In *Inorganic Polymers;* Mark, J. E., Allcock, H. R., West, R., Eds.; R. Prentice Hall, NJ, 1992.

70. Kipping, F. S. *J. Chem. Soc.* **1924**, *125*, 2291.

71. Burkhard, C. *J. Am. Chem. Soc.* **1949**. *71*.963.

72. Yajima, S.; Hayashi, J.; Omori, M. *Chem. Lett.* **1975**, 931.

73. Yajima, S.; Okamura, K.; Hayashi, J. *Chem. Lett.* **1975**, 1209.

74. Yajima, S.; Hasegawa, Y.; Hayashi, J.; Iimura, M. *J. Mater. Sci.* **1978**, *13*, 2569.

75. Trefonas, P.; West, R.; Miller, R. D.; Hofer, D. *J. Polym. Sci., Polym. Lett. Ed.* **1983**, *21*, 823.

76. Trefonas, P., III.; Damewood, J. R., Jr.; West, R.; Miller, R. D. *Organometallics* **1985**,*4*, 1318.

77. Michl, J.; West, R. Electronic Structure and Spectroscopy of Polysilanes. In *Silicon-Based Polymers The Science and Technology of their Synthesis and Applications;* Chojnowski, J., Jones, R. G., Ando, W., Eds.; Kluwer, Dordrecht, The Netherlands, 2000.

78. Schweitzer, K. S. *J. Chem. Phys.* **1986**, *85*, 1156.

79. Klingensmith, K. A.; Downing, J. W.; Miller, R. D.; Michl, J. *J. Am. Chem. Soc.* **1986**, *108*, 7438.

80. Cotts, P. M.; Miller, R. D.; Trefonas III, P.; West, R.; Fickes, G. *Macromolecules* **1987**, *20*, 1046.

81. Shukla, P.; Cotts, P. M.; Miller, R. D.; Russell, T. P.; Smith, B. A.; Waalraff, G. M.; Baier, M.; Thyagarajan, P. *Macromolecules* **1991**, *24*, 5606.

82. Miller, R. D.; Waalraaf, G. M.; Baier, M.; Cotts, P. M.; Shukla, P.; Russell, T. P.; De Schryver, F. C.; Declerq, D. *J. Inorg. Organomet. Polym.* **1991**, *1*, 505.

83. Oka, K.; Fujiue, N.; Nakanishi, S.; Takata, T.; West, R.; Dohmaru, T. *J. Organomet. Chem.* **2000**, *611*, 45.

84. Harrah, L. A.; Zeigler, J. M. In *Photo hysics of Polymers;* Hoyle, C. E., Torkelson, J. M., Eds.; ACS Symposium Series 358; American Chemical Society:,Washington, DC, 1987.

85. .H arrah. L. A.: Zeirrler, J. M. *J . Polvm. Sci., Polvm. Lett. Ed.* **1985**, *23*, 209.

86. Charlesby, A. *Atomic Radiation and Polymers;* Pargamon Press, Oxford, 1960.

87. Chapiro, A. *Radiation Chemistry of Polymeric System;* Wiley, New York, 1962.

88. Guilmeau, I.; Esnouf, S.; Betz, N.; Le Moel, A. *Nucl. Instrum. Meth. Phys. Res. B* **1997**, *131*, 270.

89. Betz, N.; Begue, J.; Goncalves, M.; Gionnet, K.; Deleris, G.; Le Moel, A. *Nucl. Instrum. Meth. Phys. Res. B* **2003**, *208*, 434.

90. Chapiro, A. *Radiat. Phys. Chem.* **1977**, *9*, 55.

91. Abdel-Bary, E. M.; El-Nesr, E. M. Methods, characterization, and application of grafting. In *Handbook of engineering polymeric materials;* Cheremisinoff, P., Ed.; Marcel Dekker, New York, 1997.

92. Nasef, M. M.; Hegazy, E. S. A.; *Prog. Polym. Sci.* **2004**, *29*, 499.

93. Nasef, M.; Saidi, H.; Nor, H. *Nucl. Sci. J. Malaysia* **1999**, *17*, 27.

94. Aydinli, B.; Tincer, T. *Radiat. Phys. Chem.* **2001**, *60*, 237.

95. Corkill, J. M.; Godman, J. F.; Harrold, S. P. *Trans. Faraday. Soc.* **1964**, *64*, 202.

96. Price, C. Colloidal properties of block copolymers. In *Developments in block copolymers 1.;* Goodman, I., Ed.; Applied Science, London, 1982.

97. Quintana, J. R.; Villacampa, M.; Katime, I. Block copolymers: micellization in solution. In *Polymer material encyclopedia, vol. 1.;* Salamone, J. C., Ed.; CRC

Press, Boca Raton, 1996.

98. Alexandridis, P.; Holtzwarth, J. F.; Hatton, T. A. *Macromolecules* **1994**, *27*, 2414.
99. Riess, G. *Prog. Polym. Sci.* **2003**, *28*, 1107.
100. Blodgett, K. B. *J. Am. Chem. Soc.* **1934**, *56*, 495.
101. Blodgett, K. B. *J. Am. Chem. Soc.* **1935**, *57*, 1007.
102. Langmuir, I. *Trans. Faraday Soc.* **1920**, *15*, 62.
103. Blodgett, K. B.; Langmuir, I. *Phys. Rev.* **1937**, *51*, 964.
104. Laschewsky, A.;Ringsdort, H.; Schmidt, G.; Schneider, J. *J. Am. Chem. Soc.* **1987**, *109*, 788.
105. Schneider, J.; Ringsdort, H.; Rabolt, F. J. *Macromolecules* **1989**, *22*, 205.

Part I

Chapter 2

Radiation-Induced Graft Polymerization of Amphiphilic Monomers with Different Polymerization Characteristics onto Hydrophobic Polysilane

2.1. Introduction

Polysilane has attracted much attention because it has unique properties arising from delocalized electrons along the silicon backbone.[1-3] If polysilane is applied to fabricate ordered materials in the nanometer scale, further unique properties can be developed. The utilization of self-assemblies is considered as a powerful method for preparing ordered structures. Since it is widely known that amphiphilic block or graft copolymers can form self-assemblies such as micelles and oriented Langmuir monolayers,[4-6] amphiphilic polysilane copolymers are also expected to serve as ordered materials.

For the synthesis of polysilane copolymers with hydrophilic or amphiphilic chains, we can consider the following two approaches: the modification of presynthesized hydrophobic polysilane and the direct polymerization of monomeric silanes with hydrophilic or amphiphilic groups. In the latter case, however, the Wurtz-type coupling reaction, which is commonly used for the synthesis of polysilane, can not be applied because sodium metal used in the reaction violently attacks reactive functional groups.[1,2] Thus, this way is limited in its use. In contrast, the former way is free from such a limitation. Therefore the author studied the modification of presynthesized polysilane to obtain polysilane-based amphiphilic graft copolymers

by utilizing γ-ray-induced graft polymerization.

In this chapter, the author investigates the structures of amphiphilic graft polysilane modified under various irradiation conditions to establish optimized irradiation. As a hydrophobic base polymer for the graft polymerization, poly(methyl-*n*-propylsilane) (PMPrS) was employed. For grafted molecules, three types of monomers bearing hydrophilic groups were used: methyl methacrylate (MMA), diethyl fumarate (DEF) and maleic anhydride (MAH). MMA and DEF are homopolymerizable monomers having different propagation rate constants, while MAH is known as a non-homopolymerizable monomer in radical polymerization.[7,8] It can be expected that the structure and property of modified PMPrS differ according to the polymerization characteristics of these grafted monomers. In each experiment performed with the grafting monomers, the author tried to control grafting yield, which is defined as monomer units of grafted chains per silicon atom of PMPrS, by changing irradiation conditions such as total absorption dose, dose rate and the concentrations of grafting monomers.

2.2. Experimental Section

2.2.1. Monomers

Methyl-*n*-propyldichlorosilane (Shin-Etsu Chemical, Co.), methyl methacrylate (MMA) (Nakalai Tesque, Inc.) and diethyl fumarate (DEF) (Nakalai Tesque, Inc.) were used after purification by reduced-pressure distillation. Maleic anhydride (MAH) was employed after purification by re-crystallization with toluene.

2.2.2. Synthesis of PMPrS

PMPrS was synthesized via the Wurtz-type coupling reaction of methyl-*n*-propyldichlorosilane. Crude PMPrS was purified by re-precipitation from a toluene solution into methanol, and then pure PMPrS was obtained by freeze-drying from a benzene solution. The number average molecular weight of PMPrS used in the following experiments is listed in Table 2.1. PMPrS1, PMPrS2 and PMPrS3 were employed for grafting poly(methyl methacrylate) (PMMA), poly(diethyl fumarate) (PDEF) and MAH, respectively.

Table 2.1. Number average molecular weight (M_n) and polydispersity index (PDI) of PMPrS.

	$M_n \times 10^{-4}$ [a]	PDI [b]
PMPrS1	1.3	2.4
PMPrS2	1.2	3.8
PMPrS3	1.1	3.8

[a,b] Determined by GPC (RI detector) with polystyrene standards and a THF eluent.

2.2.3. Radiation-Modification of PMPrS

PMMA-grafted PMPrS (PMPrS-*g*-PMMA), PDEF-grafted PMPrS (PMPrS-*g*-PDEF) and MAH-grafted PMPrS (PMPrS-*g*-MAH) were synthesized as follows: PMPrS and each monomer were co-dissolved in toluene. The toluene solution was degassed and sealed in a glass tube, and then irradiated with ^{60}Co-γ-rays at room temperature.

In the case of PMPrS-*g*-PMMA, the toluene solution after γ-irradiation was poured into methanol to precipitate a product. To remove PMMA homopolymer contained in the crude product, the precipitate was purified by fractional precipitation with acetone/methanol. Acetone is a good solvent for PMMA but a poor solvent for PMPrS, and methanol is a poor solvent for both PMMA and PMPrS. When a small amount of a toluene solution of the crude product was dropped into a large amount of acetone, PMPrS-*g*-PMMA formed emulsions. By adding methanol into the acetone solution containing the emulsions of the product, four regimes were found according to the methanol amount. In the first regime, no changes were recognized in spite of methanol addition. In the second regime, however, further methanol addition caused the solution more opaque and the amount of centrifuged precipitates was increased. In the third regime, the amount of precipitates was constant independently of the methanol amount, but in the fourth regime, precipitates obtained were again increased with increasing methanol amount. PMPrS-*g*-PMMA was successfully recovered in the second regime. After the fractional precipitation, PMPrS-*g*-PMMA was freeze-dried with benzene.

The purity of PMPrS-*g*-PMMA obtained was verified by iodine-staining thin-layer chromatography (TLC) with a silica plate and an eluent of a tetrahydrofuran (THF)/toluene (4/6, v/v) mixture. The eluent could separate PMPrS-*g*-PMMA and PMMA homopolymer completely. In the TLC experiment with purified PMPrS-*g*-PMMA, the author could not recognize the spot of PMMA homopolymer. This fact indicates that the amount of PMMA contained was under the detection limit in the purified product. The detection limit of PMMA was determined in another TLC experiment, and finally the content of PMMA homopolymer in

PMPrS-*g*-PMMA was found to be less than 1.0 wt%.

In the case of PMPrS-*g*-PDEF, solvent toluene was removed by evaporation from the reaction solution after irradiation, and then crude PMPrS-*g*-PDEF was freeze-dried from a benzene solution. Next, PMPrS-*g*-PDEF was precipitated from a THF solution into water, and recovered again by freeze drying after unreacted DEF monomers contained in the precipitate were removed by filtration. This reprecipitation procedure was repeated 3 – 5 times. Some products containing PDEF homopolymer above 1.0 wt% were further purified by fractional precipitation with THF/hexane. THF is a good solvent for both PMPrS and PDEF, while hexane is a good solvent only for PMPrS but not for PDEF. When hexane is added to the THF solution of the product, PMPrS-*g*-PDEF forms emulsions and PDEF homopolymer precipitates. Accordingly, PDEF homopolymer could be removed by centrifugation after successive addition of hexane. Finally, the product was freeze-dried twice from a benzene solution and then vacuum-dried for 40 hours to remove water completely.

The purity of PMPrS-*g*-PDEF was verified by TLC with a methanol eluent and a sulfuric acid stain in the same manner as described above. The content of PDEF homopolymer was also found to be less than 1.0 wt%.

In the case of PMPrS-*g*-MAH, solvent toluene was removed by evaporation from the reaction solution after irradiation. Pure PMPrS-*g*-MAH was isolated from the crude product by solvent extraction with hexane and then obtained by freeze-drying from a benzene solution. The content of unreacted MAH was checked to be less than 0.5 wt% by GPC with a UV detector.

2.2.4. Spectroscopy

^{1}H NMR spectra were recorded on a JEOL EX 400 spectrometer at 25 or 55 ℃ in deuterated chloroform solutions.

2.2.5. Evaluation of Grafting Yield

Grafting yield, which the author defines as the number of monomer unit per silicone atom of PMPrS, was calculated from the intensity ratio of ^{1}H NMR signals. In reference to the integrated signal intensity for a methyl proton of PMPrS ($SiCH_3$, δ 0.25 ppm), the intensity rations of a methyl proton of PMMA ($COOCH_3$, δ 3.7 ppm) for PMPrS-*g*-PMMA, a methylene proton of PDEF ($COOCH_2CH_3$, δ 4.2 ppm) for PMPrS-*g*-PDEF and a methine proton of MAH (CHCH, δ 2.0 – 5.0 ppm) for PMPrS-*g*-MAH were calculated to evaluate their grafting yields.

2.3. Results and Discussion

2.3.1. Irradiation Effect on PMPrS

The molecular weight of PMPrS modified with grafted chains should become larger than that of PMPrS irradiated without monomers. Therefore, the author examined the change of molecular weight of PMPrS when PMPrS was irradiated by γ-rays with and without MMA monomers in toluene. Figure 2.1 shows the variation of molecular weight depending on dose. When PMPrS alone is irradiated with γ-rays, its molecular weight decreases with an increase of dose. This result indicates that PMPrS is degraded by γ-rays. When PMPrS is irradiated together with MMA, on the other hand, the decrease of the molecular weight is smaller. One reason is that MMA monomers shows protection effect on PMPrS degradation

by absorbing γ-rays and consuming radicals. Moreover, PMMA grafting on PMPrS is also responsible for this smaller molecular weight decrease. The result obtained here suggests that γ-irradiation successfully cause the graft polymerization of MMA onto PMPrS in spite of degradation of PMPrS.

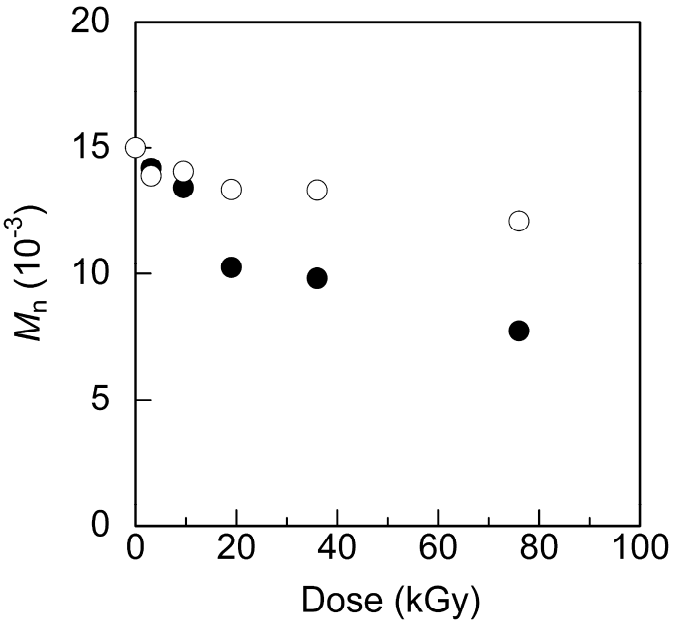

Figure 2.1. Variation of molecular weight of PMPrS depending on dose. Dose rate was 3.1 kGy/h. Open and closed circles indicate the molecular weight of PMPrS irradiated with and without MMA, respectively. The molecular weight was measured by GPC with RI detector.

2.3.2. Grafting Yield of PMPrS-g-PMMA

The author tried to control grafting yield by changing irradiation conditions. Figure 2.2a shows the dependence of grafting yield of PMPrS-*g*-PMMA on dose at a constant dose rate of 3.1 kGy/h. Although grafting yield obviously rises with increasing dose, the increase rate of grafting yield gradually reduces at higher doses. The reason for this rate reduction is partly attributed to the consumption of MMA monomers by graft- and homo-polymerization of MMA. The concentration of MMA monomers available for graft polymerization decreases at higher doses.

Figure 2.2b exhibits that grafting yield decreases with increasing dose rate despite the total absorption dose is the same. This decrease of grafting yield is explained by PMMA homopolymerization. At higher dose rates, γ-rays generate more MMA radicals simultaneously in the reaction solution, which leads to more facile homopolymerization of MMA. Thus, MMA monomers available for graft polymerization diminish, and consequently grafting yield decreases in spite of the same dose.

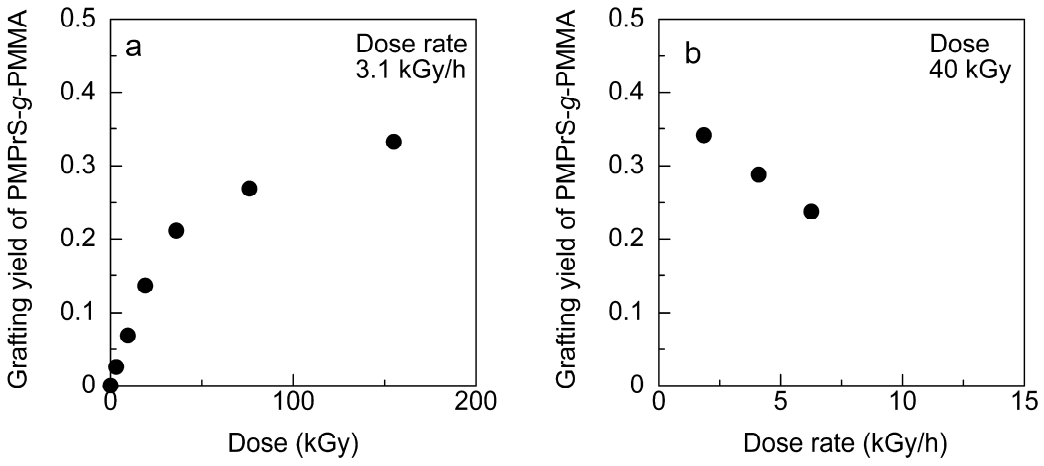

Figure 2.2. Dependence of grafting yield of PMPrS-*g*-PMMA on (a) dose and (b) dose rate. The concentrations of PMPrS and MMA were both 10 wt%.

Figure 2.3 depicts the dependence of grafting yield of PMPrS-*g*-PMMA on the concentration of MMA. Grafting yield rises in proportion to the MMA concentration under 40 wt%. Above MMA concentrations of 60wt%, gelation took place upon irradiation and therefore it was impossible to isolate PMPrS-*g*-PMMA from the product. This indicates that crosslinking of PMMA occurs at higher concentrations.

Thus, the author demonstrated that grafting yield of PMPrS-*g*-PMMA could be controlled by the irradiation conditions such as dose, dose rate and the concentration of MMA.

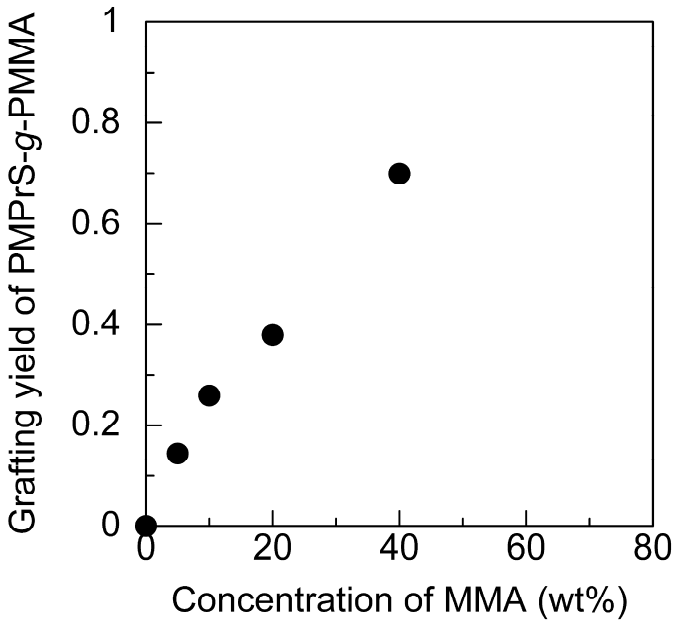

Figure 2.3. Dependence of grafting yield of PMPrS-*g*-PMMA on the concentration of MMA. The concentration of PMPrS was 10 wt%. Dose rate was 1.9 kGy/h and dose was 40 kGy.

2.3.3. Characterization of PMPrS-g-PMMA

Polysilane has a strong absorption band in UV region due to the σ-σ* transition of delocalized electrons along its backbone. However, polysilane is degraded by γ-irradiation as described above. Therefore, the author checked whether or not PMPrS-*g*-PMMA keeps this electronic property after γ-irradiation from UV absorption spectra of PMPrS and PMPrS-*g*-PMMA. The shape of the spectra and the molar absorption coefficients were little changed by irradiation. These results indicate that the electronic property derived from the delocalized electrons along the

silicon backbone is scarcely affected by the radiation-modification.

ESR and ^{1}H NMR measurements were attempted to define the reactive sites on PMPrS and to clarify the structure of PMPrS-*g*-PMMA, but resulted in little success. The ESR result suggests that alkyl radicals were generated at room temperature, but it is difficult to determine exact positions of those radicals. In ^{1}H NMR measurement, it is also hard to specify the position where graft chains attach to the main chain.

Therefore, the author assumed the structure of radiation-modified polysilane by reference to other studies on radiation chemistry of polysilane. Seki et al. reported the γ-ray-induced process on poly(dimethylsilane) by ESR study.[9] They demonstrated that radicals are generated on silicon atoms by elimination of side-chain methyl radicals upon γ-irradiation at 77 K. Kumagai et al. studied the effect of γ-irradiation on poly(diethylsilane) and poly(cyclohexylmethylsilane) at 77 K.[10] They clarified that radicals are generated on alkyl side chains of these polysilanes by homolytic cleavage of C-H bonds. In both cases, the initial process caused by γ-irradiation is the formation of radicals at an alkyl side-chain position. In consideration of the similar structure having relatively longer alkyl side chains, Kumagai's case is more safely applicable to the author's case. Although the radicals often cause the homolytic cleavage of Si-Si bonds at elevated temperatures and therefore block type copolymers might be formed, main products are considered to be copolymers with grafted chains growing from alkyl side chains of PMPrS since radicals initially formed at a side-chain position can facilely attack surrounding MMA monomers.

For quantitative discussion, two indexes were evaluated: the degree of

polymerization of PMMA graft chains, d_{PMMA}, and the number of PMMA graft chains per silicon atom, n_{PMMA}. It is possible to evaluate d_{PMMA} from the ratio of the number of MMA units to that of PMMA chain ends and n_{PMMA} from the ratio of the number of PMMA chain ends to methyl-*n*-propylsilane (MPrS) units. Two signals observed at δ 5.5 and 6.2 ppm in ^{1}H NMR spectra of PMPrS-*g*-PMMA reveal that the terminal unit of PMMA graft chains has an unsaturated bond due to termination by disproportionation. Contrary to the author's expectations, a chain transfer reaction from growing PMMA chains to solvent toluene molecules during irradiation is negligible, judging from the absence of toluene-derived signals in ^{1}H NMR spectra. Other terminal structures of PMMA graft chains should exist, but signals due to them could not be clearly distinguished in ^{1}H NMR spectra because of interference by other signals. In this study, consequently, PMMA terminal units were counted by measuring the signals from the unsaturated bond.

For the following analysis based on ^{1}H NMR spectra, the ratio of integral intensity for a methoxy proton of PMMA (δ 3.7 ppm) to that for a methylene proton of the unsaturated terminal of PMMA (δ 6.2 ppm) is expressed as r_{d1}, and the ratio of integral intensity for a methylene proton of the unsaturated terminal of PMMA to that for a methyl proton of PMPrS (δ 0.25 ppm) as r_{n1}. In addition, the number of the unsaturated terminals per graft chain is symbolized by N_{PMMA}. Because the absolute value of N_{PMMA} is hard to be determined by ^{1}H NMR measurement, the author assumed N_{PMMA} as 1.0 for each PMPrS-*g*-PMMA. Then, the degree of polymerization of PMMA chains (d_{PMMA}) and the number of PMMA chains per silicon atom (n_{PMMA}) are described as $d_{PMMA} = r_{d1}$ $N_{PMMA} = r_{d1}$ and $n_{PMMA} = r_{n1}/N_{PMMA} = r_{n1}$, respectively. Figure 2.4 depicts the dependence of d_{PMMA} and

n_{PMMA} on the concentration of MMA in the graft polymerization. As shown in the figure, d_{PMMA} rises with increasing concentration of MMA, but n_{PMMA} scarcely changes. These results demonstrate that the rise of grafting yield with an increase of MMA concentration (Figure 2.3) is due to the growth of the degree of polymerization but not to the growth of the number of graft chains.

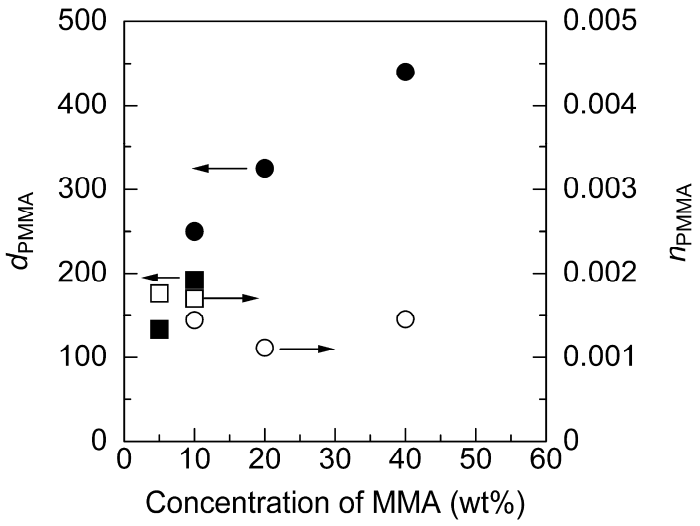

Figure 2.4. Dependence of d_{PMMA} and n_{PMMA} on the concentration of MMA. The concentration of PMPrS was 10 wt% and dose rate was 1.9 kGy/h. Closed and open symbols indicate d_{PMMA} and n_{PMMA}, respectively. Circles and squares corresponds to doses of 40 and 95 kGy, respectively.

Figure 2.5 shows the dependence of d_{PMMA} and n_{PMMA} on dose. The d_{PMMA} decreases with increasing dose, which indicates that PMMA graft chains are degraded more readily at higher doses. In contrast, n_{PMMA} rises with an increase of dose, showing that PMMA graft chains increase in number. These results reveal that the rise of grafting yield with increasing dose, which is shown in Figure 2.2a, is mainly caused by the increase of a graft density.

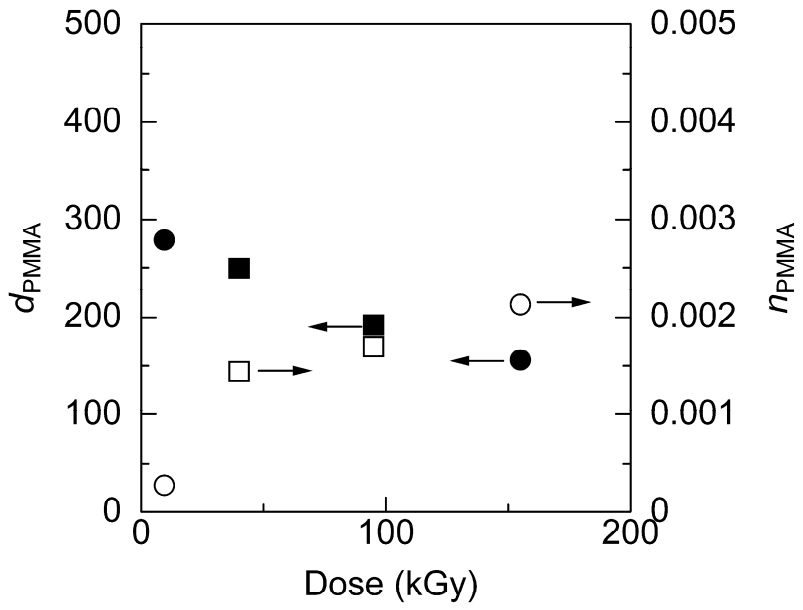

Figure 2.5. Dependence of d_{PMMA} and n_{PMMA} on dose. The concentrations of PMPrS and MMA were both 10 wt%. Closed and open symbols indicate d_{PMMA} and n_{PMMA}, respectively. Circles and squares correspond to dose rates 3.1 and 1.9 kGy/h, respectively.

If M_n of PMPrS1 in Table 2.1 is used, the number of PMMA chains per PMPrS chain is estimated as ca. 0.32 for PMPrS-*g*-PMMA with grafting yield of 0.33. The cause of such a low graft density is explained as follows. In PMMA graft polymerization, the initiation reaction by γ-rays is considerably slower than the chain propagation reaction. Then, PMMA chains grown at an early stage of the reaction sterically cover other initiation sites on the same polysilane chain. Due to this steric hindrance by graft chains, monomers can hardly access to the reactive sites and the grafting from these sites scarcely occurs. As a result, the graft density becomes low.

Therefore, it is required to depress the steric hindrance by use of a monomer with a small propagation rate constant to attain high graft density.

2.3.4 Grafting Yield of PMPrS-g-PDEF

DEF was employed as a grafting monomer with smaller propagation rate constant (k_p = 0.21 $Lmol^{-1}s^{-1}$) than that of MMA (k_p = 290 $Lmol^{-1}s^{-1}$).[11,12] The dependence of grafting yield of PMPrS-*g*-PDEF on dose and dose rate is shown in Figure 2.6. Grafting yield rises with an increase of dose in Figure 2.6a as in the case of PMPrS-*g*-PMMA, but the leveling-off behavior at higher doses as observed for PMPrS-*g*-PMMA is hardly recognized. This result can be explained as follows. Reduction of DEF monomers is more moderate than that of MMA monomers because DEF has the smaller propagation rate constant and the amount of DEF consumed by homopolymerization is small. As a result, more monomers are available for graft polymerization compared to the case of PMPrS-*g*-PMMA.

On the other hand, grafting yield of PMPrS-*g*-PDEF decreases with increasing

dose rate in Figure 2.6b. This relationship between grafting yield and dose rate is consistent with that shown in Figure 2.2b. DEF has a smaller propagation rate constant than MMA does, but the competition between graft polymerization and homopolymerization also occurs as in the case of PMPrS-*g*-PMMA.

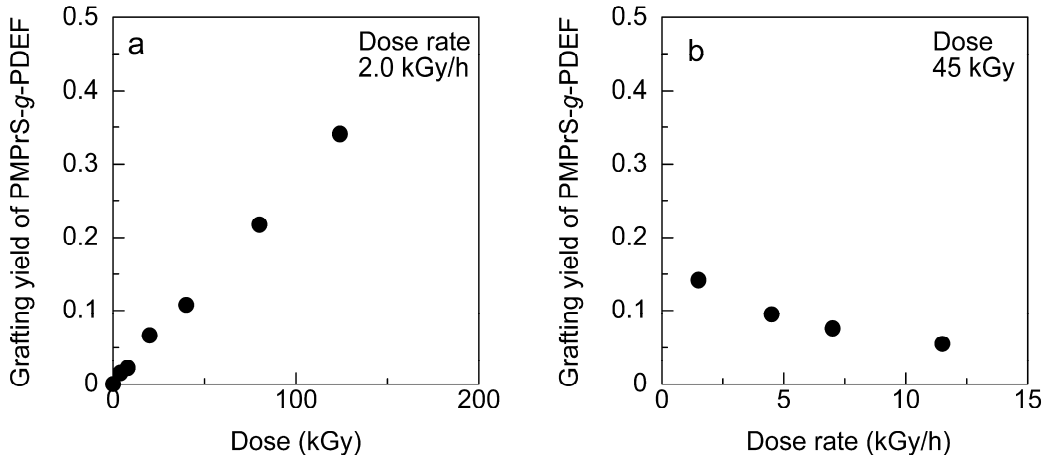

Figure 2.6. Dependence of grafting yield of PMPrS-*g*-PDEF on (a) dose and (b) dose rate. The concentrations of PMPrS and DEF were 10 and 30 wt%, respectively.

Figure 2.7 depicts the dependence of grafting yield on the concentration of DEF. Similarly to the case of PMPrS-*g*-PMMA, grafting yield rises with increasing concentration of DEF.

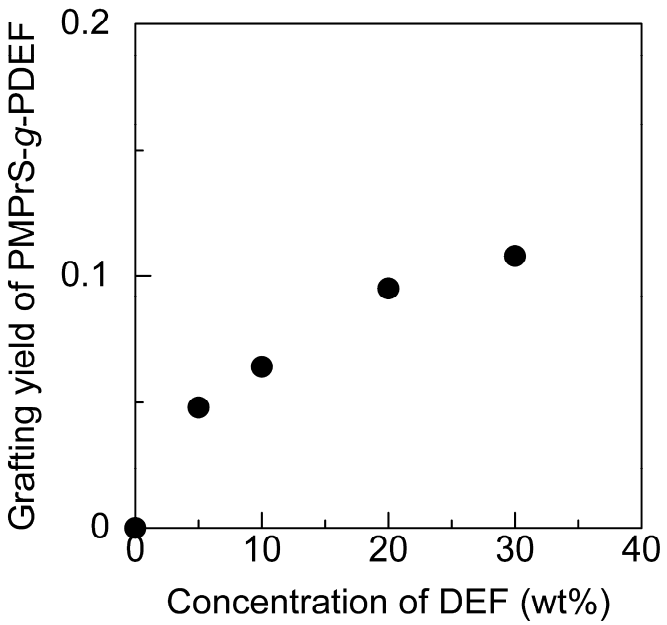

Figure 2.7. Dependence of grafting yield of PMPrS-*g*-PDEF on the concentration of DEF. The concentration of PMPrS was 10 wt%. Dose rate was 2.0 kGy/h and dose was 40 kGy.

2.3.5. Characterization of PMPrS-g-PDEF

In ^{1}H NMR spectra of PMPrS-*g*-PDEF, a signal owing to PDEF chain ends was observed at δ 6.7-6.9 ppm. Other signals due to the chain ends were not distinguished. The observed signals indicate that the terminal unit of PDEF graft chains has an unsaturated structure.

In the same manner described above, the author hereafter uses the following quantities: the degree of polymerization of PDEF graft chains, d_{PDEF}, the number of PDEF graft chains per silicon atom, n_{PDEF}, and the number of the unsaturated

terminals, N_{PDEF}. The following values are also defined: r_{d2} as the ratio of integral intensity for a methylene proton of PDEF (δ 4.2 ppm) to that for a methine proton of the unsaturated terminals (δ 6.7-6.9 ppm), and r_{n2} is one for a methine proton of the unsaturated terminals to that of a methyl proton of PMPrS. As in the case of PMPrS-*g*-PMMA, the author assumes N_{PDEF} as 1.0 for each PMPrS-*g*-PDEF. Then, d_{PDEF} and n_{PDEF} are expressed by $d_{PDEF} = r_{d2}$ and $n_{PDEF} = r_{n2}$, respectively.

Figure 2.8 shows the dependence of d_{PDEF} and n_{PDEF} on dose. Contrary to the d_{PMMA} of PMPrS-*g*-PMMA, d_{PDEF} rises with increasing dose. This indicates that the PDEF chains are less degradable than PMMA chains and the growth of PDEF chains is predominant over the degradation except at higher doses. In Figure 2.8, n_{PDEF} also rises with increasing dose. The rise of grafting yield of PMPrS-*g*-PDEF shown in Figure 2.6a is due to the increase of both the degree of polymerization and the number of grafted chains, unlike the PMPrS-*g*-PMMA case.

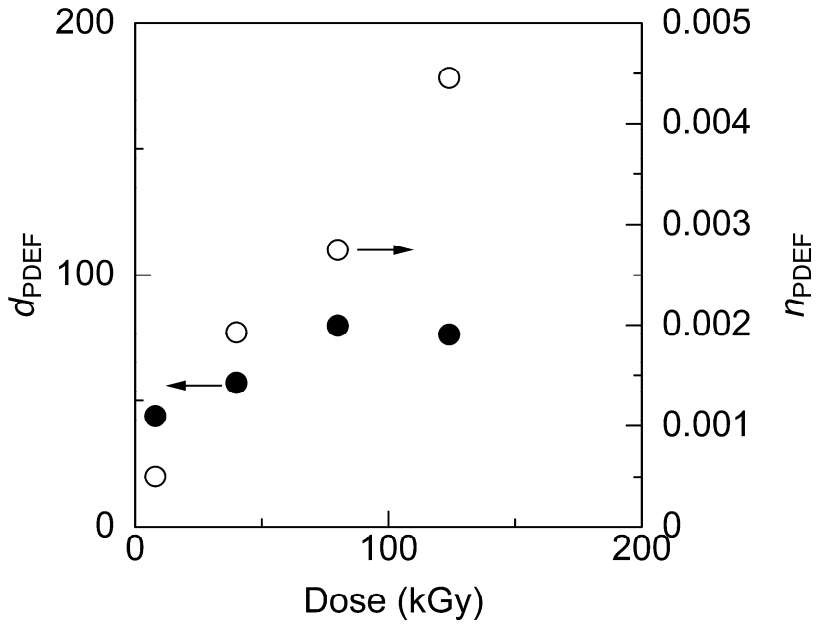

Figure 2.8. Dependence of d_{PDEF} (closed circles) and n_{PDEF} (open circles) on dose. The concentrations of PMPrS and DEF were 10 and 30 wt%, respectively. Dose rate was 2.0 kGy/h.

For further quantitative discussion, the author estimated the graft density of PMPrS-*g*-PDEF in the same way as shown above.

If M_n of PMPrS2 in Table 2.1 is employed, the number of PDEF chains per PMPrS chain is estimated as ca. 0.62 for PMPrS-*g*-PDEF with grafting yield of 0.34. Although the graft density of PMPrS-*g*-PDEF is higher than that of PMPrS-*g*-PMMA, this value is still lower than the author has expected. The propagation of PDEF graft chains is still too fast to overcome steric hindrance by grafted chains. Therefore, the author adopted a monomer with no ability of

homopolymerization, MAH.

2.3.6. Grafting Yield of PMPrS-g-MAH

Because MAH is a non-homopolymerizable monomer in radical polymerization,[7,8] it is expected that the steric hindrance by grafted chains is reduced and the higher graft density of PMPrS-*g*-MAH is attained compared with that of PMPrS-*g*-PMMA and PMPrS-*g*-PDEF.

Prior to using MAH for graft polymerization, the author confirmed by GPC and ^{1}H NMR measurement that MAH does not homopolymerize indeed by γ-irradiation.

Figure 2.9 depicts the dependence of grafting yield of PMPrS-*g*-MAH on dose. The grafting yield of PMPrS-*g*-MAH rises with increasing dose. The rise of grafting yield directly indicates the rise of graft density of PMPrS-*g*-MAH because the grafted chains have only one MAH unit.

The number of grafted MAH per silicon atom, n_{MAH}, is calculated by multiplying grafting yield by the number of MPrS units of PMPrS. For PMPrS-*g*-MAH with grafting yield of 0.24, n_{MAH} is calculated as 4.2; in other expression, the number of MAH bonded to one PMPrS chain is ca. 30. It is thus demonstrated that higher graft density is attained by MAH grafting as the author expected.

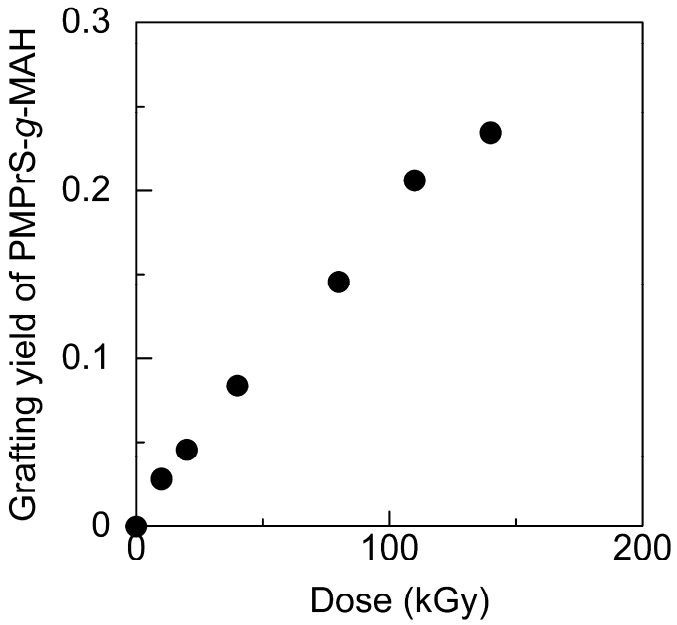

Figure 2.9. Dependence of grafting yield of PMPrS-*g*-MAH on dose. The concentrations of PMPrS and MAH were 10 wt%. Dose rate was 2.0 kGy/h.

With an aim to attain larger grafting yield, i.e., higher graft density, higher dose of γ-rays was irradiated for synthesizing PMPrS-*g*-MAH. The results are summarized in Table 2.2. Grafting yield listed in Table 2.2 is higher than that shown in Figure 2.9. However, UV absorption spectra of these PMPrS-*g*-MAH samples show peak shifts of σ-σ* absorption to shorter wavelength, which reflects the degradation of PMPrS main chains by high dose of γ-rays.

Table 2.2. Grafting yield of PMPrS-*g*-MAH at higher doses. The concentrations of PMPrS and MAH were both 10 wt%.

Dose (kGy)	Dose rate (kGy/h)	Grafting yield
275	5.0	0.32
550	10.0	0.50
1100	20.0	0.62

The author used higher concentration of MAH to attain higher grafting yields, but PMPrS could not be dissolved in a toluene solution of MAH with a concentration above 11 wt%. Accordingly, relative concentration of MAH with reference to PMPrS was increased by reducing the concentration of PMPrS for a fixed MAH concentration. However, grafting yield was almost constant even with changing the concentration of PMPrS. This result presumably indicates that the rate-determing step is generation of reactive sites on PMPrS and the grafting rate of MAH is independent of the concentration of PMPrS. As a result, the grafting yield is also irrelevant to the concentration of PMPrS. In the case of PMPrS-*g*-PMMA and PMPrS-*g*-PDEF, on the other hand, grafting yield depends on the concentration of grafting monomers as discussed above. Generation of reactive sites on PMPrS would be a rate-determining step also in this case, but the grafting yield of these polymers is determined by graft chain length which is subject to monomer concentration.

2.4. Conclusion

The author demonstrated that γ-ray-induced graft polymerization is a simple but effective method for the modification of polysilane. For the grafting of MMA and DEF to PMPrS, grafting yield rises with increasing dose and concentrations of the monomers, but the number of grafted chains per PMPrS chain was estimated to be less than 1.0. Such low graft density was due to the steric hindrance of growing grafted chains on PMPrS. To depress the steric hindrance and increase the graft density of modified PMPrS, non-homopolymerize monomer MAH was used not to form bulky grafted chains. With an increase of dose, grafting yield of PMPrS-*g*-MAH and consequently the graft density increases as the author has expected. The highest graft density obtained in this study was one MAH unit for 4.2 silicone atoms of a PMPrS backbone.

In this way, the author revealed the structure of radiation-modified polysilane-based graft copolymers. In particular, the graft chain length and density were clarified. It was also demonstrated that grafting yield of radiation-modified polysilane can be controlled by the irradiation conditions such as dose, dose rate and concentration of monomers.

References

1. Miller, R. D.; Michl, J. *Chem. Rev.* **1989**, *89*, 1359.
2. West, R. *J. Organomet. Chem.* **1986**, *300*, 327-346.
3. West, R. Polysilanes and Related Polymers. In *Inorganic Polymers;* Mark, J. E., Allcock, H. R., West, R., Eds.; R. Prentice Hall, NJ, 1992.
4. Alexandridis, P.; Lindman, B. *Amphiphilic Block Copolymers: Self-Assembly and Application*; Elsevier, Amsterdam, 2000.
5. Riess, G.. *Prog. Polym. Sci.* **2003**, *28*, 1107.
6. Webber, S. E., Munk, P., Tuzar, Z., Eds. *Solvents and Self-Organization of Polymers;* Kluwer, The Netherlands, 1996.
7. Hodge, P.; Khoshdel, E.; Tredgold, R. H.; Vickers, A. J.; Winter, C. S. *Br. Polym. J.* **1985**, *17*, 368.
8. Hodge, P.; Davis, F.; Tredgold, R. H.; Silver, J.; Coles, H. *J. Philos. Trans. R. Soc. Lond.* **1990**, *A330*, 153.
9. Seki, S.; Tagawa, S.; Ishigure, K.; Cromack, K. R.; Trifunac, A. D. *Radiat. Phys. Chem.* **1996**, *47*, 217.
10. Kumagai, J.; Oyama, K.; Yoshida, H.; Ichikawa, T. *Radiat. Phys. Chem.* **1996**, *47*, 631.
11. Brandrup, J., Immergut, E. H., Grulke, E. A., Eds. *Polymer Handbook 4th Edition;* Wiley, New York, 1999.
12. Otsu, T.; Ymada, B.; Ishikawa, T. *Macromolecules* **1991**, *24*, 415.

Chapter 3

Synthesis of pH-Responsive Polysilane with Polyelectrolyte Side Chains through γ-ray-Induced Graft Polymerization

3.1. Introduction

In Chapter 2, the author describes the synthesis and characterization of polysilane-based graft copolymers with amphiphilic chains such as poly(methyl methacrylate) (PMMA) and poly(diethyl fumarate) (PDEF) obtained through γ-ray-induced grafting of corresponding monomers.[1] As a further development of these studies, the author focused on stimuli-responsive polysilane-based graft copolymers with polyelectrolyte side chains. Ordered materials built up with this type of polymers are expected to be responsive to external stimuli such as pH and ionic strength, which attracts both industrial and scientific interest.

In this study, poly(acrylic acid) (PAA) or poly(methacrylic acid) (PMAA) chains are grafted onto poly(methyl-*n*-propylsilane) (PMPrS) through γ-ray-induced graft polymerization. PAA-grafted PMPrS (PMPrS-*g*-PAA) was obtained by hydrolysis of poly(methyl acrylate) (PMA) graft chains of radiation-presynthesized PMA-grafted PMPrS (PMPrS-*g*-PMA), while PMAA-grafted PMPrS (PMPrS-*g*-PMAA) was directly synthesized with γ-ray-induced grafting of methacrylic acid (MAA) monomers onto PMPrS. To verify pH-responsiveness of ordered structures of these polysilane-based graft copolymers, surface pressure-area (π-A) isotherms of PMPrS-*g*-PMAA monolayers on the water subphase with different pH were examined.

3.2. Experimental Section

3.2.1. Synthesis

PMPrS was synthesized via the Wurtz-type coupling reaction of methyl-*n*-propyldichlorosilane. PMPrS was purified by re-precipitation from a toluene solution into methanol, and then pure PMPrS was obtained by freeze-drying from a benzene solution. Number average molecular weight (M_n) and polydispersity index (PDI) were determined by GPC (RI detector) with polystyrene standards and a THF eluent. M_n and PDI of PMPrS used in the following experiments are listed in Table 3.1. PMPrS1 and PMPrS2 were employed for grafting PMA and PMAA, respectively.

Table 3.1. M_n and PDI of PMPrS used in the following experiments.

	$M_n \times 10^{-4}$ [a]	PDI [b]
PMPrS1	1.1	2.9
PMPrS2	1.8	2.8

[a,b] Determined by GPC (RI detector) with polystyrene standards and a THF eluent.

PMPrS-*g*-PMA and PMPrS-*g*-PMAA were synthesized in the following manner. PMPrS and purified each monomer were dissolved in toluene to given concentrations. The toluene solution in a glass tube was degassed, and then irradiated with ^{60}Co γ-rays at room temperature.

The toluene solution of PMPrS-*g*-PMA after γ-irradiation was poured into methanol to obtain a crude product. Because the product contained PMA

homopolymer, it was purified by fractional precipitation with toluene/hexane. From the thin-layer chromatography (TLC) with toluene/methanol = 2/8 (v/v) eluent, the content of PMA homopolymer in PMPrS-*g*-PMA was confirmed to be less than 0.5 wt%.

PMPrS-*g*-PAA was prepared by hydrolysis of PMA graft chains of PMPrS-*g*-PMA. A sodium hydroxide aqueous solution containing 1.5 equivalents of hydroxide ions to an MA unit of the graft chains was added into a 1.0 wt% tetrahydrofuran (THF) solution of PMPrS-*g*-PMA. The solution was stirred at 60 ℃ for 5 h. After being cooled to room temperature, the solution was neutralized by adding hydrochloric acid and then the solvent was evaporated. NaCl salt contained in the crude product was removed by solvent extraction of the graft copolymer with THF. The yield of hydrolysis was confirmed with ^{1}H NMR spectra. As the hydrolysis proceeds, the signal intensity at 3.65 ppm derived from methyl proton of PMA decreases. Accordingly, the yield was calculated from the intensity ratio of 3.65 ppm signals of PMPrS-*g*-PMA and PMPrS-*g*-PAA.

In the case of PMPrS-*g*-PMAA, the toluene solution after γ-irradiation was poured into a large amount of toluene to precipitate PMAA homopolymer. To remove residual PMAA homopolymer, a toluene solution of the product was centrifuged repeatedly. The content of PMAA homopolymer in the final product was confirmed by TLC to be less than 2.0 wt%.

3.2.2. Spectroscopy

^{1}H NMR spectra were recorded on a JEOL EX 400 spectrometer at 25 ℃ in deuterated chloroform solutions. UV absorption spectra were recorded on a Hitachi

U-3400 spectrophotometer at room temperature. IR spectra were obtained with a PERKIN-ELMER 1800 by the KBr pellet method at room temperature.

3.2.3. Grafting Yield

Grafting yield is defined as the number of each monomer units per silicon atom of PMPrS. Grafting yield of PMPrS-*g*-PMA was determined from the integrated intensity ratio of ^{1}H NMR signals (methyl proton of PMA ($COOCH_3$, δ 3.65 ppm) to methyl proton of PMPrS ($SiCH_3$, δ 0.25 ppm)).

Grafting yield of PMPrS-*g*-PMAA was estimated from the UV absorption spectra of its THF solution. The molar absorption coefficient of PMPrS is not changed by γ-irradiation as described in the following section. Therefore, the molar absorption coefficient of PMPrS-*g*-PMAA (ε) is expressed by $\varepsilon = \varepsilon_0 / (1 + M_r f)$, where ε_0 is the molar absorption coefficient of PMPrS homopolymer, M_r the ratio of molecular weight of a MAA unit to that of a methyl-*n*-propylsilane unit, and f grafting yield. If the concentration of PMPrS homopolymer and PMPrS-*g*-PMAA solutions is the same, ε and ε_0 in the above equation are replaced by the corresponding absorption intensity A and A_0. Thereby grafting yield f is evaluated by $f = (A_0 / A - 1) / M_r$.

3.2.4. π-A Isotherm

Benzene solutions of 0.1 g/L of PMPrS-*g*-PMAA were spread at 20 °C on the subphase water, which was previously purified by deionization with a Millipore filtration system followed by distillation and then pH-adjusted by adding hydrochloric acid or sodium hydroxide aqueous solutions. The monolayers at the air/water interface were compressed at a speed of 20 cm^2/min and the π-A isotherms

were monitored with a Wilhelmy plate.

3.3. Results and Discussion

3.3.1. Synthesis of PMPrS-g-PAA

Firstly the author tried to hydrolyze PMMA chains of PMMA-grafted PMPrS (PMPrS-*g*-PMMA) described in Chapter 2,[1] but the result was less than satisfactory. Thus the author planned to presynthesize the PMPrS-based graft copolymer whose graft chains have higher reactivity in hydrolysis. PMA was selected as such graft chains because it is more susceptible to hydrolysis due to lack of α-methyl groups exerting inductive effects. Figure 3.1 shows the dependence of grafting yield of PMPrS-*g*-PMA on total absorption dose. Grafting yield increases as dose rises, which indicates that grafting yield of PMPrS-*g*-PMA can be controlled by changing dose.

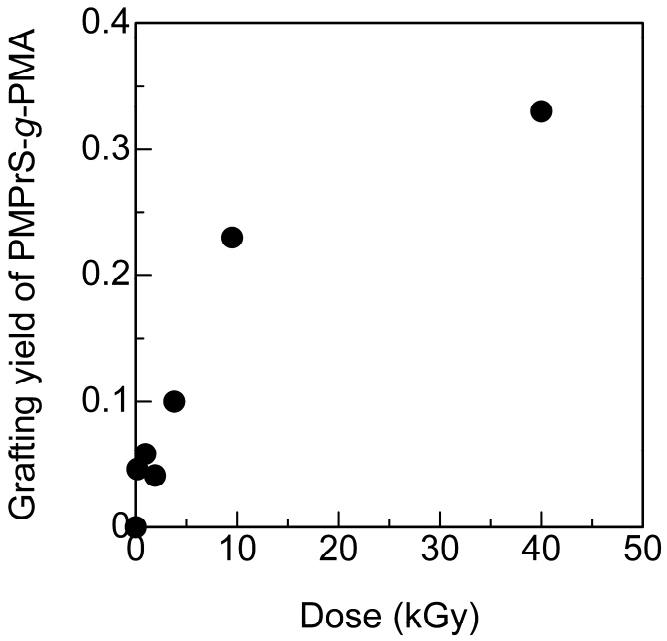

Figure 3.1. Dependence of grafting yield of PMPrS-*g*-PMA on dose. The concentrations of PMPrS and MA were 10 and 20 wt%, respectively.

A graft density of PMPrS-*g*-PMA can be estimated by referring to the author's previous study on PMPrS-*g*-PMMA.[1] PMPrS-*g*-PMMA has a low graft density, and the number of PMMA graft chains per PMPrS main chain is estimated to be less than 1.0. Such a low graft density is explained by the high propagation rate constant of methyl methacrylate (MMA). Since methyl acrylate (MA) has the higher propagation rate constant than MMA, it is supposed that PMPrS-*g*-PMA also has a low graft density and the number of PMA graft chains per PMPrS main chain is less than 1.0.

Polysilanes have generally larger *G* values for scission, *G*(s), than those for cross-linking, *G*(x), upon γ-irradiation, which indicates that polysilanes predominantly undergo chain scission by γ-rays.[2] For example, *G*(s) and *G*(x) values of poly(di-*n*-butylsilane) which has the similar structure to PMPrS are 0.42 and 0.023, respectively. Although aryl-substituted polysilanes have relatively higher *G*(x) values than alkyl-substituted polysilanes due to the protecting effect by aryl groups, still the chains of aryl-substituted polysilanes are also degraded by γ-rays.[3] The author also confirmed that PMPrS is degraded by γ-irradiation.[1] Accordingly, it was verified that PMPrS-*g*-PMA keeps the electronic property of PMPrS even after γ-irradiation. As shown in Figure 3.2, UV absorption spectra of PMPrS and PMPrS-*g*-PMA are scarcely different. The molar absorption coefficient neither changes by irradiation. This result indicates that the electronic property derived from the delocalized electrons along the silicon backbone is scarcely affected by the radiation-modification.

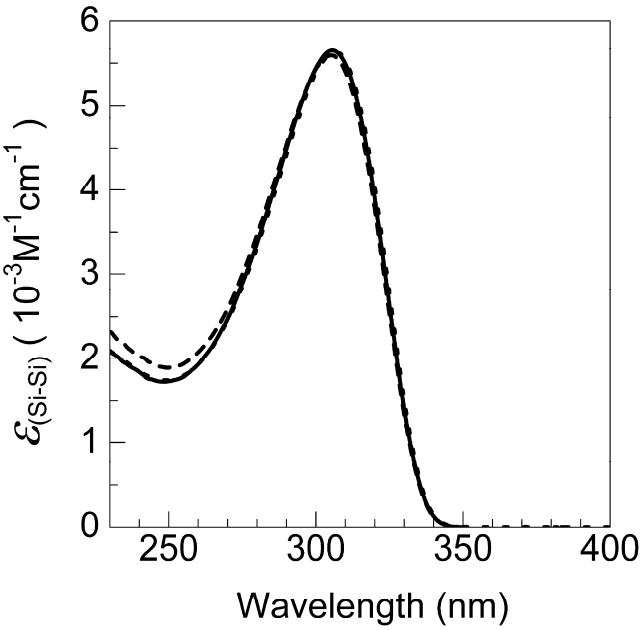

Figure 3.2. UV absorption spectra of THF solutions of PMPrS (dotted line), PMPrS-*g*-PMA (broken line) and PMPrS-*g*-PAA (solid line) with grafting yield of 0.33.

Next, PMA chains of PMPrS-*g*-PMA were hydrolyzed to PAA chains in the manner described in the experimental section. The yield of the hydrolysis was ca. 97%. Since sodium hydroxide is strong base, there is some possibility that PMPrS main chains are also hydrolyzed and its electronic property is changed. As seen in Figure 3.2, however, the spectral profile and the molar absorption coefficient of PMPrS-*g*-PAA are almost the same as those of PMPrS homopolymer, which shows that the electronic property of PMPrS main chains is not changed by hydrolysis.

Thus, PMPrS-*g*-PAA was successfully synthesized by hydrolysis of grafted PMA chains.

3.3.2. Synthesis of PMPrS-g-PMAA

The preparation method described in the previous section includes two reaction steps. As a simpler method to prepare similar polysilane, the author tried direct synthesis of polysilane with polyelectrolyte side chains.

Figure 3.3 shows IR spectra of PMPrS-*g*-PMAA irradiated with different doses. The absorption peaks at 1120, 1280, and 1700 cm^{-1} derived from carboxyl groups of PMAA chains increase with rising dose. This result demonstrates that PMAA chains are successfully grafted onto PMPrS chains through γ-ray-induced grafting of MAA monomers.

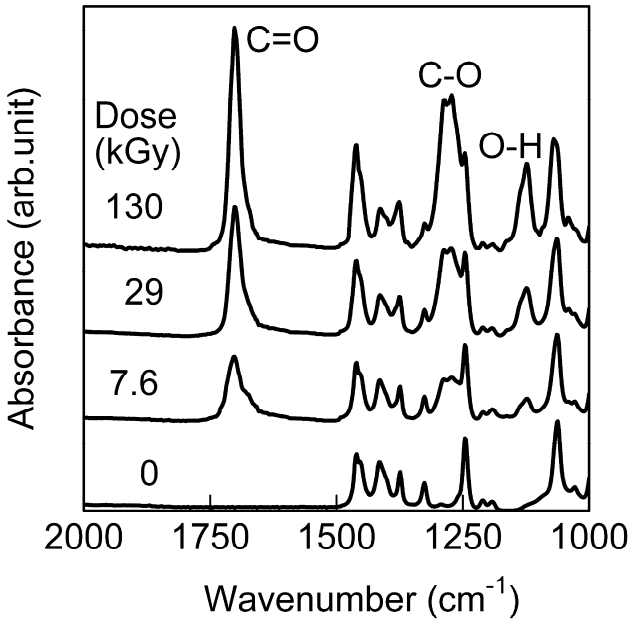

Figure 3.3. IR spectra of PMPrS-*g*-PMAA irradiated with different doses. Dose rate was 1.9 kGy/h. The concentrations of PMPrS and MAA were 10 and 20 wt%, respectively.

Figure 3.4a shows the dependence of grafting yield of PMPrS-*g*-PMAA on dose. Grafting yield increases with rising dose. This tendency is consistent with the case of PMPrS-*g*-PMMA.[1] However, grafting yield of PMPrS-*g*-PMAA is lower than that of PMPrS-*g*-PMMA at the similar doses. Because PMAA chains is almost insoluble in toluene, solutions of PMPrS-*g*-PMAA become gel-like by γ-irradiation and the fluidity of the PMPrS-*g*-PMAA solutions declines. Consequently, the efficiency of the radical reaction in the PMPrS-*g*-PMAA solutions lowers compared

to that in PMPrS-*g*-PMMA solutions, and grafting yield of PMPrS-*g*-PMAA becomes lower than that of PMPrS-*g*-PMMA.

The same phenomenon appears in the dependence of grafting yield of PMPrS-*g*-PMAA on dose rate. Grafting yield decreases with rising dose rate in Figure 3.4b. This tendency is also consistent with the case of PMPrS-*g*-PMMA, but grafting yield of PMPrS-*g*-PMAA is lower than that of PMPrS-*g*-PMMA at the similar dose rates.

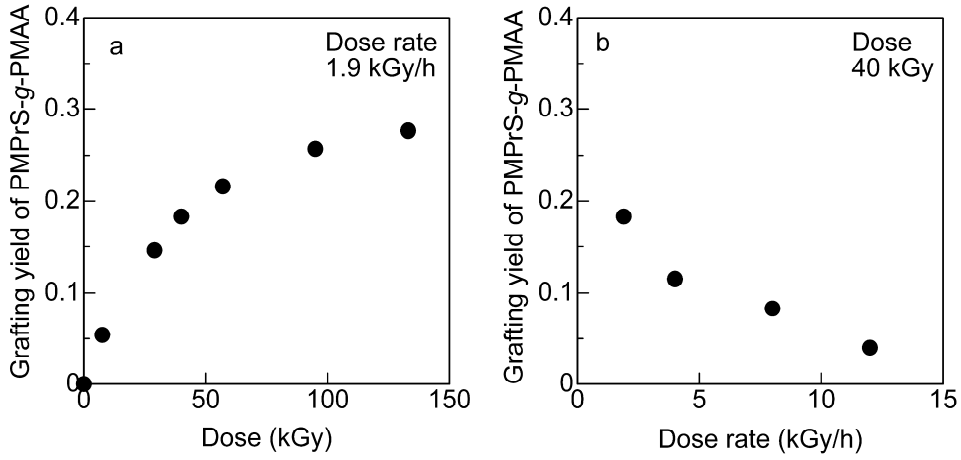

Figure 3.4. Dependence of grafting yield of PMPrS-*g*-PMAA on (a) dose and (b) dose rate. The concentrations of PMPrS and MAA were 10 and 20 wt%, respectively.

Figure 3.5 depicts the dependence of grafting yield of PMPrS-*g*-PMAA on the concentration of MAA. Grafting yield increases in the range from 0 to 20 wt%. However, the change of grafting yield is scarcely recognized in the range from 20 to 30 wt%, and finally the grafting yield decreases at 40 wt%. At higher MAA concentrations, solutions of PMPrS-*g*-PMAA become solid by γ-irradiation. Diffusion of MAA monomers to PMPrS chains is reduced in the radical reaction, which results in the decrease of grafting yield at high MAA concentrations.

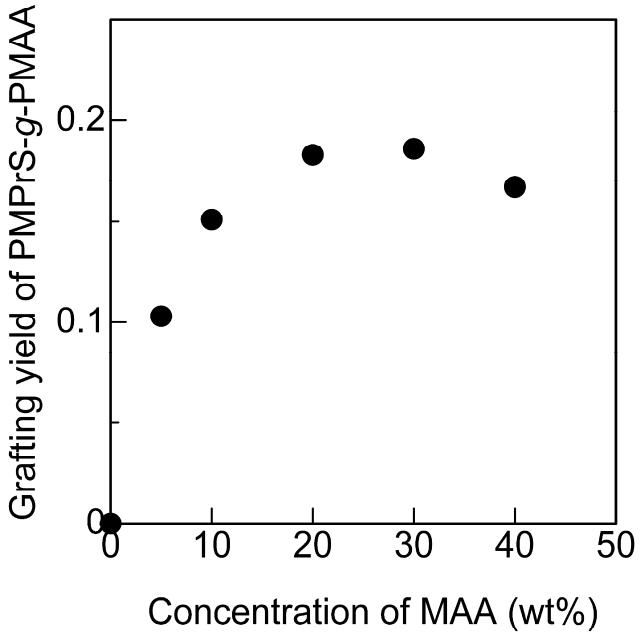

Figure 3.5. Dependence of grafting yield of PMPrS-*g*-PMAA on the concentration of MAA. The concentration of PMPrS was 10 wt%. Dose rate was 1.9 kGy/h and dose was 40 kGy.

PMPrS-*g*-PMAA indicates different solubility to water depending on its pH. PMPrS-*g*-PMAA is soluble in neutral and alkaline water, but not in acidic water. In addition, PMPrS-*g*-PMAA dissolved in the neutral water forms emulsion, while that in the alkaline water gives a transparent solution. This fact indicates that PMPrS-*g*-PMAA shows better solubility in higher-pH water, which corresponds to the characteristics of PMAA. The result obtained here demonstrates that PMPrS becomes responsive to ambient pH condition due to introduction of PMAA graft chains.

3.3.3. π-A Isotherms of PMPrS-g-PMAA

The interfacial behavior of PMPrS-*g*-PMAA was investigated by π-A isotherm measurements. Figure 3.6 displays π-A isotherms of PMPrS-*g*-PMAA monolayers at the air/water interface. The π-A isotherm of polysilane homopolymer exhibits a condensed profile because hydrophobic PMPrS cannot spread over the water surface. On the other hand, the π-A isotherms of PMPrS-*g*-PMAA show expanded profiles, and the limiting area of the PMPrS-*g*-PMAA monolayer increases with rising grafting yield.

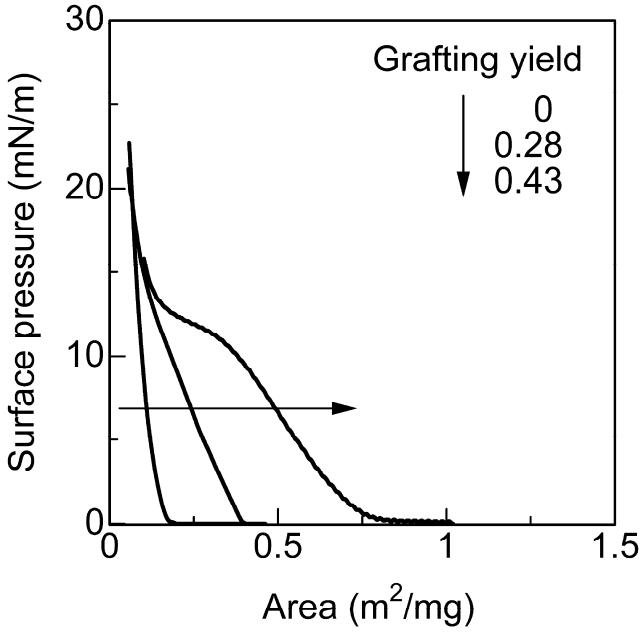

Figure 3.6. π-A isotherms of PMPrS-*g*-PMAA monolayers at the air/water interface. The pH of the water subphase is 7.

Next, the author investigated π-A isotherms of PMPrS-*g*-PMAA monolayers on the water of different pH values to verify the pH-responsiveness of PMPrS-*g*-PMAA. Figure 3.7a and 3.7b display π-A isotherms of PMPrS-*g*-PMAA with different grafting yield. In Figure 3.7a, the limiting area increases with rising pH. At pH = 7 and 12, PMAA graft chains are negatively charged because pK_a of PMAA is 5.65 and the carboxyl groups of PMAA graft chains release protons.[4] Under such conditions, PMAA graft chains repel each other on the water subphase due to the negative charge. On the other hand, PMAA graft chains are not charged at pH = 2 because the carboxyl groups are protonated. Consequently, the π-A isotherms at

pH = 7 and 12 show more expanded profiles than that at pH = 2. The number of negatively charged MAA units and the repulsive force among PMAA chains become larger at pH = 12 than at pH = 7. As a result, the limiting area increases in this order.

Figure 3.7b displays π-A isotherms of PMPrS-*g*-PMAA with higher grafting yield. The π-A isotherm at each pH shows more expanded profile than that in Figure 3.7a. However, the limiting area in Figure 3.7b decreases with rising pH contrary to that in Figure 3.7a. The water solubility of the graft copolymer is responsible for this result. PMPrS-*g*-PMAA with higher grafting yield is more soluble in neutral and alkaline water than that with lower grafting yield. The solubility of PMPrS-*g*-PMAA to alkaline water is higher than that to neutral one. As the monolayers are compressed to a smaller surface area, some of the polymer lying on the water surface dissolve into the water. Accordingly, the limiting area at pH = 12 becomes smaller than that at pH = 7. In contrast, PMPrS-*g*-PMAA does not dissolve in acidic water. As a result, the π-A isotherm at pH = 2 exhibits more expanded profile than those at pH = 7 and 12.

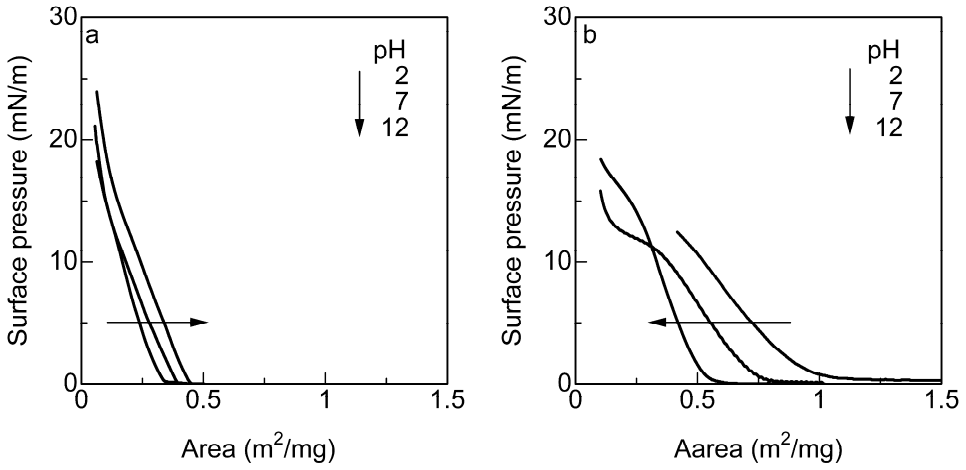

Figure 3.7. π-A isotherms of PMPrS-*g*-PMAA with grafting yield of (a) 0.28 and (b) 0.43 on the water of different pH values.

3.4. Conclusion

Polysilanes with polyelectrolyte graft chains were successfully obtained by two different methods: one is the hydrolysis of graft chains of a polysilane-based graft copolymer presynthesized through γ-ray-induced grafting, and the other is the direct grafting of electrolyte monomers onto polysilane chains by γ-irradiation. In the first method, the hydrolysis yield of graft-chain ester units of PMPrS-*g*-PMA was found to be ca. 97%, which proves that this method is useful for obtaining polysilane with polyelectrolyte graft chains, PMPrS-*g*-PAA. In the second method, PMPrS-*g*-PMAA was directly synthesized through γ-ray-induced grafting of MAA monomers onto PMPrS chains. It was thus shown that γ-ray-induced grafting is useful to give polysilane with polyelectrolyte graft chains.

By utilizing PMPrS-*g*-PMAA obtained by the second method, it was observed that

polysilane with polyelectrolyte graft chains shows pH responsive behaviors. As an instant result of this, the solubility in water becomes dependent on its pH. PMPrS-*g*-PMAA is soluble in neutral and alkaline water, but not in acidic water. Interfacial behavior is also pH-dependent. Limiting areas of PMPrS-*g*-PMAA monolayers with lower grafting yield increase with rising pH due to the repulsive force among negatively charged PMAA chains. On the other hand, limiting areas of PMPrS-*g*-PMAA monolayers with higher grafting yield decrease with rising pH due to the water solubility of the graft copolymer. These results demonstrate that the fabrication of ordered materials responsive to external stimuli is feasible by utilization of radiation-modified polysilane with polyelectrolyte side chains.

References

1. Tanaka, H.; Iwasaki, I.; Kunai, Y.; Sato, N.; Matsuyama, T. *Radiat. Phys. Chem.* **2011**, *80*, 884.
2. Miller, R. D.; Michl, J. *Chem. Rev.* **1989**, *89*, 1359.
3. Seki, S.; Cromack, K. R.; Trifunac, A. D.; Yoshida, Y.; Tagawa, S.; Asai, K.; Ishigure, K. *J. Phys. Chem. B* **1998**, *102*, 8367.
4. Greenwald, H. L.; Luskin, L. S. In *Handbook of water-soluble gums and resins;* Davidson, R. L., Ed.; McGraw-1E11, New York, 1980.

Part II

Chapter 4

Conformational Transition of the Core Chain in Radiation-Modified Polysilane Micelles Formed in Selective Solvents

4.1. Introduction

Among the several properties of polysilane,[1-8] optical property is quite intriguing because polysilane possesses a strong absorption band in the UV region due to the σ-σ* transition of the delocalized electrons along the silicon backbone.[1,2,9] This absorption band is related to the conformation of the backbone. For example, the maximum absorption wavelength of poly(methyl-*n*-propylsilane) (PMPrS) is 305 nm for a random conformation, and 325 nm is for a more extended conformation. The latter conformation of PMPrS has been considered as an all-trans (all-anti) conformation.[10,11] However, Chunwachirasiri et al. revealed by an X-ray diffraction measurement and a pair correlation functional analysis that the conformation showing the absorption peaking at 325 nm consists of an intermediate conformation between a helical form and the all-trans one, that is, a D+T+D–T– repeated construction (D, deviant; T, transoid).[12] In this chapter, hereafter, this conformation is denoted as the quasi-all-trans conformation. As described above, information on the conformation of polysilane chains is available through optical absorption spectroscopy.

Because of such unique properties, application of polysilane to the ordered materials in the nanometer scale is a very interesting theme both scientifically and technologically.[13-15] For this purpose, utilization of self-assemblies such as micelles

and vesicles could be one of powerful methods to construct nano-ordered structures. It is well known that block or graft copolymers consisting of both hydrophobic and hydrophilic or amphiphilic chains form micelles in selective solvents.[16,17] If hydrophobic polysilane is modified to be amphiphilic by the introduction of hydrophilic or amphiphilic chains, polysilane is also expected to be applicable to ordered functional materials in the nanometer scale.[18-20]

In this study, the author prepared two amphiphilic graft copolymers as modified polysilane, poly(methyl acrylate)-grafted PMPrS (PMPrS-*g*-PMA) and poly(acrylic acid)-grafted PMPrS (PMPrS-*g*-PAA), through γ-ray-induced grafting of methyl acrylate onto PMPrS. The author describes here the micelle formation from PMPrS-*g*-PMA and PMPrS-*g*-PAA in selective solvents. In particular, conformational transition of PMPrS chains in the micelle core is closely examined by analyzing UV absorption spectra, which will demonstrate the usefulness of polysilane as an optical probe. Moreover, the overall process of micelle formation was clarified experimentally by utilizing excitation energy transfer to a coexisting fluorescent probe, perylene.

4.2. Experimental Section

4.2.1. Synthesis and Characterization of PMPrS and Radiation-Modified PMPrS

PMPrS was synthesized via the Wurtz-type coupling reaction of distilled methyl-*n*-propyldichlorosilane (Shin-Etsu Chemical, Co.).[1,2] Crude PMPrS obtained was purified by the reprecipitation from a toluene solution into methanol, and then pure PMPrS was freeze-dried from its benzene solution. The number average molecular weight determined by GPC with polystyrene standards was 11000

– 15000 (Table 4.1).

Table 4.1. Conditions of irradiation and the grafting yields of PMPrS-*g*-PMA.

M_n of PMPrS $\times 10^{-4}$ [b]	Dose (kGy)	Dose rate (kGy/h)	Grafting yield [a]
1.1	0.16	1.9	0.046
1.1	0.95	1.9	0.058
1.1	1.9	1.9	0.041
1.1	3.8	1.9	0.10
1.1	9.5	1.9	0.23
1.5	40	1.9	0.33

[a] Determined by ^{1}H NMR. [b] Number average molecular weight of PMPrS used in the graft polymerization. Determined by GPC using polystyrenes as a standard.

PMPrS-*g*-PMA was synthesized in the following manner. PMPrS and purified methyl acrylate (MA) (Nakalai Tesque, Inc.) were dissolved in toluene to concentrations of 10 and 20 wt%, respectively. The solution was degassed and then irradiated with ^{60}Co-γ-rays at room temperature. The conditions of the irradiation are shown in Table 4.1. After the irradiation, the solution was poured into methanol to precipitate the products. Because the products contained PMPrS-*g*-PMA and PMA homopolymer, PMA was removed by the fractional precipitation with toluene/hexane. From the thin-layer chromatography with toluene/methanol = 2/8 (v/v) eluent, the content of PMA homopolymer in PMPrS-*g*-PMA was confirmed to

be less than 0.5 wt%. Grafting yield, defined as the number of introduced MA units per silicon atom, was determined from the integrated intensity ratio of ^{1}H NMR signals (methyl proton of PMA (3.65 ppm) to methyl proton of PMPrS (0.25 ppm)). The results are summarized in Table 4.1. From the author's work on PMMA-grafted PMPrS, the number of grafted chains per one PMPrS chain was found to be as less than 1. In the present system, the number of grafted chains is likely to be at the same level as described in Chapter 3.

PMPrS-*g*-PAA was prepared by the hydrolysis of PMA chains of PMPrS-*g*-PMA listed in Table 4.1. A sodium hydroxide aqueous solution containing 1.5 equiv of hydroxide ions to an MA unit was added into a 1 wt% tetrahydrofuran (THF) solution of PMPrS-*g*-PMA. The solution was stirred at 60 ℃ for 5 h. After being cooled down to room temperature, the solution was neutralized by adding hydrochloric acid and then the solvent was evaporated. Because the product contained PMPrS-*g*-PAA and salt, PMPrS-*g*-PAA alone was extracted with THF. The yield of the hydrolysis was ca. 97%, which was calculated from the intensity ratio of 3.65 ppm signals of PMPrS-*g*-PMA and PMPrS-*g*-PAA in ^{1}H NMR spectra.

4.2.2. Measurements

To investigate the association behavior of these graft copolymers in selective solvents, the author used a dimethyl sulfoxide (DMSO)/THF mixture for PMPrS-*g*-PMA and a water/THF mixture for PMPrS-*g*-PAA. THF is a good solvent for the PMPrS main chain, while DMSO and water are poor solvents for PMPrS and good solvents for PMA and PAA, respectively. In the experiment were used deionized distilled water, spectral grade THF and DMSO. In a typical

procedure of sample preparation, PMPrS-*g*-PMA was first dissolved in THF, and then a proper amount of DMSO was added to give a desired composition. For PMPrS-*g*-PAA, water was added instead of DMSO. Throughout this study, the concentration of the graft copolymers was fixed at 1.5×10^{-2} g/L unless otherwise noted. A spin-coated film of PMPrS was prepared from a toluene solution onto a quartz substrate.

^{1}H NMR spectra were obtained for a deuterated chloroform solution at 25 ℃ by a JEOL EX 400 spectrometer. UV absorption and fluorescence emission spectra were recorded at room temperature using Hitachi U-3400 and F-4500 spectrophotometers, respectively. To evaluate the size of the PMPrS-*g*-PAA micelle (grafting yield = 0.33) in a solution of water/THF = 99/1 (v/v), dynamic light scattering (DLS) experiments were carried out at 25 ℃ in the range of scattering angle from 30° to 150° using ALV-5000. The size was analyzed by a simple exponential fitting method.

4.3. Results and Discussion

4.3.1. UV Absorption and Emission Spectra of the Graft Copolymers

Before investigating the association behavior of amphiphilic PMPrS-*g*-PMA and PMPrS-*g*-PAA, that of hydrophobic PMPrS homopolymer in selective solvents was checked. Its UV absorption in DMSO/THF is depicted in Figure 4.1. At a DMSO content of 0%, an absorption band appeared at 305 nm, indicating that PMPrS completely dissolved in THF adopts the random conformation. When the DMSO content was increased, the intensity of the band decreased with little change of the spectral shape and disappeared at a DMSO content of 40%. This fact shows that

PMPrS cannot be dissolved stably in DMSO/THF and gradually precipitates with an increase of DMSO content. In the experiment, powder-like white precipitates floating in the solution were actually observed at a high content of DMSO. This behavior was also seen in water/THF.

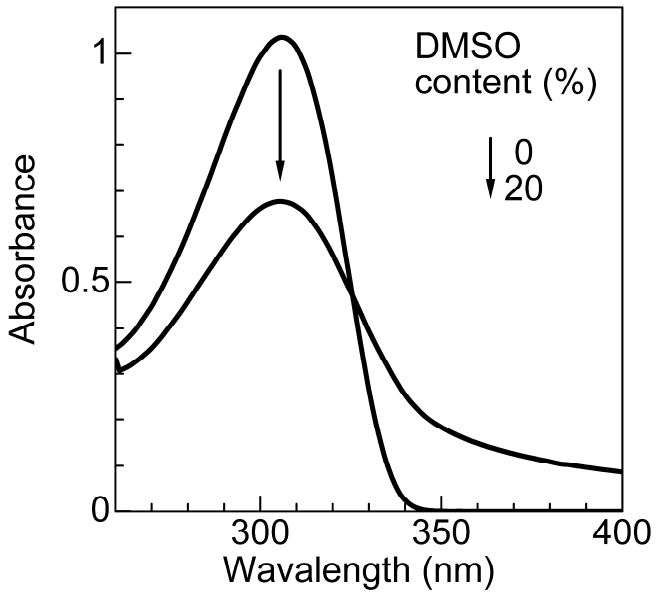

Figure 4.1. UV absorption spectra of PMPrS in DMSO/THF mixed solvents. PMPrS precipitates at DMSO contents more than 20%.

On the other hand, the graft copolymers showed different behavior in selective solvents. PMPrS-*g*-PMA with grafting yield of 0.33 in DMSO/THF appeared homogeneous, and no precipitation was recognized even at high contents of DMSO. This phenomenon indicates the formation of PMPrS-*g*-PMA micelles in this mixed

solvent. Judging from the solubility of each chain, the micelle consists of PMPrS chains in the core and PMA chains in the corona.

Figure 4.2 shows the optical absorption spectra of PMPrS-*g*-PMA in various compositions of DMSO/THF mixture. In the range of DMSO content lower than 90%, the absorption spectra showed a band peaking at 305 nm with little change in its intensity and shape. With a further increase of DMSO content, however, the band profile peaking at 305 nm was rapidly changed into that peaking at 325 nm. The absorption band at 305 nm, which is also observed for a solution or melt, corresponds to the random conformation of PMPrS chains, whereas that at 325 nm also seen for the solid-state PMPrS indicates the quasi-all-trans conformation (Figure 4.3). Here, it is convenient to define the transition point as the content of the poor solvent for PMPrS (hereafter referred to as just "poor solvent") at which the absorbance at 305 nm is equal to that at 325 nm. In this system, the transition point was evaluated to be 94.5%. The transition point stands for the poor solvent content at which the PMPrS chains undergo the conformational transition from the random conformation in the dissolved state to the quasi-all-trans conformation in the solid state. A water/THF solution of PMPrS-*g*-PAA with grafting yield of 0.33 also appeared homogeneous. Solvatochromism was also observed, and the transition point was found to be 95.0%.

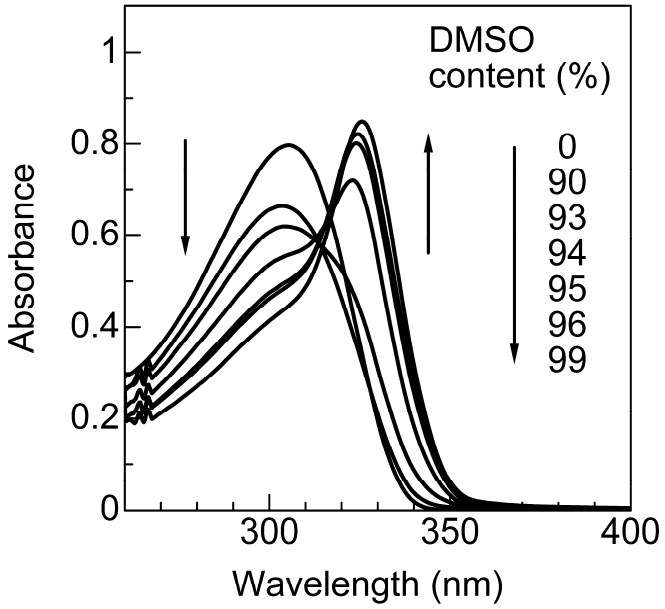

Figure 4.2. UV absorption spectra of PMPrS-*g*-PMA in DMSO/THF mixed solvents.

Fluorescence spectroscopy of both systems under excitation at 305 nm showed a spectral shift accompanying a change in the content of poor solvents, as depicted in Figure 4.4 for PMPrS-*g*-PMA in DMSO/THF. The shift is small at DMSO contents under 90%, but it is quite large in the range from 92 to 96%. In addition, the initial and final spectra are in good agreement with those of PMPrS in a solution and a solid-state spin coated film (Figure 4.3), respectively. Because these results are consistent with those obtained from the absorption measurement, the emission data in Figure 4.4 again support the conformational transition of PMPrS chains.

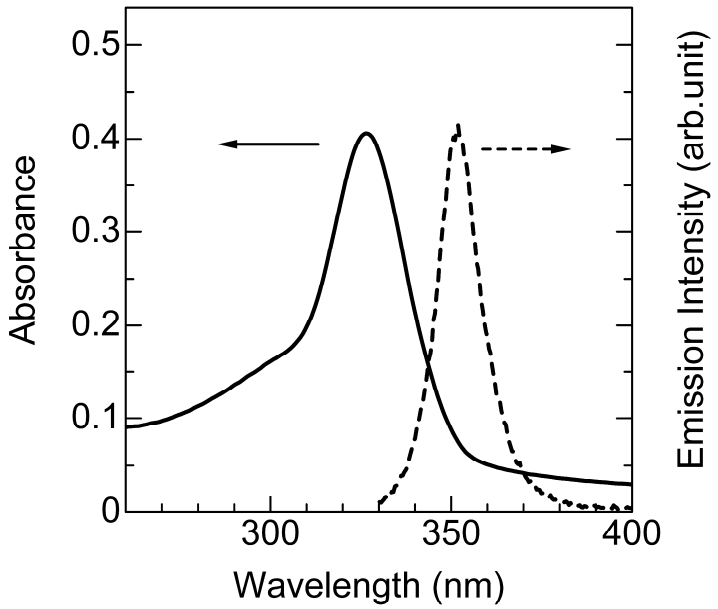

Figure 4.3. UV absorption and fluorescence emission spectra of a spin-coated film of PMPrS. Excitation wavelength is 325 nm.

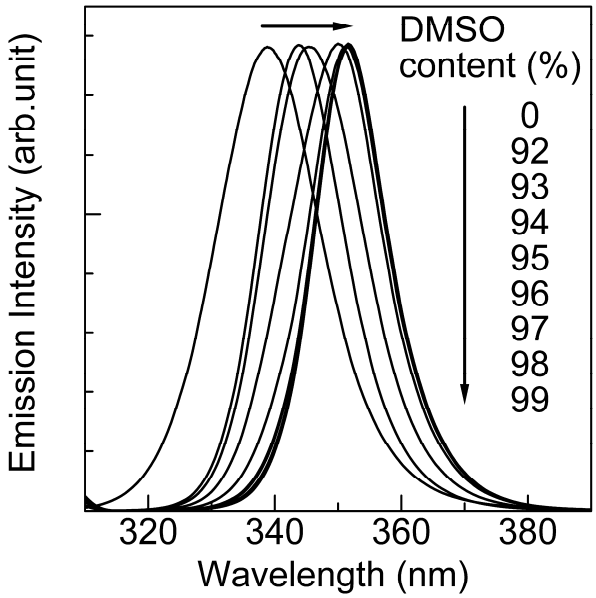

Figure 4.4. Emission spectra of PMPrS-*g*-PMA in DMSO/THF mixed solvents. Excitation wavelength is 305 nm. All spectra are normalized by their peak intensity.

4.3.2. Formation of Solid-Core Micelles and Their Size

Even though PMPrS chains are in the solid state above the transition point, the solutions were homogeneous and precipitation was not observed. This fact indicates that solid-core micelles are formed above the transition point. To make this sure, the critical micelle concentration (CMC) was examined with PMPrS-*g*-PMA with grafting yield of 0.33 in a DMSO/THF mixture at a DMSO content of 99%. In this solvent, DMSO content is beyond the transition point. Therefore, if micelles are formed, emission from the solid core with the quasi-all-trans conformation is expected to be detected at 350 nm as seen in Figure 4.4 under excitation at 305 nm. Figure 4.5 shows the emission spectra obtained as a function of the PMPrS-*g*-PMA concentration. The observed emission intensity was below the background level when the concentration was lowered to 1.5×10^{-7} g/L. This means that the CMC of the solid-core micelle exists between the copolymer concentration of 1.5×10^{-6} and 1.5×10^{-7} g/L. CMC was also evaluated by the surface tension measurement, which gave the same result. Thus, existence of CMC proved that solid-core micelles are formed.

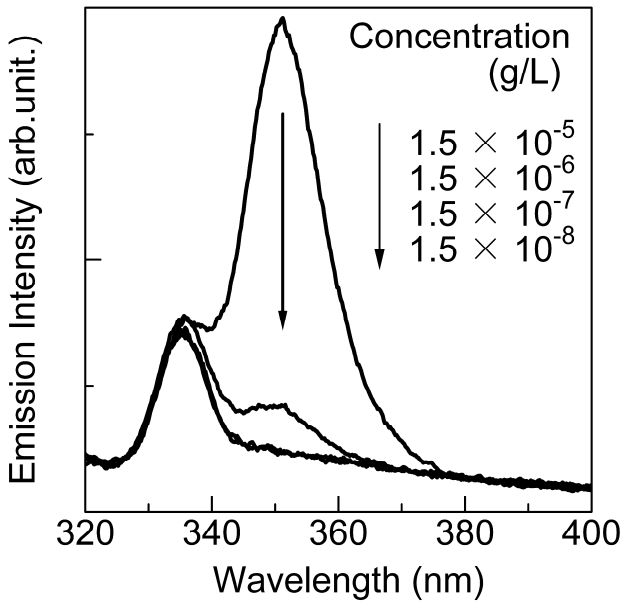

Figure 4.5. Emission spectra of PMPrS-*g*-PMA in a DMSO/THF mixture at a DMSO content of 99%. The spectra are normalized by the intensity at 335 nm. The peak at 335 nm is due to Raman scattering of DMSO.

Because the formation of solid-core micelles was demonstrated above, the author tried to estimate the size of the solid-core micelle by DLS for PMPrS-*g*-PAA with grafting yield of 0.33 in a water/THF mixture at a water content of 99%. The data shown in Figure 4.6 indicate that the decay rate depends on the scattering vector and the micelle has a sharp distribution in size. From the slope of the line in the figure, the size of the micelle was determined to be about 95.3 nm in radius.

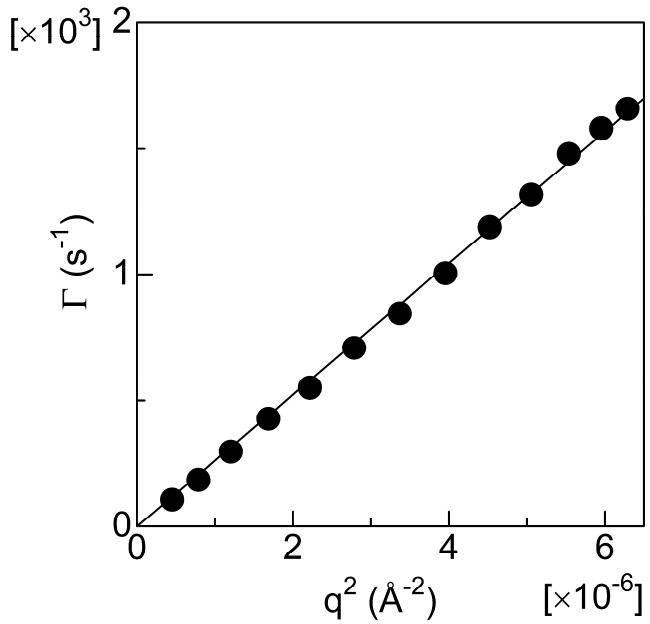

Figure 4.6. Decay rate Γ versus q^2 plot for the micelle formed from PMPrS-*g*-PAA in water/THF = 99/1 (v/v) mixed solvent. q is the scattering vector.

4.3.3. Grafting Yield Dependence of the Transition Point

In the preceding sections, the formation of solid-core micelles was revealed only for a copolymer with grafting yield of 0.33. Next, the author investigated the grafting yield dependence of the transition point using the other graft copolymers listed in Table 4.1. The results are shown in Figure 4.7. It is seen from the figure that the transition points are constant at ca. 95% for all of the systems independent of the grafting yield. They are also irrelevant to the sort of grafted chains and poor solvents.

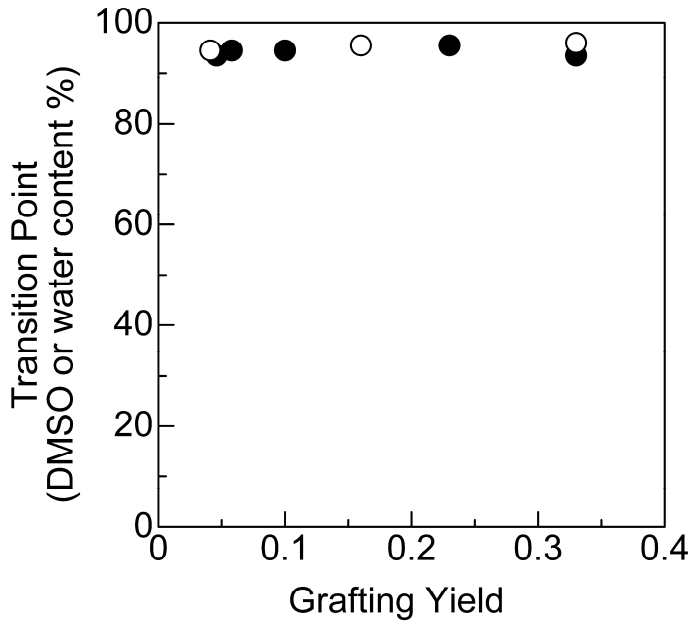

Figure 4.7. Grafting yield dependence of the transition point. ●, PMPrS-*g*-PMA in DMSO/THF mixed solvents. ○, PMPrS-*g*-PAA in water/THF mixed solvents.

Because grafted chains play an important role in stabilizing micelles in mixed solvents, the grafting yield should affect the formation of micelles. Nevertheless, the transition point did not depend on the grafting yield. To explain this discrepancy, the author considers the following scenario on the behavior of the graft copolymers in the selective solvents: at a low content of the poor solvents for hydrophobic PMPrS, amphiphilic PMPrS-*g*-PMA and PMPrS-*g*-PAA can disperse homogeneously as unimers with the random conformation of PMPrS chains. By increasing content of poor solvents, however, their homogeneous dispersion becomes harder. They then start to associate together and assemble into micelles with PMPrS chains in the core. At this stage, there are two possibilities concerning

the PMPrS core of the micelle. One is that solid-core micelles with the quasi-all-trans conformation are formed directly from separately dissolved PMPrS unimers. In this case, micelles are formed just at the transition point. The other is that micelles with PMPrS chains in the random conformation are formed at a poor solvent content lower than the transition point. In this case, the core of the micelle is swollen with the good solvent, THF, because the random conformation means that PMPrS chains are dissolved. Independence of the transition point on the grafting yield makes the latter case more plausible.

4.3.4. Presence of Swollen-Core Micelles before Formation of Solid-Core Micelles

As discussed in the previous section, the author assumes the formation of swollen-core micelles instead of direct formation of solid-core micelles from unimers in the solution. It is expected that swollen-core micelles are formed below the transition point. To verify this, the author utilized the excitation energy transfer using perylene as a fluorescent probe. The excitation energy can transfer from PMPrS chains to perylene at a certain rate depending on their separation, because the absorption spectrum of perylene overlaps the emission spectrum of PMPrS as illustrated in Figure 4.8. Even if a PMPrS/perylene mixed system is excited at 305 nm where perylene has much less absorption than PMPrS, emission from perylene can be observed as a result of the energy transfer with the intensity according to the distance between perylene molecules and PMPrS chains.

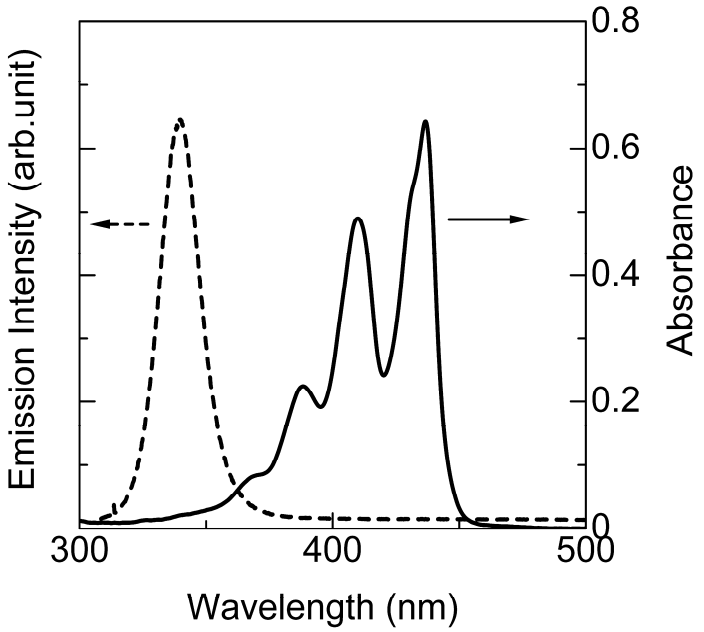

Figure 4.8. Emission spectrum of PMPrS-*g*-PAA (excitation wavelength is 305 nm) and absorption spectrum of perylene in THF (the concentration is 5.0×10^{-3} g/L).

Prior to examining the energy transfer, the author checked the emission of perylene alone in various compositions of water/THF solvents with 305 nm excitation light. Closed circles in Figure 4.9 represent emission intensity at 445 nm as a function of the water content in water/THF. It is seen that the intensity is almost constant up to the water content of ca. 70% and is hardly discernible from noise signals above that. This disappearance of emission at high contents of water is caused by the precipitation of perylene in the selective solvent because water is a poor solvent for perylene.

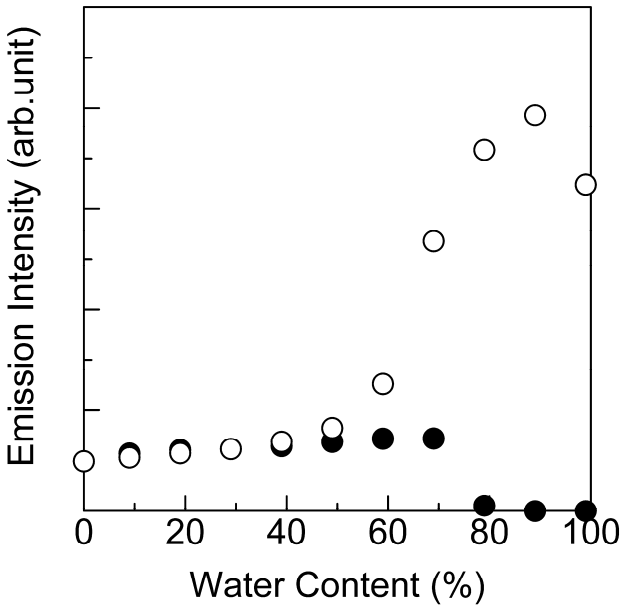

Figure 4.9. Emission intensity of perylene at 445 nm in a water/THF mixed solvent. ●: perylene; ○: perylene dissolved together with PMPrS-*g*-PAA.

When perylene was codissolved with PMPrS-*g*-PAA, in contrast, the emission intensity of perylene behaved dissimilarly as shown as open circles in Figure 4.9. It is clearly recognized that the intensity starts to increase at a water content of ca. 50%, although it is almost constant below that content. This fact indicates that the energy transfer from excited PMPrS chains to perylene molecules becomes significant and consequently the distance between PMPrS chains and perylene molecules becomes shorter at a water content of around 50%. This shortening of the distance is understood by the formation of micelles. Hydrophobic perylene molecules are hard to dissolve in a high water content solvent of water/THF. Accordingly, when the

micelles are formed with a THF-rich solvent inside, perylene molecules are preferentially incorporated within the micelles. Thus, the distance between perylene molecules and PMPrS chains becomes short and the energy transfer occurs efficiently. As discussed in the previous section, micelles formed in this composition range should be swollen-core micelles.

The formation of swollen-core micelles also explains the increasing intensity above 50% shown in Figure 4.9. As the water content increases, that is, the THF content decreases, solubility of the PMPrS chains in the micelles reduces and thus the PMPrS chains become more contracted. As a result, PMPrS chains and perylene molecules get closer to give a higher energy transfer rate. From these results, therefore, it can be safely said that swollen-core micelles are formed at poor solvent contents lower than the transition point. By a further increase of the water content, PMPrS chains finally undergo transition from the random conformation to the quasi-all-trans conformation around the poor solvent content represented by the transition point. Solidified core chains will squeeze out the incorporated perylene. The drop of the emission intensity above the transition point as seen in Figure 4.9 is interpreted by this reason.

The intensity behavior similar to Figure 4.9 was also observed for other PMPrS-*g*-PAA with different grafting yields. This fact implies that the formation of swollen-core micelles is also independent of the grafting yield. For PMPrS-*g*-PMA in DMSO/THF, on the contrary, such behavior was not found because DMSO has better solvation power for perylene than does water. However, the author believes that PMPrS-*g*-PMA also forms swollen-core micelles with the random conformation below the transition point.

The author tried to obtain information on the size of swollen-core micelles by DLS at several points lower than 90% of the water content. However, clear information was not available due to poor reproducibility of DLS signals. The indefinite and unstable structure of the swollen-core micelles may be responsible for this poor reproducibility.

4.3.5. The Process of Micelle Formation

The process of micelle formation is summarized as follows: at a low content of the poor solvents, the graft copolymers dissolved homogeneously as unimers. With increasing content of poor solvents, they avoid the unfavorable interaction between PMPrS chains and the poor solvent molecules to self-assemble into swollen-core micelles containing THF-rich solvents inside. The absorption spectra at this stage indicate the random conformation of polysilane chains because polysilane chains are solvated by THF within the micelles. With further increasing content of the poor solvents, polysilane chains can no longer adopt the random conformation and undergo transition to the quasi-all-trans conformation. At this stage, the micelles with the core consisting of solid-state polysilane chains are formed, as the unfavorable interaction between polymer chains and poor solvent molecules is replaced by the interaction among the polymer chains.[21,22]

4.4. Conclusion

The association behavior of polysilane-based graft copolymers in selective solvents was clarified by spectroscopic measurements. Fluorescence spectroscopy utilizing excitation energy transfer to codissolved perylene demonstrated that

micelles are formed in the mixed solvent above a certain content of the poor solvents for polysilane main chains. Furthermore, detailed examination of the absorption spectra of these systems elucidated the conformational transition of micelle-core polysilane chains. Utilization of a unique property of polysilanes, that is, solvatochromic behavior based on the conformational transition, proved to be an effective means of revealing the inner structure of micelles. Unfortunately, a noticeable difference due to variation in grafting yields was not found in this study. However, large variation of the grafting yield and proper selection of solvent systems can enable the fine control of the three distinct stages of these graft copolymer systems: unimer, swollen-core micelle, and solid-core micelle.

The present polysilane-based graft copolymers were prepared simply by a radiation-chemical method. Combined with unique properties of polysilane, the micelles are expected to be applicable to functional materials in the nanometer scale. In the present system, solvation power of the solvents works as an external stimulus and the response to it is detectable as the chromic change in the UV region. If it is possible to design artificially polysilane-based graft copolymers whose conformation is changeable by various stimuli, those micelles would be applicable to new optical sensors.

References

1. West, R. *J. Organomet. Chem.* **1986**, *300*, 327.
2. Miller, R. D.; Michl, J. *Chem. Rev.* **1989**, *89*, 1359.
3. Fujino, M. *Chem. Phys. Lett.* **1987**, *136*, 451.
4. Kepler, R. G.; Zeigler, J. M.; Harrah, L. A.; Kurtz, S. R. *Phys. Rev.* **1987**, *B35*, 2818.
5. Stolka, M.; Yuh, H. J.; McGrane, K.; Pai, D. M. *J. Polym. Sci., Polym. Chem.* **1987**, *25*, 823.
6. Abkowitz, M. A.; Knier, F. E.; Yuh, H. J.; Weagley, R. J.; Stolka, M. *Solid State Commun.* **1987**, *62*, 547.
7. Yuan, C. H.; Hoshino, S.; Toyoda, S.; Suzuki, H.; Fujiki, M.; Matsumoto, N. *Appl. Phys. Lett.* **1997**, *71*, 3326.
8. Suzuki, H.; Hoshino, S.; Furukawa, K.; Ebata, K.; Yuan, C. H.; Bleyl, I. *Polym. Adv. Technol.* **2000**, *11*, 460.
9. West, R. Polysilanes and Related Polymers. In *Inorganic Polymers;* Mark, J. E., Allcock, H. R., West, R., Eds.; R. Prentice Hall, NJ, 1992.
10. Jambe, B.; Jonas, A.; Devaux, J. *J. Polym. Sci., Polym. Phys.* **1997**, *35,* 1533.
11. Furukawa, S. *J. Organomet. Chem.* **2000**, *611*, 36.
12. Chunwachirasiri, W.; Kanaglekar, I.; Winokur, M. J.; Koe, J. C.; West, R. *Macromolecules* **2001**, *34*, 6719.
13. Nagano, S.; Seki, T.; Ichimura, K. *Langmuir* **2001**, *17*, 2199.
14. Nagano, S.; Seki, T. *J. Am. Chem. Soc.* **2002**, *124*, 2074.
15. Fujiki, M.; Koe, J. R.; Terao, K.; Sato, T.; Teramoto, A.; Watanabe, J. *Polym. J.* **2003**, *35*, 297.

16. Webber, S. E., Munk, P., Tuzar, Z., Eds. *Solvents and Self-Organization of Polymers;* Kluwer, The Netherlands, 1996.
17. Riess, G. *Prog. Polym. Sci.* **2003**, *28*, 1107.
18. Alexandridis, P.; Lindman, B. *Amphiphilic Block Copolymers: Self-Assembly and Application*; Elsevier, Amsterdam, 2000.
19. Sanji, T.; Kitayama, F.; Sakurai, H. *Macromolecules* **1999**, *32*, 5718.
20. Sanji, T.; Nakatsuka, Y.; Ohnishi, S.; Sakurai, H. *Macromolecules* **2000**, *33*, 8524.
21. Quintana, J. R.; Villacampa, M.; Katime, I. A. *Macromolecules* **1993**, *26*, 601.
22. Villacampa, M.; Apodaca, E. D.; Quintana, J. R.; Katime I. *Macromolecules* **1995**, *28*, 4144.

Chapter 5

Core Phase Transition of Radiation-Modified Polysilane Micelles As Revealed from Their Thermochromism

5.1. Introduction

The micelle formation of graft and block copolymers in selective solvents is an interesting topic on polymer self-assemblies.[1,2] Although various micellar systems have been investigated, their detailed structure still remains to be clarified since micelles composed of at least two component chains are complex to examine discretely.

In Chapter 4, the author describes solvatochromism of the micelles of poly(methyl acrylate)-grafted poly(methyl-*n*-propylsilane) (PMPrS-*g*-PMA) and poly(acrylic acid)-grafted PMPrS (PMPrS-*g*-PAA) synthesized through γ-ray-induced graft polymerization.[3] Polysilane is well-known for its chromic behavior[4-15] caused by the main-chain conformational change as well as for its unique electronic and photonic properties.[16,17] By taking advantage of the chromic changes of PMPrS, the author disclosed the inner structure of the PMPrS-*g*-PAA micelles in water/tetrahydrofuran (THF) mixed solvents.

In this chapter, the author reports core phase transition of PMPrS-*g*-PAA micelles in water/THF solvents as revealed from their thermochromism. The conformational transition of PMPrS core chains induced by a temperature change was closely examined by UV spectroscopy. In addition, light scattering measurements and a fluorescent method were also employed for clarifying the

physical state of the micelles in the solution.

5.2. Experimental Section

5.2.1. Synthesis

PMPrS was synthesized via the Wurtz-type coupling reaction of distilled methyl-*n*-propyldichlorosilane (Shin-Etsu Chemical, Co.). GPC measurement showed that the number average molecular weight of PMPrS used was 15000 against polystyrene standards.

PMPrS-*g*-PMA was synthesized through γ-ray-induced graft polymerization. PMPrS was dissolved together with methyl acrylate monomer in toluene and then irradiated with γ-rays after degassing. PMPrS-*g*-PAA was prepared by the hydrolysis of PMA chains of PMPrS-*g*-PMA. The grafting yield (the number of grafted monomer units per silicon atom) was 0.33 for PMPrS-*g*-PAA determined from ^{1}H NMR signals. The details of preparation and characterization are described in Chapter 3.[3]

5.2.2. Measurements

PMPrS-*g*-PAA micelles were prepared in water/THF mixed solvents. Water and THF are poor and good solvents for PMPrS, respectively. In a typical procedure of sample preparation, PMPrS-*g*-PAA was first dissolved in THF, and then a proper amount of water was added to give a desired solvent composition. Throughout this study, concentration of PMPrS-*g*-PAA was fixed at 1.5×10^{-2} g/L. A spin-coated film of PMPrS was prepared from a toluene solution on a quartz substrate.

Optical absorption and emission spectra were measured under controlled

temperature. Temperature was measured by immersing a thermocouple in the solution or by attaching it directly to the film just before data acquisition. Static light scattering (SLS) and dynamic light scattering (DLS) measurements were carried out with ALV-5000. The detection angle in the SLS measurements was 90°. Those in the DLS measurements were 30°, 60°, 90° and 120°. The hydrodynamic size of the micelles was analyzed from DLS results by a single exponential fitting method.

5.3. Results and Discussion

5.3.1. UV Absorption Spectra of a PMPrS Film

Before investigating micelles, UV absorption spectra of a PMPrS spin-coated film were briefly examined for comparison. With increasing temperature from 20 to 50 °C, a thermochromic change was observed as seen in the literature.[18] The absorption band peaking at 320 nm diminished and that peaking at 305 nm grew correlatively, which corresponds to the transition from the quasi-all-trans conformation explained in Chapter 4 to the random conformation of PMPrS chains. Here, the author defines transition temperature as the temperature at which the absorbance at 305 nm is equal to that at 325 nm. The evaluated transition temperature of the PMPrS film, 46 °C, is in consistence with the literature value,[18] and then this thermochromic behavior indicates melting of PMPrS chains. Thus, the conformational change in association with the phase transition was demonstrated to appear as the thermochromism.

5.3.2. Temperature Effect on Solid-Core Micelles

PMPrS-*g*-PAA forms solid-core micelles in a water/THF mixed solvent with a water content of 99% (in volume, likewise hereinafter) at room temperature as reported in Chapter 4.[3] The solid-core micelle consists of PMPrS core chains and PAA corona chains, where PMPrS chains are in the solid state and adopt the quasi-all-trans conformation at room temperature.

Figure 5.1 shows UV absorption spectra of PMPrS-*g*-PAA at a water content of 99% obtained with increasing temperature. The spectral behavior observed was parallel to that of the PMPrS spin-coated film and reversible with hysteresis upon a temperature change as described in the following section. The spectral transition indicates the conformational change of PMPrS chains from quasi-all-trans to random with rising temperature. Moreover, the transition temperature, 42 °C, is close to that of the PMPrS film. It is judged from this result that the solid core consisting of PMPrS chains changes into a molten core at this temperature.

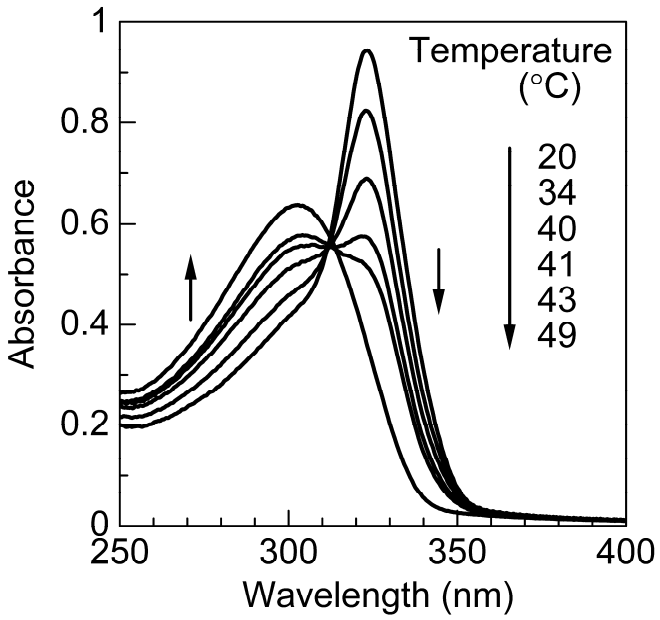

Figure 5.1. UV absorption spectra of PMPrS-*g*-PAA micelles at a water content of 99% measured with increasing temperature.

The open circles in Figure 5.2 shows the SLS results of PMPrS-*g*-PAA micelles at a water content of 99% plotted against temperature. The scattering light intensity is almost constant in the shown temperature range, indicating that the aggregation number of the polymer chains in each micelle does not vary.[19,20] This fact also indicates that the conformational transition demonstrated in Figure 5.1 is not caused by the dissolution of the micelles.

Next, the change in the micellar size was investigated by the DLS experiment with rising temperature. Also in Figure 5.2, the evaluated size is plotted by closed circles against temperature. Below the transition temperature, the micellar size becomes smaller with increasing temperature. This reduction of the size is

interpreted in terms of the shrinkage of PAA corona chains because the hydrogen bonds between carboxyl groups of PAA and water molecules become weaker with rising temperature.[19] Due to the breakage of hydrogen bonds, PAA corona chains are less solvated by water molecules and shrink with increasing temperature. Thus, the micellar size decreases as shown in the figure. Above the transition temperature, the size is almost constant. The reason for this is not fully clarified but the author considers that it is due to the competition between the shrinkage of PAA corona chains and the increase of the core volume within the micelle. Since PMPrS core chains melt above the transition temperature as demonstrated above, the core volume should increase with the phase transition of PMPrS. This increase of the core volume compensates the corona shrinkage and the apparent size appears constant above the transition temperature.

When the temperature was risen from 20 to 60 °C and then lowered to 20 °C again, the micellar size was recovered. This thermal reversibility supports the idea that micellar structure is maintained after experiencing phase transition in the micelle core.

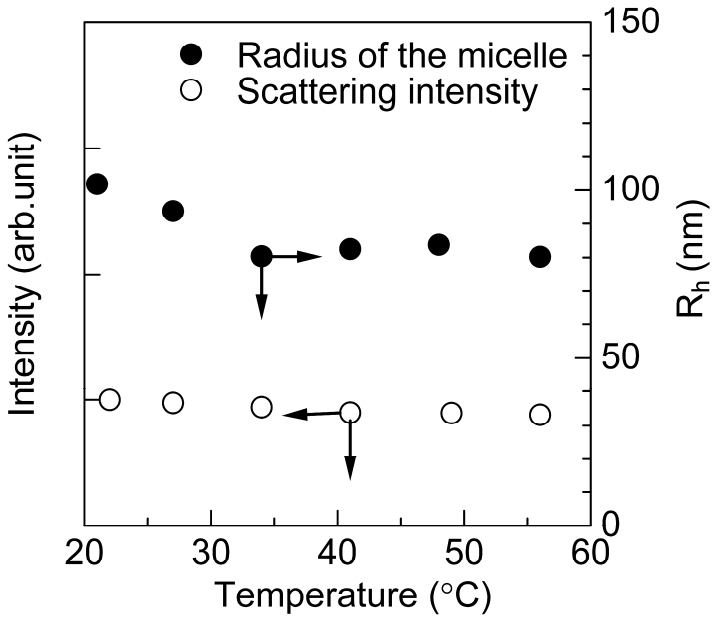

Figure 5.2. Temperature dependence of the static light-scattering intensity at 90° (○) and the hydrodynamic radius (R_h) of PMPrS-*g*-PAA micelles (●) at a water content of 99% evaluated from DLS.

5.3.3. Transition Temperature and Solvent Composition

PMPrS-*g*-PAA forms swollen-core micelles at water contents from 50 to 95% at room temperature. The swollen-core micelle contains THF within the core, which dissolves PMPrS chains. Fluorescence measurement using perylene proved that the swollen-core micelle becomes smaller with increasing water content.[3]

Thermochromic behavior at water contents of 95% and 89% is similar to that at a water content of 99%, but the transition temperature varies as shown in Figure 5.3. The transition temperature lowers with decreasing water content. This result is explained by local concentration of PMPrS chains within the core.[21] In the solid

core, PMPrS chains contact with each other and therefore the local concentration of the PMPrS chains is high. The conformational transition of PMPrS chains requires large thermal energy because of the restriction of the chain motion. In the swollen core, on the contrary, the local concentration of PMPrS chains is lower than that of the solid core because THF partially solvates the core chains. The chain motion is less hindered and the conformational transition requires smaller energy. As a result, the transition temperature falls with decreasing water content as shown in Figure 5.3.

The transition temperature in the cooling process is always lower than that in the heating process as shown by open circles in Figure 5.3. Similar hysteresis was observed also for the PMPrS film: its transition temperature was 46 °C on heating but 43.5 °C on cooling. This is a supercooling phenomenon commonly found in polymer systems and that of polysilane is also reported in several studies by DSC measurements.[12,14]

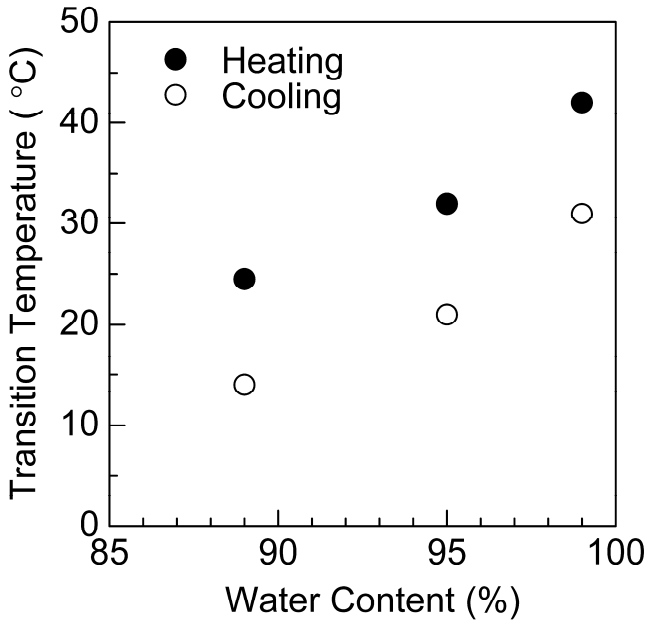

Figure 5.3. Relationship between the transition temperature and the solvent composition of PMPrS-*g*-PAA solutions. The data shown by ● and ○ are obtained in the heating and cooling process, respectively.

5.3.4. Temperature Effect on Highly Swollen Micelles

Lastly, the author briefly discusses temperature effect on the swollen-core micelles that exhibited no phase transition. Below water contents of 69%, the absorption spectra exhibited a peak around 305 nm and no spectral transition in the temperature range shown in Figure 5.3. This means that no conformational transition of the PMPrS chains occurs in this temperature range. Size information of the swollen-core micelles by the DLS measurement was also unavailable owing to the poor reproducibility of DLS data as described in Chapter 4. Accordingly, the

author estimated the micelle structure by utilizing the excitation energy transfer method in the same manner as shown in the chapter.[3]

The principle is as follow. When perylene is codissolved with the graft copolymer, hydrophobic perylene is incorporated in the micelle at low water contents. In this situation, energy transfer based on the Förster mechanism occurs from PMPrS chains to perylene molecules by selective excitation of PMPrS with 305 nm light, and thus fluorescence emission from perylene can be observed. If the core of micelles is shrinked, perylene emission should become stronger because the density of PMPrS chains increases and perylene can approach closer to PMPrS chains.

Figure 5.4 shows the emission intensity from perylene at 445 nm observed for the micellar solution at a water content of 69%. The emission intensity decreases with rising temperature. It is presumed that the Förster radius hardly changes with temperature because little change was observed for the spectral overlap between PMPrS emission and perylene absorption as well as for the emission intensity of PMPrS. Emission intensity from perylene alone in the solvent was also independent of temperature. Therefore, this decrease of the emission intensity is solely ascribable to the less efficient energy transfer due to extended distance between PMPrS chains and perylene molecules. This result indicates that the micelle core becomes more swollen because the solubility of PMPrS for THF increases with rising temperature. The graft copolymers more loosely aggregate in the micelles and get closer to the unimer state at higher temperature.

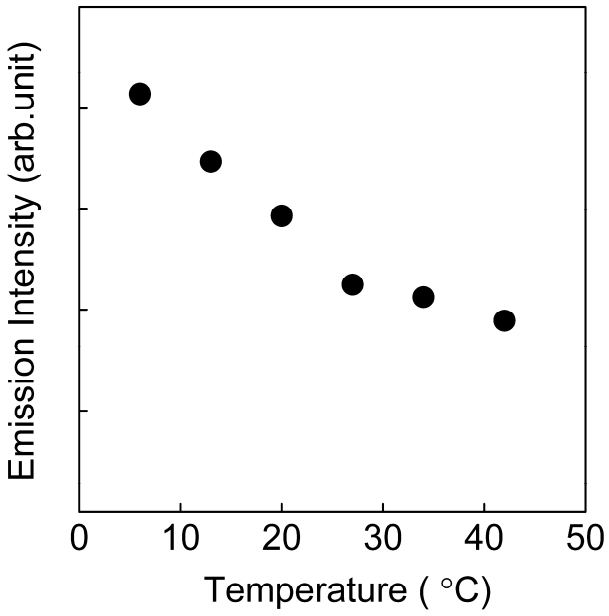

Figure 5.4. Emission intensity from perylene at 445 nm at a water content of 69%. The concentration of perylene is 5.0×10^{-3} g/L.

5.4. Conclusion

The author disclosed the core phase transition of PMPrS-*g*-PAA micelles formed in water/THF mixed solvents. The core of the solid-core micelle transitions to the molten state with increasing temperature. In Chapter 4, the author reveals that there are two types of core states, that is, swollen and solid states depending on the solvent composition. The molten state is the third state that the author found for the polysilane micelle, which is induced by a temperature rise. Through this study, the author successfully demonstrated that the physical state of inner chains within micelles can be revealed by taking advantage of the optical property unique to polysilane. In the present system, temperature works as an external stimulus and

the response appears as thermochromic behavior in UV absorption. It was proved thus that polysilane is expected to serve as a stimuli-responsive optical probe molecule.

References and Notes

1. Webber, S. E., Munk, P., Tuzar, Z., Eds. *Solvents and Self-Organization of Polymers;* Kluwer, The Netherlands, 1996.
2. Alexandridis, P.; Lindman, B. *Amphiphilic Block Copolymers: Self-Assembly and Application*; Elsevier, Amsterdam, 2000.
3. Tanaka, H.; Sato, N.; Matsuyama, T. *Langmuir* **2005**, *21*, 7696.
4. Oka, K.; Fujiue, N.; Nakanishi, S.; Takata, T.; Dohmaru, T.; Yuan, C. H.; West, R. *Chem. Lett.* 1995, 875.
5. Oka, K.; Fujiue, N.; Dohmaru, T.; Yuan, C. H.; West, R. *J. Am. Chem. Soc.* **1997**, *119*, 4074.
6. Yuan, C. H.; West, R. *J. Chem. Soc. Chem. Commun.* **1997**, 1825.
7. Toyoda, S.; Fujiki, M.; Yuan, C. H.; West, R. *Macromolecules* **2000**, *33*, 1503.
8. Fujino, M.; Hisaki, T.; Matsumoto, N. *Macromolecules* **1995**, *28*, 5017.
9. Song, K.; Kuzumany, H.; Wallraf, G. M.; Miller, R. D.; Rabolt, J. F. *Macromolecules* **1990**, *12*, 3870.
10. Harrah, L. A.; Zeigler, J. M. *J. Polym. Sci., Polym. Lett. Ed.* **1985**, *23*, 209.
11. Miller, R. D.; Hofer, D.; Robolt, J.; Fickes, G. N. *J. Am. Chem. Soc.* **1985**, *107*, 2172.
12. Rabolt, J. F.; Hofer, D.; Miller, R. D.; Fickes, G. N. *Macromolecules* **1986**, *19*, 611.
13. Sakamoto, K.; Yoshida, M.; Sakurai, H. *Macromolecules* **1990**, *23*, 4494.
14. Yuan, C. H.; West, R. *Macromolecules* **1998**, *31*, 1087.
15. Sanji, T.; Sakamoto, K.; Sakurai, H.; Ono, K. *Macromolecules* **1999**, *32*, 3788.
16. West, R. *J. Organomet. Chem.* **1986**, *300*, 327.

17. Miller, R. D.; Michl, J. *Chem. Rev.* **1989**, *89*, 1359.

18. Chunwachirasiri, W.; Kanaglekar, I.; Winokur, M. J.; Koe, J. C.; West, R. *Macromolecules* **2001**, *34*, 6719.

19. Pispas, S.; Hadjichristidis, N. *Macromolecules* **2003**, *36*, 8732.

20. The association number of the micelle was not determined from light scattering measurement, but if the micelle is approximated by the same-size solid sphere with the density of PMPrS-*g*-PAA, 1.0 g/cm^3, then the association number of the solid-core micelle is estimated as 1.4×10^5. A similar treatment is also found in the literature (Zhang, L.; Eisenberg, A. *J. Am. Chem. Soc.* **1996**, *118*, 3168.)

21. Furukawa, K.; Ebata, K.; Ichikawa, D.; Matsumoto, N. *Macromolecules* **2003**, *36*, 7681.

Part III

Chapter 6

Effect of the Graft Chain Length and Density on the Morphology of Radiation-Modified Polysilane Monolayers at the Air/Water Interface

6.1. Introduction

In Chapter 4, the author reveals that radiation-modified polysilane forms nanoscale micelles in selective solvents.[1,2] As another method to construct nano-ordered structures of polysilane, the Langmuir-Blodgett (LB) film with amphiphilic polysilane is a promising candidate.

The LB film is an ultra thin film with well-defined layer structure fabricated through layer-by-layer deposition of monolayers at the air/water interface. Amphiphilic polysilanes to form monolayers at the air/water interface have been intensely studied,[3-7] but there is no report about how the structure of amphiphilic polysilanes affects the morphology of their monolayers.

In Chapter 2, the author describes the γ-ray-induced grafting of amphiphilic monomers onto hydrophobic polysilane to obtain amphiphilic polysilanes by a simple and easy technique under moderate chemical condition. In the course of this study, the author found that amphiphilic polysilanes with different structures can be obtained by changing a type of grafted monomers.[8] While poly(diethyl fumarate)-grafted PMPrS (PMPrS-*g*-PDEF) has long but sparsely grafted chains, maleic anhydride-grafted PMPrS (PMPrS-*g*-MAH) has short (just one MAH unit) but densely grafted units. From this fact, it can be expected that the morphology of

monolayers formed by these amphiphilic polysilanes is quite different according to the difference of graft chain length and density. In order to obtain high quality polysilane LB films, it is essential to establish optimum way of radiation-modification of polysilanes.

To clarify the effect of the grafting manner of amphiphilic polysilanes on the morphology of their monolayers at the air/water interface, surface pressure-area (π-A) isotherms of the monolayers at the air/water interface and AFM images for the monolayers transferred onto solid substrates are closely examined in this study. Moreover, the deposition of LB films is demonstrated to construct the nano-ordered structure of polysilane.

6.2. Experimental Section

6.2.1. Synthesis and Characterization of PMPrS and Radiation-Modified PMPrS

The preparation and characterization of PMPrS-*g*-PDEF and PMPrS-*g*-MAH are as follows. Details of the synthetic procedure are described in Chapter 2.[8]

PMPrS was synthesized via the Wurtz-type coupling reaction with distilled methyl-*n*-propyldichlorosilane (Shin-Etsu Chemical, Co.). Number average molecular weight determined by GPC with an RI detector is shown in Table 6.1.

PMPrS-*g*-PDEF was synthesized through γ-ray-induced graft polymerization. PMPrS was dissolved together with diethyl fumarate (DEF; Nakalai Tesque, Inc.) in toluene and then irradiated with γ-rays after degassing (PMPrS 10 wt%, DEF 30 wt%, dose rate 2.0 kGy/h). PMPrS-*g*-MAH was also prepared in a similar manner (PMPrS 10 wt%, MAH 10 wt%, dose rate 2.0 kGy/h). Irradiation conditions and the number average molecular weights of the radiation-modified polysilanes are

summarized in Table 6.1. Grafting yield, which is defined as the number of DEF or MAH units per silicon atom of PMPrS, was calculated from the integrated intensity ratio of ^{1}H NMR signals. Grafting yields of PMPrS-*g*-PDEF and PMPrS-*g*-MAH are also listed in Table 6.1.

The graft density of PMPrS-*g*-PDEF was evaluated from ^{1}H NMR spectra by quantitatively analyzing signals of the unsaturated end of PDEF graft chains. As a result, the number of PDEF graft chains per PMPrS main chain was found to be less than 1.0. On the other hand, PMPrS-*g*-MAH was more densely grafted. For example, PMPrS-*g*-$MAH_{0.24}$ has one MAH unit per 4.2 silicone atoms, in other words, the number of MAH bonded to one PMPrS chain is ca. 30 units.

Table 6.1. Number average molecular weight (M_n) and grafting yield of the radiation-modified polysilanes on various doses.

	Dose (kGy)	M_n[a]	Grafting yield[b]
PMPrS		1.2×10^4	
PMPrS-*g*-$PDEF_{0.07}$	20	1.1×10^4	0.07
PMPrS-*g*-$PDEF_{0.11}$	40	9.4×10^3	0.11
PMPrS-*g*-$PDEF_{0.22}$	80	7.8×10^3	0.22
PMPrS-*g*-$PDEF_{0.34}$	124	6.7×10^3	0.34
PMPrS		1.1×10^4	
PMPrS-*g*-$MAH_{0.05}$	20	1.1×10^4	0.05
PMPrS-*g*-$MAH_{0.08}$	40	1.0×10^4	0.08
PMPrS-*g*-$MAH_{0.15}$	80	8.8×10^3	0.15
PMPrS-*g*-$MAH_{0.24}$	140	6.6×10^3	0.24

[a] Determined by GPC (RI detector) with polystyrene standards and a THF eluent.

[b] Determined by ^{1}H NMR measurement.

6.2.2. Film Preparation

A spin-coated film was prepared on a quartz substrate from a toluene solution of PMPrS homopolymer or the radiation-modified PMPrS.

Monolayers of the radiation-modified PMPrS on solid substrates were prepared in the following manner: a benzene solution of 0.1 g/L of the radiation-modified PMPrS was spread on the water surface. A monolayer at the air/water interface was

compressed up to a given surface pressure in a similar manner described in the section of π-A isotherm measurements. Then, the monolayer was transferred onto a hydrophilic quartz substrate, which was facing perpendicular to the compression direction, by the up-stroke of the vertical dipping technique at a speed of 5 mm/min. Only for AFM observation, the monolayer was transferred onto a hydrophilic silicon substrate.

LB films were fabricated by the Y-type deposition of the monolayers at the air/water interface. Hydrophilic quartz substrates facing perpendicular to the compression direction were dipped at a speed of 5 mm/min for both up- and down-strokes.

6.2.3. π-A Isotherm

A benzene solution of 0.1 g/L of PMPrS or the radiation-modified PMPrS was spread on the water surface at 20 °C. The water for subphase was purified by deionizing with a Millipore filtration system after distillation. The monolayer at the air/water interface was compressed at a speed of 20 cm^2/min and the π-A isotherm was monitored with a Wilhelmy plate.

6.2.4. AFM Observation

AFM observation was performed with a Shimadzu SPM 9500J system by the contact mode at room temperature. The spring constant of a micro-cantilever was 0.02 N/m. The transfer ratio of the monolayers used for AFM observation was 1.0 in all experiments.

6.2.5. UV Absorption Spectroscopy

UV absorption spectra of spin-coated and LB films were recorded at room temperature with a Hitachi U-3400 spectrophotometer. *In-situ* UV absorption spectra of monolayers at the air/water interface were obtained with the apparatus as shown in Figure 6.1. Light from a D_2-lamp was guided over the water surface with an optical fiber. The light passing through a monolayer was reflected by a mirror at the bottom of a trough and again passed through the monolayer. Then, the light was captured and led to a detector with another optical fiber. As the light source and the detector, a Shimazu UV-3500PC spectrophotometer was used.

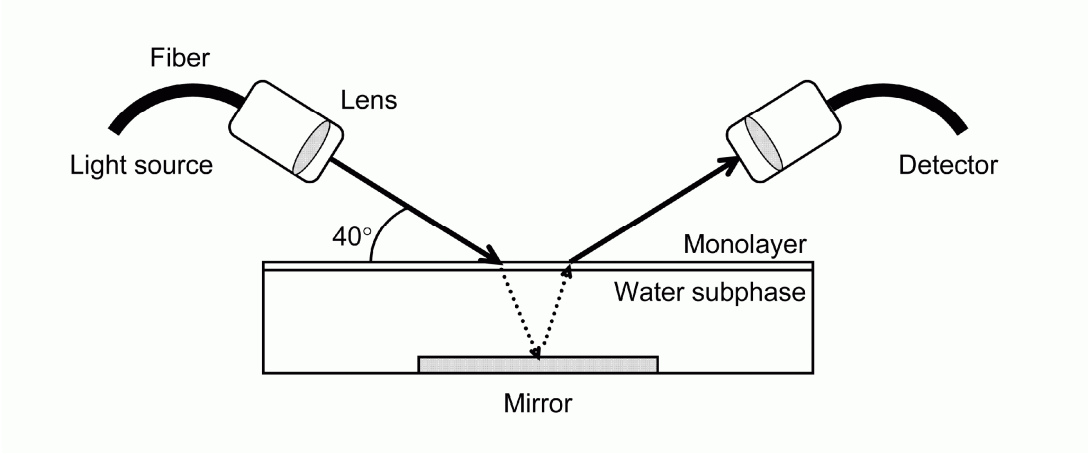

Figure 6.1. Apparatus for *in-situ* UV absorption spectroscopy of a monolayer at the air/water interface.

6.3. Results and Discussion

6.3.1. Conformation of PMPrS in PMPrS-g-PDEF Spin-Coated Films

The absorption peaks of PMPrS appearing at 305 and 325 nm correspond to random and quasi-all-trans conformations, respectively. The absorption intensity of PMPrS-*g*-$PDEF_{0.34}$ spin-coated films around 300 nm was a little larger than that of PMPrS homopolymer, which means that PDEF graft chains slightly inhibit crystallization of PMPrS main chains to increase the fraction of the random conformation of PMPrS. However, it was also confirmed that UV absorption spectra of PMPrS-*g*-PDEF do not change in the range of grafting yield listed in Table 6.1. From these facts, it is supposed that PMPrS main chains and PDEF graft chains separately form their domains in the film.

6.3.2. Monolayers and LB Films of PMPrS-g-PDEF

Figure 6.2 shows π-A isotherms of PMPrS-*g*-PDEF monolayers at the air/water interface. The isotherm of PMPrS homopolymer shows a very condensed profile because hydrophobic PMPrS cannot spread over the water surface and aggregates together. On the other hand, π-A isotherms of PMPrS-*g*-PDEF display more expanded profiles with an increase of grafting yield. The area at the lift-off point of the π-A isotherm has nearly linear relationship with the composition of DEF units. This result offers a piece of evidence that PDFE graft chains have the dominant effect on the behavior of PMPrS-*g*-PDEF monolayers at the air/water interface.

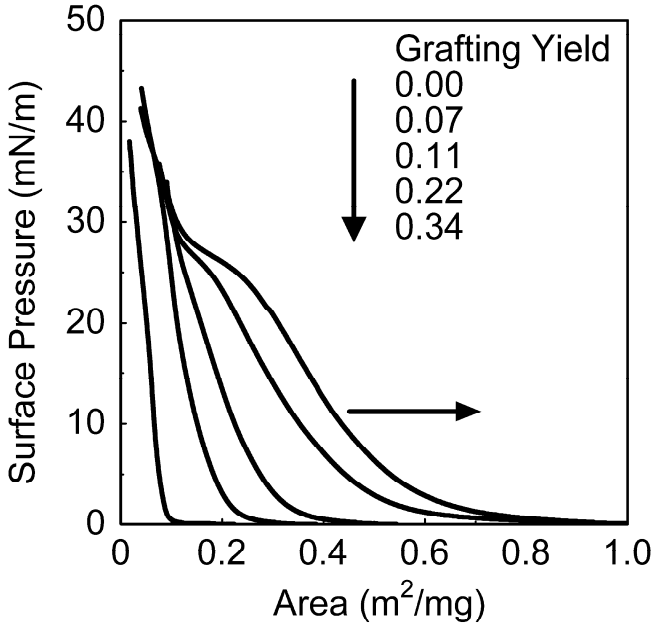

Figure 6.2. π-A isotherms of PMPrS-*g*-PDEF monolayers at the air/water interface.

The collapse pressure of PMPrS-*g*-PDEF monolayers also shows that PDEF chains have the most influence over their interfacial behavior. The collapse pressure of the monolayer of PDEF homopolymer was 28 mN/m in the author's another π-A measurement, which is consistent with those of PMPrS-*g*-$PDEF_{0.22}$ and PMPrS-*g*-$PDEF_{0.34}$ monolayers as seen in Figure 6.2.

Next, AFM observation was carried out to reveal the morphology of PMPrS-*g*-PDEF monolayers transferred onto silicon substrates below the collapse pressure. AFM images of PMPrS-*g*-$PDEF_{0.22}$ monolayers are displayed in Figure 6.3. Both images indicate inhomogeneous features containing string-like

microstructures. The density of the microstructures becomes higher with an increase of surface pressure. This morphology is formed due to the structure made of three-dimensionally contracted hydrophobic PMPrS chains escaping from the water surface and amphiphilic PDEF chains spreading over the water surface. This consideration is confirmed also by the fact that the height of the string-like microstructure evaluated from the AFM line profile (3–5 nm) is comparable with the root-mean-square diameter of PMPrS used in this experiment.

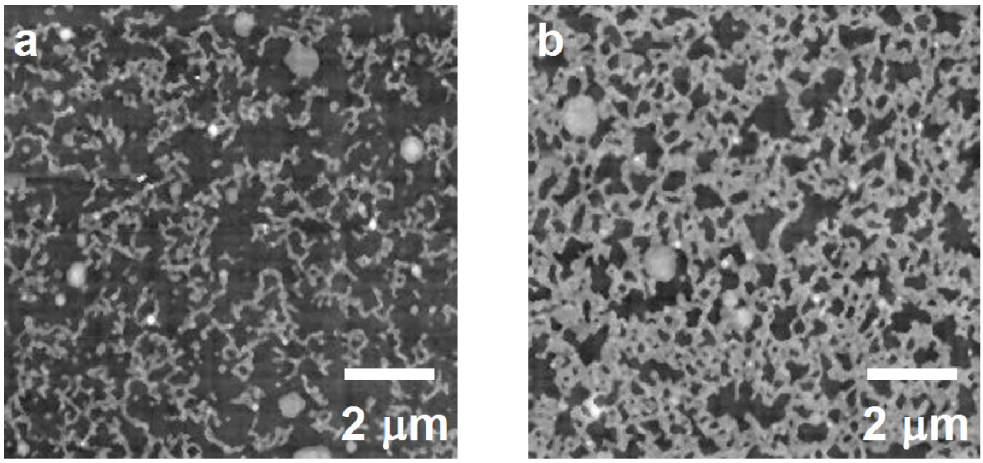

Figure 6.3. AFM images of PMPrS-*g*-PDEF$_{0.22}$ monolayers transferred at surface pressures of (a) 5 mN/m and (b) 20 mN/m.

After AFM observation, the author tried to build up LB films of PMPrS-*g*-PDEF. The first layer could be transferred onto a quartz substrate by the up-stroke with the

transfer ratio ca. 1.0, but it was peeled off by the down-stroke in the next step. PDEF homopolymer has no ability to form multilayers, and consequently PMPrS-*g*-PDEF monolayers, whose interfacial behavior is strongly affected by PDEF graft chains, are also hard to be built up for LB films.

6.3.3. Conformation of PMPrS in PMPrS-g-MAH Spin-Coated Films

The conformation of PMPrS main chains of PMPrS-*g*-MAH in the solid state was examined as in the case of PMPrS-*g*-PDEF. As shown in Figure 6.4, UV absorption spectra of PMPrS-*g*-MAH spin-coated films reveal that the fraction of the quasi-all-trans conformation indicated by the absorption peak at 325 nm decreases with an increase of grafting yield. When the ratio of the absorption intensity at 305 nm ($Abs._{305}$) to that at 325 nm ($Abs._{325}$) is plotted against grafting yield, it decreases with increasing grafting yield as shown in Figure 6.5. This fact means that crystallization of PMPrS chains is hindered by grafted MAH units and the fraction of the quasi-all-trans conformation of PMPrS main chains decreases. In the case of PMPrS-*g*-PDEF, each of PMPrS and PDEF chains forms separate domains and the ratio of random and quasi-all-trans conformations is independent of the grafting yield as described in the former section. However, the graft chains of PMPrS-*g*-MAH are too short to form such separate domains. Thus, grafting yield directly affects the conformation of PMPrS main chains and the ratio of the absorption intensity is dependent on the grafting yield.

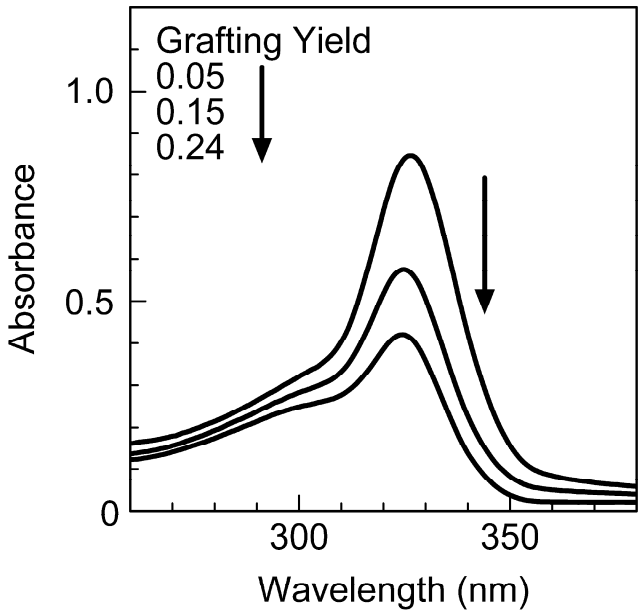

Figure 6.4. UV absorption spectra of spin-coated films of PMPrS-*g*-MAH.

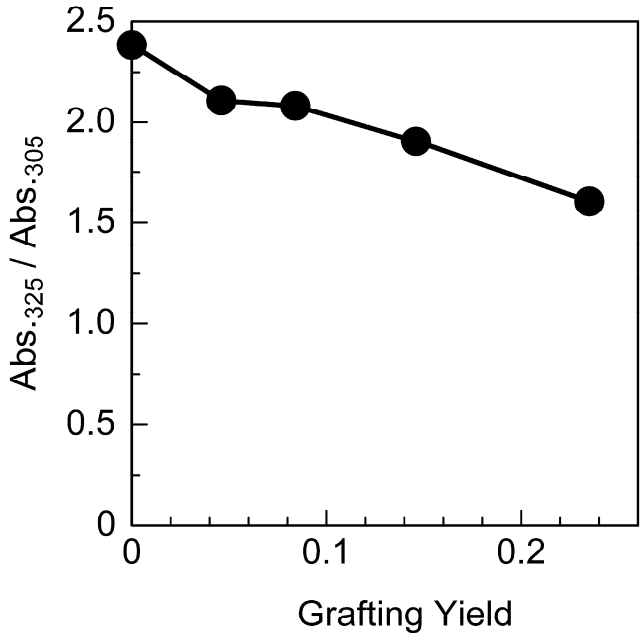

Figure 6.5. Relation between the ratio of the absorption intensity ($Abs._{325}$ / $Abs._{305}$) and grafting yield.

6.3.4. Monolayers of PMPrS-g-MAH

π-A isotherms of PMPrS-*g*-MAH monolayers are shown in Figure 6.6. Similarly to PMPrS-*g*-PDEF, PMPrS-*g*-MAH spreads more readily than PMPrS homopolymer does. However, the occupied area of PMPrS-*g*-MAH monolayers is smaller than that of PMPrS-*g*-PDEF monolayers with comparable grafting yield. The author considers that this difference is attributed to the dissimilar structure of these two monolayers at the air/water interface due to the disparity in the length and density of the grafted chains. While the long PDEF chains of PMPrS-*g*-PDEF extensively spread on the water surface, MAH graft units are short and cannot spread so extensively as PDEF chains can. Besides, ungrafted parts of PMPrS chains between MAH-grafted parts are detached from the water surface. As a result, the occupied area of PMPrS-*g*-MAH monolayers is smaller than that of PMPrS-*g*-PDEF monolayers. At high grafting yields, however, PMPrS-*g*-MAH monolayers spread extensively enough. This fact suggests that the PMPrS chains are firmly confined on the water surface by densely grafted MAH units.

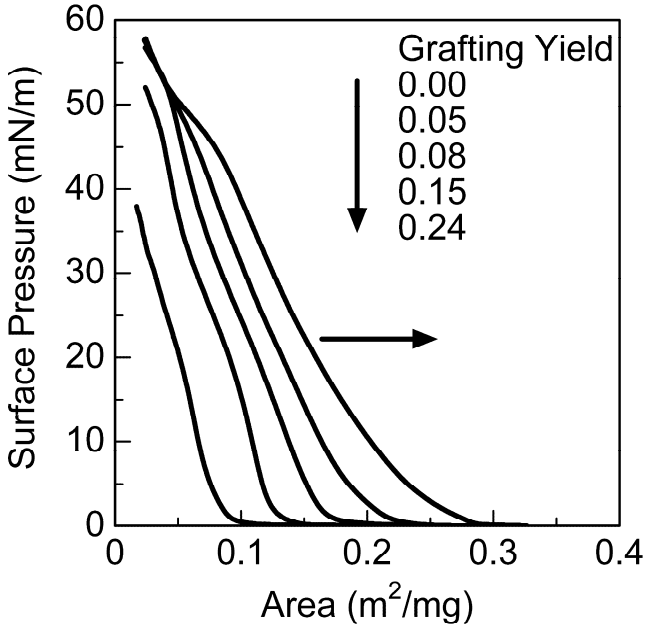

Figure 6.6. π-A isotherms of PMPrS-*g*-MAH monolayers at the air/water interface.

It is important to know the collapse pressure of monolayers at the air/water interface when the monolayers are transferred to solid substrates, but PMPrS-*g*-MAH monolayers do not show definite collapse pressure as shown in Figure 6.6. Accordingly, the author judged the collapse pressure by examining the hysteresis of π-A isotherms of a PMPrS-*g*-MAH monolayer in a compression-expansion process. The π-A isotherm of a PMPrS-*g*-$MAH_{0.24}$ monolayer on the second compression indicates the same profile as that on the first compression up to 35 mN/m. When the monolayer is compressed up to 50 mN/m, however, the π-A isotherm shows no reproducibility, which indicates collapse of the monolayer. Therefore, the author assumes that the bending points around the

surface pressure of 50 mN/m on the π-A isotherms in Figure 6.6 indicate the collapse pressure of the monolayers.

A typical AFM image of a PMPrS-*g*-$MAH_{0.24}$ monolayer transferred onto a quartz substrate below the collapse pressure is displayed in Figure 6.7. PMPrS-*g*-MAH forms a uniform monolayer in contrast to PMPrS-*g*-PDEF as shown in Figure 6.3 because hydrophobic PMPrS chains are confined in the two-dimensional interface by MAH graft units acting like anchors and fully spread on the water surface.

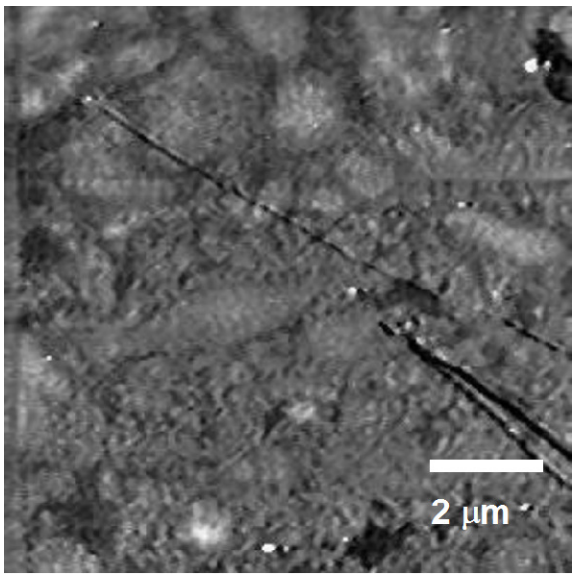

Figure 6.7. AFM image of a PMPrS-*g*-$MAH_{0.24}$ monolayer transferred at a surface pressure of 5 mN/m.

In-situ UV absorption spectra of PMPrS-*g*-MAH monolayers at the air/water interface are depicted in Figure 6.8. Both for PMPrS-*g*-$MAH_{0.15}$ and PMPrS-*g*-$MAH_{0.24}$ monolayers, the absorption intensity entirely rises with increasing surface pressure because the surface density of the monolayers is heightened by the compression. However, comparing the spectra in detail, it is found that the absorption around 305 nm of PMPrS-*g*-$MAH_{0.24}$ monolayers is larger than that of PMPrS-*g*-$MAH_{0.15}$ monolayers especially at lower surface pressures, which means the larger fraction of random conformation of PMPrS main chains in PMPrS-*g*-$MAH_{0.24}$ monolayers. In the case of PMPrS-*g*-MAH with lower grafting yield, ungrafted PMPrS chains are detached from the water surface and crystallize by aggregating together. On the other hand, for PMPrS-*g*-MAH with higher grafting yield, PMPrS chains are more firmly confined on the water surface, and therefore hardly aggregate for crystallization. Nevertheless, the fraction of the quasi-all-trans conformation of PMPrS-*g*-$MAH_{0.24}$, which corresponds to the relative absorption intensity around 325 nm, rises with increasing surface pressure in Figure 6.8. One reason for this is that the two-dimensional crystallization occurs on compression of the monolayer. PMPrS chains are prone to align perpendicular to the compression direction. As a result, the PMPrS chains are forced to take the quasi-all-trans conformation.

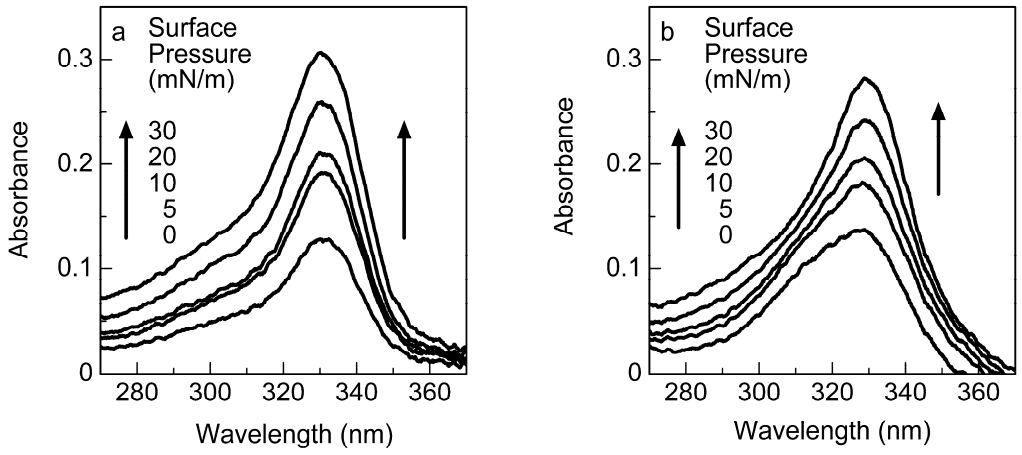

Figure 6.8. *In-situ* UV absorption spectra of (a) PMPrS-*g*-$MAH_{0.15}$ and (b) PMPrS-*g*-$MAH_{0.24}$ monolayers at the air/water interface.

Here, the thickness of the PMPrS-*g*-MAH monolayers is estimated to verify the monolayer structure. The thickness, D, is calculated by the following equation: $D = 1 / (d_{Si}\, w_{Si} + d_{MAH}\, w_{MAH})\, A$. In this equation, d_{Si} and d_{MAH} are the mass densities of PMPrS (1.14 g/cm^3) and MAH (1.48 g/cm^3) in the bulk state,[9,10] respectively, w_{Si} and w_{MAH} are the weight fractions of PMPrS graft chains and MAH graft units, respectively, and A is the occupied surface area of a PMPrS-*g*-MAH monolayer. The result of the calculation is listed in Table 6.2. The thickness decreases with an increase of grafting yield. This fact strongly suggests that the densely grafted PMPrS-*g*-MAH can spread more extensively and the PMPrS chains are firmly confined on the water surface by grafted MAH units.

Table 6.2. Thickness of the PMPrS-*g*-MAH monolayers.

Surface pressure	PMPrS-*g*-MAH$_{0.08}$	PMPrS-*g*-MAH$_{0.15}$	PMPrS-*g*-MAH$_{0.24}$
(mN/m)	*D* (nm)	*D* (nm)	*D* (nm)
5	5.6	4.5	3.6
20	7.6	6.3	5.2
35	12	9.4	7.4
40	14	11	8.5

6.3.5. LB Films of PMPrS-g-MAH

While PMPrS-*g*-PDEF monolayers did not form multilayer films, PMPrS-*g*-MAH$_{0.24}$ monolayers were successfully deposited layer-by-layer on a solid substrate by the Y-type deposition. The successful layer-by-layer deposition was confirmed by UV absorption spectra of built-up LB films, as shown in Figure 6.9. The entire absorption intensities proportionally rise with increasing number of layers. The inset of Figure 6.9 shows the nearly linear increase of absorbance at 325 nm against the number of layers.

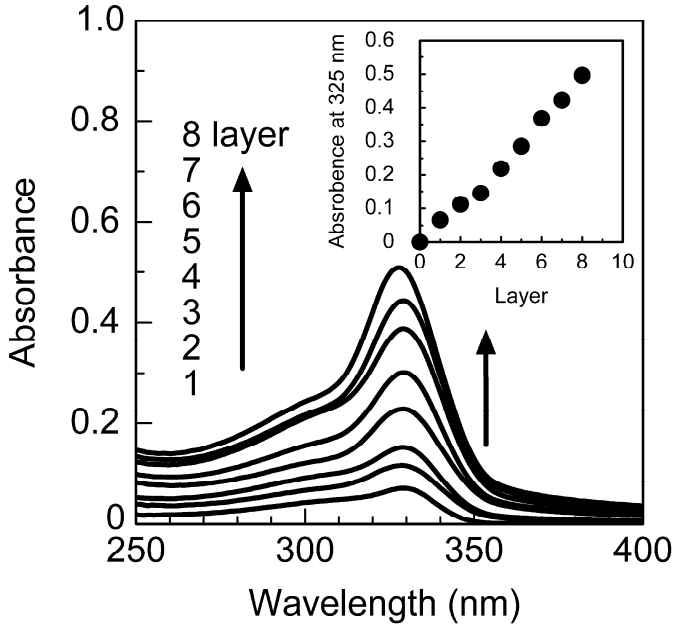

Figure 6.9. UV absorption spectra of PMPrS-*g*-$MAH_{0.24}$ LB films. The inset is a plot of absorbance at 325 nm as a function of the number of layers.

The relationship between the transfer ratio and the number of layers of a PMPrS-*g*-$MAH_{0.24}$ LB film was investigated. Up to 10 layers, the transfer ratios were 1.0 ± 0.2 for up-strokes and 0.7 ± 0.1 for down-strokes, which implies that the deposition by hydrophilic interaction of MAH is more stable than that by hydrophobic interaction of PMPrS. It can be said from the estimated thickness of Table 6.2 that the PMPrS-*g*-MAH LB film is also a nano-scale structure.

6.4. Conclusion

In this study, the author clearly demonstrated that the grafting manner of radiation-modified amphiphilic polysilanes has a significant effect on the

morphology of their monolayers. At the air/water interface, both PMPrS-*g*-PDEF and PMPrS-*g*-MAH form monolayers, but the monolayers of PMPrS-*g*-PDEF and PMPrS-*g*-MAH have quite dissimilar morphology: PMPrS-*g*-PDEF forms inhomogeneous monolayers with string-like microstructures, while the PMPrS-*g*-MAH monolayers are more uniform. It seems that higher grafting yield indicating more hydrophilic groups in the polymer leads to more uniform monolayers. However, the present study reveals that the key factor to give uniform monolayers is the density of graft chains on polymers, not the grafting yield and the length of graft chains. In most cases, graft and block copolymers composed of hydrophobic and hydrophilic chains form inhomogeneous monolayers or monolayers with regularly-structured surfaces.[11-19] Even for copolymers composed of hydrophilic chains alone, their monolayers often exhibit inhomogeneous feature due to phase separation.[20] There have been few reports on the uniform monolayers formed with amphiphilically-modified copolymers. However, the relationship between monolayer uniformity and the structure of graft copolymers clarified here offers a new principle for preparing monolayer-forming polymers.

The author's findings also provide useful information on the fabrication of high quality LB films of amphiphilic polysilanes. The interfacial property of amphiphilically grafted polysilanes inherits that of grafted chains, as seen in the layer-by-layer deposition of the LB films. Therefore, appropriate selection of grafted monomers proves to be an important factor to utilize radiation-modification for the fabrication of polysilane nano-ordered materials.

References

1. Tanaka, H.; Sato, N.; Matsuyama, T. *Langmuir* **2005**, *21*, 7696.
2. Tanaka, H.; Sato, N.; Matsuyama, T.; Inoue, R.; Kanaya, T. *Polym. J.* **2007**, *39*, 874.
3. Embs, F. W.; Wegner, G.; Neher, D.; Albouy, P.; Miller, R. D.; Willson, C. G.; Schrepp, W. *Macromolecules* **1991**, *24*, 5068.
4. Yoshida, H.; Kani, R.; Hayase, S.; Horie, K. *J. Phys. Chem.* **1993**, *97*, 5370.
5. Kani, R.; Nakano, Y.; Majima, Y.; Hayase, S.; Yuan, C. H.; West, R. *Macromolecules* **1994**, *27*, 1911.
6. Kani, R.; Yoshida, H.; Nakano, Y.; Marui, S.; Mori, Y.; Kawata, Y.; Hayase, S. *Langmuir* **1993**, *9*, 3045.
7. Seki, T.; Tanigaki, N.; Yase, K.; Kaito, A.; Tamaki, T.; Ueno, K.; Tanaka, Y. *Macromolecules* **1995**, *28*, 5609.
8. Tanaka, H.; Iwasaki, I.; Kunai, Y.; Sato, N.; Matsuyama, T. *Radiat. Phys. Chem.* **2011,** *80,* 884.
9. Brandrup, J., Immergut, E. H., Grulke, E. A., Eds. *Polymer Handbook 4th Edition;* Wiley, New York, 1999.
10. Jambe, B.; Jonas, A.; Deaux, J. *J. Polym. Sci. B. Polym. Phys.* **1997,** *35,* 1533.
11. Gabriel, N.; Njikang, L. C.; Gauthier, M. *Langmuir* **2008**, *24*, 12919.
12. Cao, B. H.; Kim, M. W.; Peiffed, D. G. *Langmuir* **1995**, *11*, 1645.
13. Webber, S. E., Munk, P., Tuzar, Z., Eds. *Solvents and Self-Organization of Polymers;* Kluwer, The Netherlands, 1996.
14. Zhu, J.; Lennox, R. B.; Eisenberg, A. *Langmuir* **1991**, *7*, 1579.
15. Li, S.; Hanley, S.; Khan, I.; Varshney, S. K.; Eisenberg, A.; Lennox, R. B.

Langmuir **1993**, *9*, 2243.

16. Seo, Y.; Im, J. H.; Lee, J. S.; Kim, J. H. *Macromolecules* **2001**, *34*, 4842.
17. Seo, Y.; Paeng, K.; Park, S. *Macromolecules* **2001**, *34*, 8735.
18. Devereaux, C. A.; Baker, S. M. *Macromolecules* **2002**, *35*, 1921.
19. Seo, Y.; Esker, A. R.; Sohn, D.; Kim, H. J.; Park, S.; Yu, H. *Langmuir* **2003**, *19*, 3313.
20. Kumaki, J.; Hashimoto, T. *J. Am. Chem. Soc.* **1998**, *120*, 423.

Chapter 7

Orientation of Radiation-Modified Polysilane in Monolayers at the Air/Water Interface As Revealed from Its Optical Property

7.1. Introduction

Application of polysilane to electronic and optical nano devices is expected due to its unique properties such as high hole drift mobility, photoconductivity and nonlinear optical effect.[1-10] Since the properties of polysilane are derived from delocalized electrons along the silicon backbone,[11-13] polysilane whose main chains are aligned in the same direction is expected to show enhanced performance in the devices.

As a method to align polymer chains, the Langmuir-Blodgett (LB) technique can be utilized. It is an effective method to prepare oriented films with nanothickness.[14] LB films and Langmuir monolayers formed by a variety of amphiphilic copolymers have been investigated, and also those formed by amphiphilic polysilane have been intensely studied.[15-21] Embs et al. first reported LB films of polysilane.[15] They demonstrated by using polysilane with bis(butoxyphenyl) groups that the orientation of rodlike polymer backbones in the LB films is parallel to the dipping direction. Hayase et al. reported the flow-induced orientation caused by a dipping procedure for LB film formation,[16-18] and Seki et al. also studied the flow- and compression-induced orientation in Langmuir monolayers.[19,20] Moreover, Tachibana et al. reported highly oriented LB films of helical polysilane, which shows high optical anisotropy due to the rigid and rod-like nature of the polymer

backbone.[21] Despite a number of research studies about LB films of amphiphilic polysilane, the relationship between the orientation and the conformation of polysilane constituting the films has not been yet disclosed.

In Chapter 6, the author revealed that poly(methyl-*n*-propylsilane) (PMPrS) can be densely grafted by maleic anhydride (MAH) units, and the graft copolymer thus obtained forms uniform monolayers at the air/water interface which can be deposited layer-by-layer on solid substrates, whereas PMPrS with low graft density forms inhomogeneous monolayers and cannot be deposited as multilayer films.[22] PMPrS main chains are anchored by densely grafted MAH units and firmly confined on the water surface, which results in MAH-grafted PMPrS (PMPrS-*g*-MAH) monolayers with a smooth surface. In this chapter, the author reports the relationship between the orientation and the conformation of polysilane main chains in both monolayers at the air/water interface and LB films of PMPrS-*g*-MAH, which is revealed by the close analysis of polarized UV absorption spectra of the monolayers and LB films.

7.2. Experimental Section

7.2.1. Synthesis

The details of preparation and characterization of PMPrS-*g*-MAH are described in Chapter 1,[23] and therefore only the principal points are noted in this chapter.

PMPrS was synthesized via the Wurtz-type coupling reaction of distilled methyl-*n*-propyldichlorosilane (Shin-Etsu Chemical, Co.). Number average molecular weight of PMPrS is shown in Table 7.1.

PMPrS-*g*-MAH was synthesized through γ-ray-induced graft polymerization. PMPrS was dissolved together with MAH (Nakalai Tesque, Inc.) in toluene (PMPrS

10 wt%, MAH 10 wt%) and then irradiated with γ-rays after degassing. Dose rate was fixed at 2.0 kGy/h, and total absorption dose was varied to give PMPrS-*g*-MAH with various grafting yield, which is defined as the number of MAH units per silicon atom of PMPrS. The number average molecular weight and grafting yield of PMPrS-*g*-MAH are summarized in Table 7.1.

Table 7.1. Number average molecular weight (M_n) and grafting yield of PMPrS-*g*-MAH.

	M_n[a]	Grafting yield[b]
PMPrS	1.1×10^4	
PMPrS-*g*-$MAH_{0.03}$	1.1×10^4	0.03
PMPrS-*g*-$MAH_{0.08}$	1.0×10^4	0.08
PMPrS-*g*-$MAH_{0.09}$	1.3×10^4	0.09
PMPrS-*g*-$MAH_{0.15}$	8.8×10^3	0.15
PMPrS-*g*-$MAH_{0.21}$	8.0×10^3	0.21
PMPrS-*g*-$MAH_{0.24}$	6.6×10^3	0.24

[a] Determined by GPC (RI detector) with polystyrene standards and a THF eluent.

[b] Calculated from the integrated intensity ratio of ^{1}H NMR signals.

7.2.2. Spin-Coated Films

Spin-coated films were prepared on quartz substrates with a hydrophilic surface from toluene solutions of PMPrS-*g*-MAH (0.01 g/L). After the spin-coating, films were dried in vacuo over 20 h. Thicknesses of the films were ca. 100 nm.

7.2.3. In-situ Polarized UV Absorption Spectroscopy

Benzene solutions of PMPrS-*g*-MAH (0.1 g/L) were spread on pure water at 20 °C. The monolayers were compressed to given surface pressures at a speed of 20 cm^2/min. *In-situ* polarized UV absorption spectra of the monolayers at the air/water interface were obtained by the following method as shown in Figure 7.1. Light from a D_2-lamp was guided just over the water surface with an optical fiber and rendered linearly polarized with a polarizer. The light passing through a monolayer was reflected by a mirror at the bottom of a trough and again passed through the monolayer. Then, the reflected light was captured and led to a detector with another optical fiber. As the light source and detector, a Shimazu UV-3500PC spectrophotometer was used. For all measurements, the incident light was *s*-polarized, and the angle of incidence was kept constant at 40°.

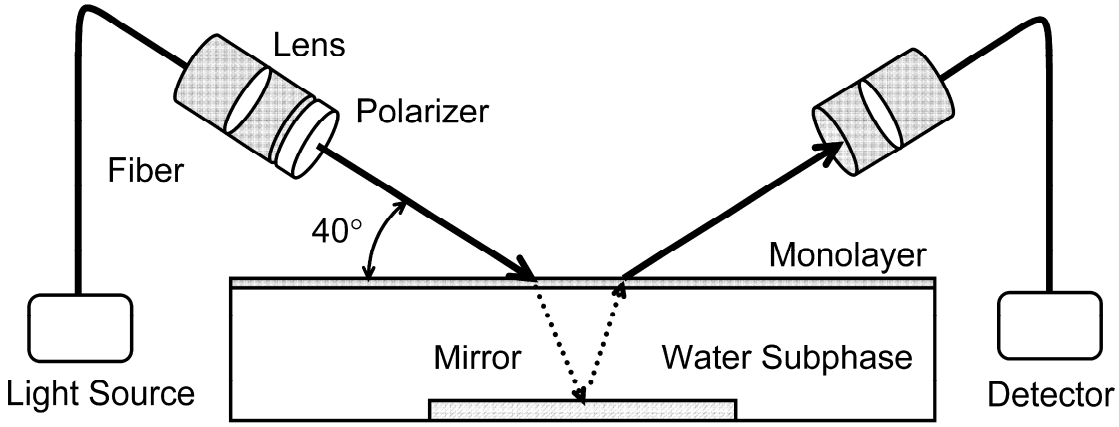

Figure 7.1. Apparatus for *in-situ* polarized UV absorption spectroscopy of a monolayer at the air/water interface.

7.2.4. UV Absorption Spectroscopy for Transferred Films

Benzene solutions of PMPrS-*g*-MAH (0.1 g/L) were spread on the water, and the monolayers were compressed by the same method as described above. The monolayers were transferred onto hydrophilic quartz substrates by a conventional vertical dipping method on the up-stroke at a dipping speed of 5 mm/min. The substrates were arranged in two different manners. One was facing perpendicular to the compression direction ($S_{\perp}$) and the other facing parallel to the compression direction ($S_{//}$) as shown in Figure 7.2. After the transferred monolayers were dried overnight in the dark, normal and polarized UV absorption spectra were measured with a Hitachi U-3400 spectrometer.

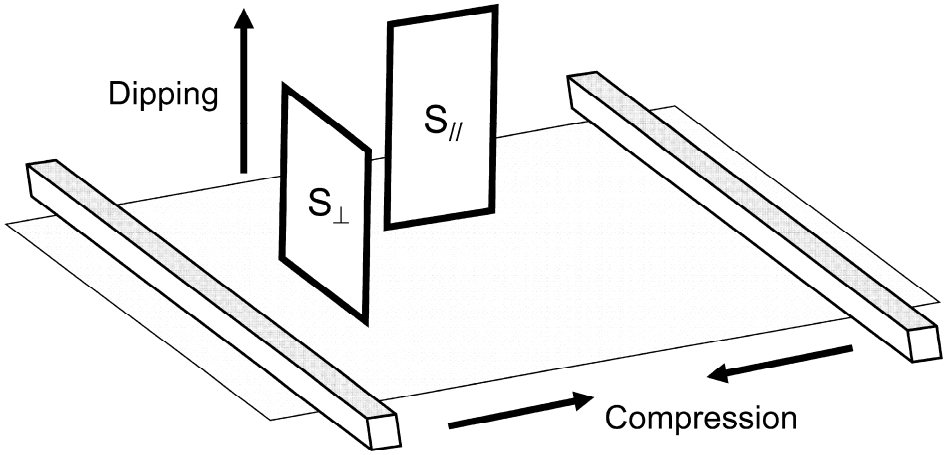

Figure 7.2. Arrangement of the substrates in reference to the compression direction during the dipping procedure.

7.3. Results and Discussion

7.3.1. Conformation of PMPrS Main Chains in Monolayers

UV absorption of polysilane is concerned with the conformation of the backbone as shown in Chapter 4. The maximum absorption wavelength of PMPrS is 305 nm for a random conformation and 325 nm for a quasi-all-trans conformation.[24] In the author's study, a spin-coated film and a transferred monolayer of PMPrS-*g*-MAH also exhibited weak absorption around 305 nm and strong absorption around 325 nm.

In Figure 7.3a, the ratio of absorbance around 325 nm to that at 305 nm, hereafter denoted by R_A, is plotted against grafting yield. Open and solid circles represent spin-coated films and monolayers transferred by the arrangement $S_\perp$ at 35 mN/m, respectively. In the spin-coated films, R_A, which expresses the population of PMPrS main chains taking the quasi-all-trans form, monotonically decreases with

increasing grafting yield. Since the decrease of R_A indicates the diminishing of the quasi-all-trans conformation, this result shows that grafted MAH units disorder the alignment of PMPrS main chains in the solid state.[22]

On the other hand, R_A of the transferred monolayers shows the inverted-V-shaped curve. The value of R_A increases as the grafting yield increases from 0.03 to 0.15, but conversely decreases above 0.15. The reason for this inverted-V-shaped behavior is explained by the competition between the conformational constraint due to the confinement of the polymer chains in two dimensions and the structural disorder evoked by the grafted MAH units. For lower grafting yields, the effect of confinement to a two-dimensional plane is predominant and responsible for the increase of R_A. PMPrS main chains at the air/water interface have contracted forms similar to the bulk state because only a few anchoring points to the water exist owing to the low graft density. However, the PMPrS main chains are gradually confined in two dimensions because PMPrS-*g*-MAH spreads more extensively on the water surface with increasing grafting yield.[22] It is well-known that the main chain conformation of polymers in two dimensions is different from that in a bulk state because the polymer chains are strongly confined in two dimensions.[25] As the confinement becomes strong, the chain conformation is gradually restricted, and consequently the ratio of the quasi-all-trans conformation increases. This is the reason why R_A increases in the range of grafting yield from 0.03 to 0.15.

Above 0.15, a disordering effect due to the grafted MAH units becomes predominant to reduce the value of R_A. Because almost all PMPrS main chains have already extended over the water surface, the effect of confinement would be unchanged. However, as seen for the spin-coated films, an increase of the grafted

MAH units disturbs the ordering of PMPrS main chains, and such disturbance is likely to work also at the air/water interface. Consequently, the highest ratio of the quasi-all-trans conformation is obtained with PMPrS-*g*-$MAH_{0.15}$ because the two-dimensional effect and the disordering effect are balanced around the grafting yield.

As shown in Figure 7.3b, R_A is also influenced by the surface pressure and R_A increases in the highly compressed region. Such piezochromic behavior demonstrates the conformational change of PMPrS main chains from random to quasi-all-trans, as reported by Yoshida et al. for an amphiphilic polysilane with alkoxyalkyl substituents.[20]

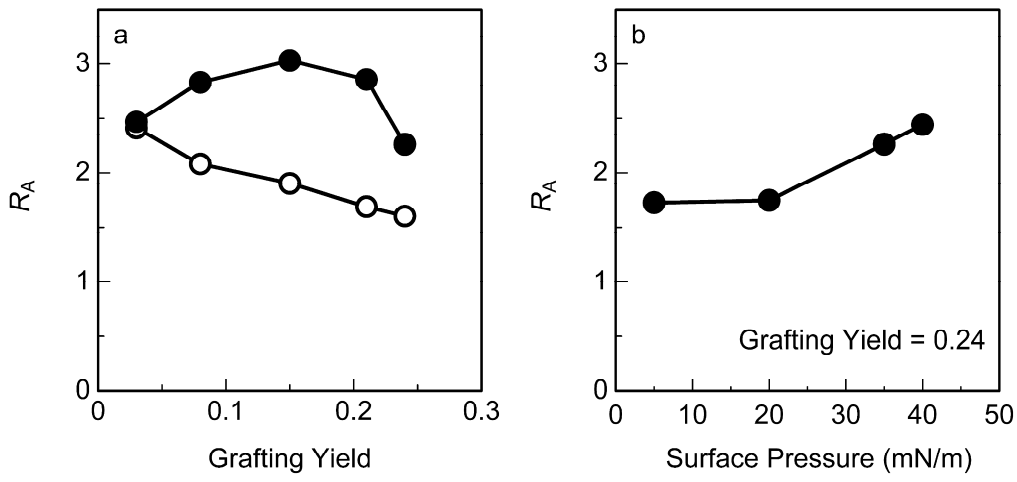

Figure 7.3. Dependence of R_A of PMPrS-*g*-MAH on (a) grafting yield and (b) surface pressure. Open and solid circles represent spin-coated films and monolayers transferred by the arrangement $S_\perp$, respectively.

7.3.2. Orientation of PMPrS Main Chains in Monolayers

Figure 7.4 displays *in-situ* polarized UV absorption spectra of PMPrS-*g*-$MAH_{0.15}$ at 0, 20 and 35 mN/m. At a surface pressure of 0 mN/m no dichroism is observed, while at higher surface pressures the absorption perpendicular to the compression direction becomes stronger than the absorption parallel to the direction. This dichroism indicates that the alignment of PMPrS main chains is perpendicular to the compression direction.

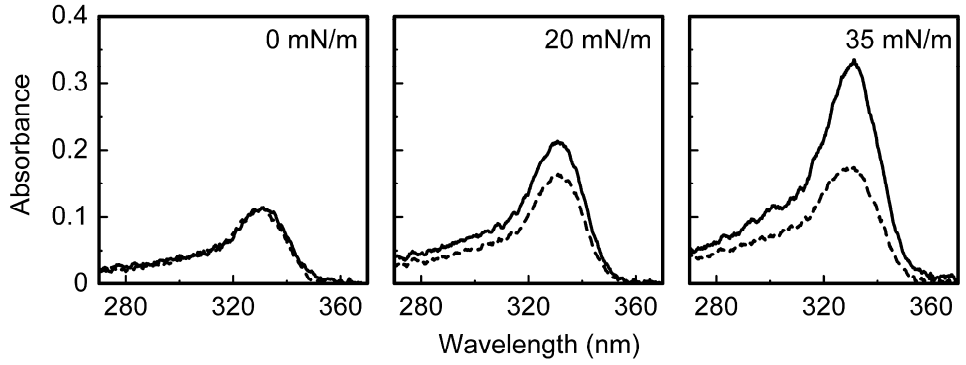

Figure 7.4. *In-situ* polarized UV absorption spectra of PMPrS-*g*-$MAH_{0.15}$ on the water surface at 0, 20 and 35 mN/m. Solid and broken lines correspond to the polarization perpendicular and parallel to the compression direction, respectively.

Polarized UV absorption spectra were also obtained for the monolayers transferred by the arrangement $S_{\perp}$. Figure 7.5 shows the spectra of PMPrS-*g*-$MAH_{0.15}$ monolayers transferred at 20 and 35 mN/m. The spectra

obtained for the transferred monolayers are almost the same as those of the monolayers at the air/water interface shown in Figure 7.4. This fact shows that the orientation of PMPrS main chains is almost maintained during the transferring process.

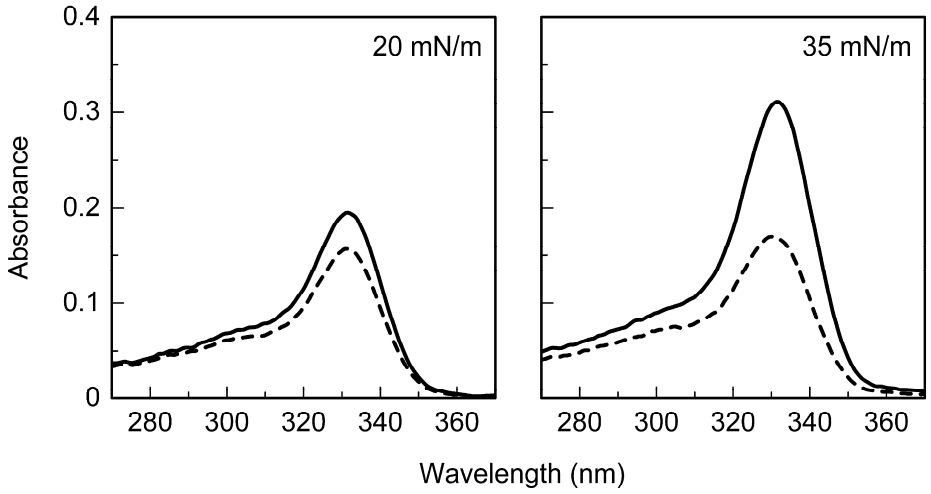

Figure 7.5. Polarized UV absorption spectra of PMPrS-*g*-$MAH_{0.15}$ monolayers transferred on solid substrates at 20 and 35 mN/m. Solid and broken lines correspond to the polarization perpendicular and parallel to the dipping direction, respectively.

Dichroic ratio (D) for the transferred monolayers is defined as $D = (A_{\perp} - A_{//}) / (A_{\perp} + A_{//})$, where $A_{\perp}$ and $A_{//}$ are the absorption intensity at 325 nm perpendicular and parallel to the dipping direction, respectively. A positive D value indicates that polysilane backbones align perpendicular to the dipping direction because the

transition moment of PMPrS aligns parallel to the backbone. Figure 7.6a shows grafting yield dependence of D of PMPrS-*g*-MAH monolayers transferred by the arrangement $S_{\perp}$ at the surface pressure of 35 mN/m. The D value increases in the range of grafting yield from 0.03 to 0.15, but conversely decreases above 0.15. This behavior is consistent with that of R_A in the transferred monolayers as shown in Figure 7.3a. Thus, it can be expected that the high D value is attained with the high ratio of the quasi-all-trans conformation to the random one. In this study, the highest D value was obtained for PMPrS-*g*-$MAH_{0.15}$.

The D value was also influenced by the surface pressure. Figure 7.6b shows the dependence of D of PMPrS-*g*-$MAH_{0.15}$ (open circles) and PMPrS-*g*-$MAH_{0.24}$ (closed circles) monolayers transferred by the arrangement $S_{\perp}$ on the surface pressure. The D value increases rapidly in the highly compressed region. This behavior is also consistent with that of R_A observed in the transferred monolayers as shown in Figure 7.3b. Thus R_A and D behave in the same way as the surface pressure increases. The negative D values at lower surface pressures are due to the flow-induced orientation to be mentioned below.

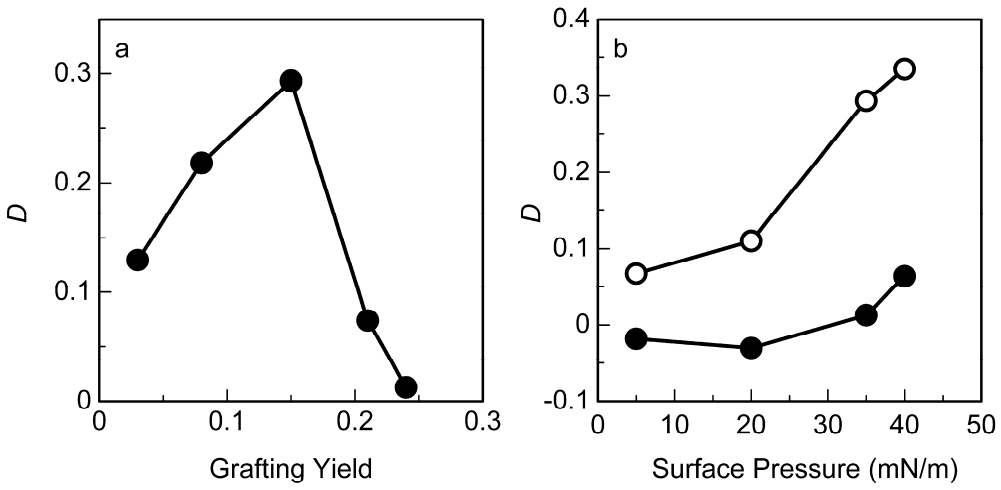

Figure 7.6. Dependence of *D* of PMPrS-*g*-MAH monolayers transferred by the arrangement $S_{\perp}$ on (a) grafting yield and (b) surface pressure. In Figure 7.6b, open and closed circles indicate *D* values of PMPrS-*g*-$MAH_{0.15}$ and PMPrS-*g*-$MAH_{0.24}$ monolayers, respectively.

Figure 7.7 shows the relation between the absolute value of *D* of PMPrS-*g*-$MAH_{0.15}$ monolayers transferred by the different arrangements and the surface pressure. The arrangement $S_{//}$ yields higher *D* values than the arrangement $S_{\perp}$ in the whole range. For some rigid rod-like polymers, it is known that in-plane orientation is brought by the flow-induced orientation during a dipping procedure. Also in the author's study, the result obtained here is caused by such a phenomenon. The cooperative effect of the compression-induced orientation and the flow-induced orientation gives rise to higher orientation as reported by Yoshida et al. for a monolayer of polysilane synthesized through masked disilene.[20]

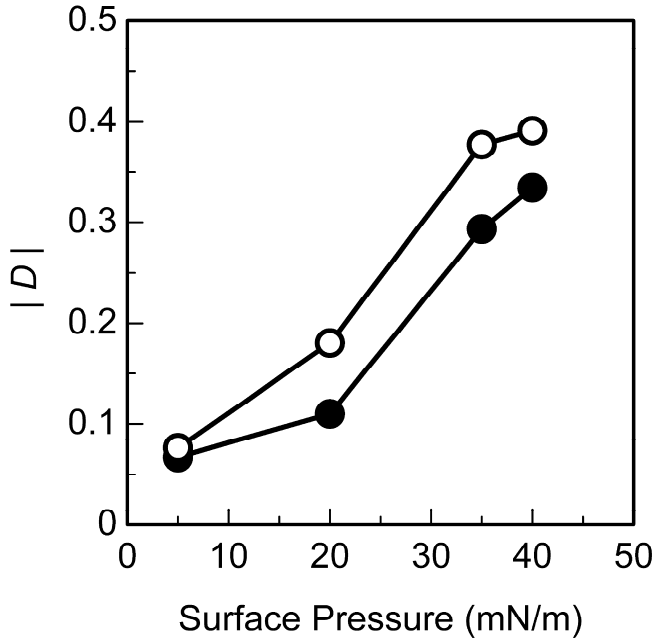

Figure 7.7. Absolute value of *D* of PMPrS-*g*-$MAH_{0.15}$ monolayers transferred by the different arrangements which is plotted against surface pressure. Open and solid circles correspond to the arrangement $S_{//}$ and $S_{\perp}$, respectively.

7.3.3. Effect of Subphase Temperature on the Orientation

The degree of orientation is dependent on subphase temperature. Solid circles in Figure 7.8 show the plot of *D* of PMPrS-*g*-$MAH_{0.09}$ monolayers transferred by the arrangement $S_{\perp}$ at 20 mN/m as a function of the subphase temperature. The *D* value increases in the range of temperature from 10 to 30 °C. However, it begins to decrease at 35 °C, and the direction of the orientation becomes completely opposite in the range 38 to 40 °C. Then, above 43 °C, no orientation is observed. The interpretation of this behavior is described below.

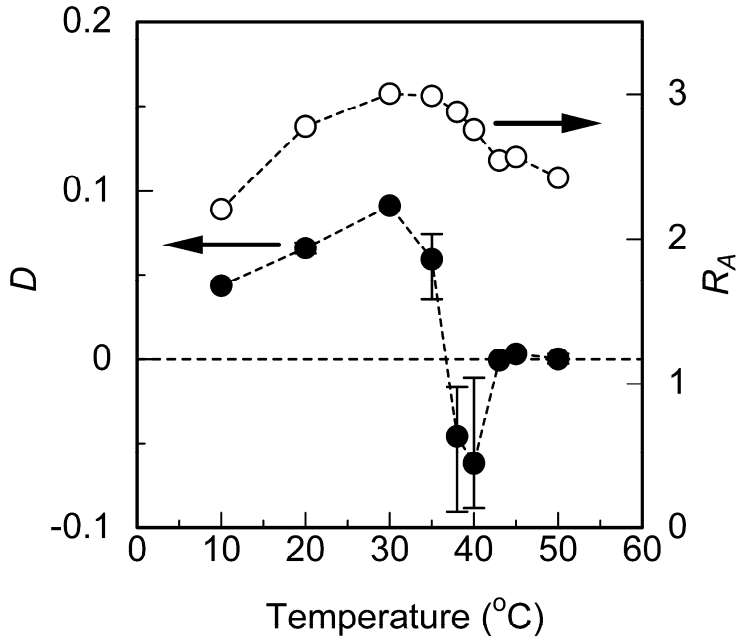

Figure 7.8. Dependence of D (solid circles) and R_A (open circles) of PMPrS-*g*-$MAH_{0.09}$ transferred monolayers on the subphase temperature.

First, the increase of the D value from 10 to 30 °C is explained by the ratio of the quasi-all-trans conformation to the random one. The value of R_A represented by open circles in Figure 7.8 becomes higher with increasing temperature from 10 to 30 °C as well as that of D. The population of the quasi-all-trans conformation increases at higher temperatures because the more facile molecular motion allows ready conformational change into the quasi-all-trans form on compression. This picture is verified from the surface pressure-area (π-A) isotherms of PMPrS-*g*-$MAH_{0.09}$ monolayers as shown in Figure 7.9, which was measured at various temperatures of the water subphase. As shown in the inset of Figure 7.9,

the surface area at 20 mN/m becomes smaller with increasing temperature from 10 to 30 °C. This result indicates that the monolayers are closely packed with an increase of the number of PMPrS main chains taking the quasi-all-trans conformation.

Second, the reason for no orientation above 43 °C is discussed. As shown in the inset of Figure 7.9, the surface area decreases abruptly in the range from 30 to 45 °C. Because the melting point (T_m) of PMPrS in the bulk state is 43.8 °C,[26] it can be said that the abrupt change in the surface area implies T_m of the monolayers. Domains of the PMPrS-*g*-MAH monolayer coalesce with one another, and the defects among them decrease because PMPrS main chains melt and become fluid above T_m. Besides, the PMPrS main chains easily take a three-dimensional contracted form escaping from the water surface. As a result, the surface area abruptly decreases. In such a fluid state, the quasi-all-trans conformation hardly exists on the water surface. Consequently, no orientation is induced even by the compression and dipping. From the open circles in Figure 7.8, it is found that the quasi-all-trans conformation exists in the transferred monolayers even above 43 °C. However, the author thinks that it appears during the cooling process of the transferred monolayers to the ambient temperature taking into consideration that the UV spectroscopic measurements of the transferred monolayers were carried out at room temperature. When isotropic monolayers at the high temperature are transferred onto a solid substrate, no preferential orientation is developed even though the conformation changes into the quasi-all-trans form.

Finally, the opposite direction of the orientation in the range of temperature from 38 to 40 °C is explained. In this region, the monolayers exhibit high fluidity

because temperature of the water subphase is close to T_m, but PMPrS main chains are still keeping the quasi-all-trans conformation. Also, the flow-induced orientation caused by the dipping exceeds the compression-induced orientation. As a result, D takes negative values.

In this experiment, only PMPrS-*g*-MAH with grafting yield of 0.09 was used. As shown in Figure 7.3a and 7.6a, other PMPrS-*g*-MAH would indicate different D and R_A values depending on grafting yield. However, it is considered that other PMPrS-*g*-MAH also shows similar change of the values because the melting point of PMPrS is the key factor of this temperature dependence.

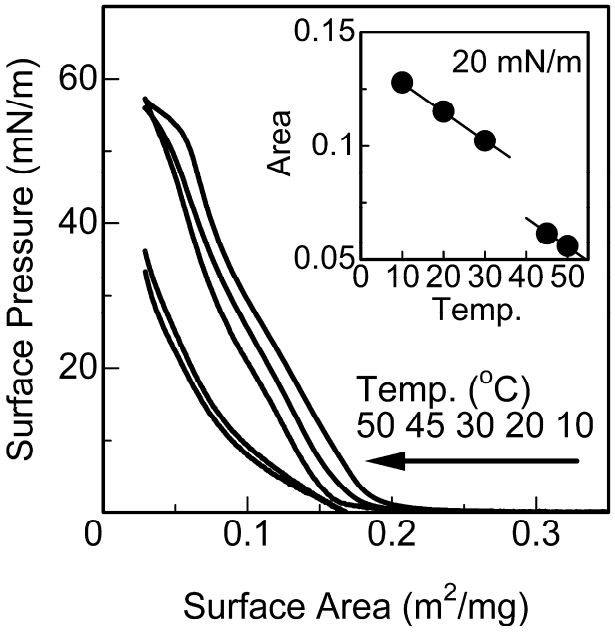

Figure 7.9. π-A isotherms of PMPrS-*g*-$MAH_{0.09}$ monolayers at various subphase temperatures. The inset shows the surface area at 20 mN/m.

7.3.4. Orientation of PMPrS Main Chains in Multilayers

The build-up of PMPrS-*g*-MAH monolayers was successfully achieved by the Y-type deposition.[22] Figure 7.10 shows R_A of PMPrS-*g*-$MAH_{0.15}$ multilayers transferred onto a hydrophilic quartz substrate at 35 mN/m. The monolayer exhibits much larger R_A values compared with a bulk state of a spin-coated film because PMPrS main chains are strongly confined in two dimensions by interaction with the hydrophilic surface. However, as the number of transferred layers increases, R_A gradually decreases to the bulk film level. This is because the layer structure in the upper layers is less stable owing to the weaker interaction between the polymers in the adjacent layers than that between the polymers and the hydrophilic substrate. Accordingly, the polymer chains take a contracted form similarly to the bulk state as the effect of two-dimensional confinement is weakened.

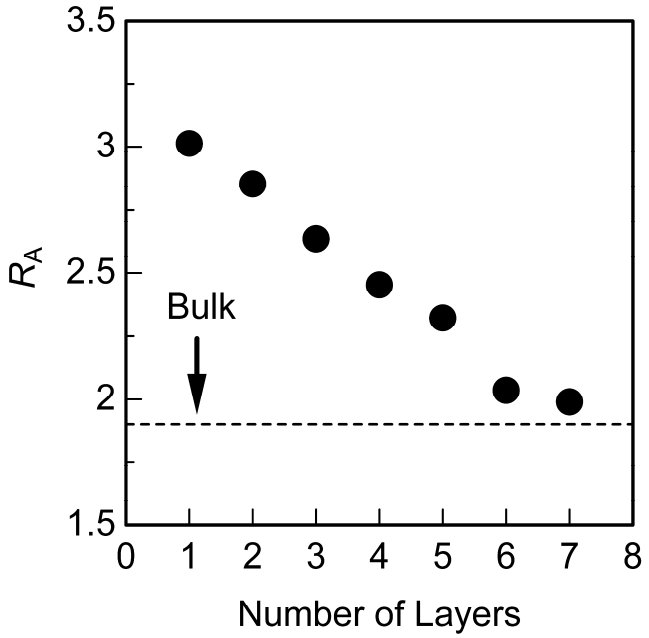

Figure 7.10. Dependence of R_A of PMPrS-*g*-$MAH_{0.15}$ multilayers dipped by the Y-type deposition on the number of layers. The dipping was conducted by the arrangement $S_{\perp}$.

Figure 7.11 shows the dependence of *D* of PMPrS-*g*-$MAH_{0.15}$ multilayers transferred at 35 mN/m. Solid circles indicate *D* values of the multilayers dipped by the arrangement $S_{\perp}$. No orientation is observed for the two-layer film, and above three layers the direction of orientation is completely against that of the monolayer film. This result means that the effect of the flow-induced orientation becomes predominant in comparison with that of the compression-induced orientation as the number of layers increases. Open circles indicate *D* values of multilayers dipped by the arrangement $S_{//}$. In this case, the compression-induced

orientation and the flow-induced orientation are in the same direction. Consequently, even in upper layers, *D* is maintained.

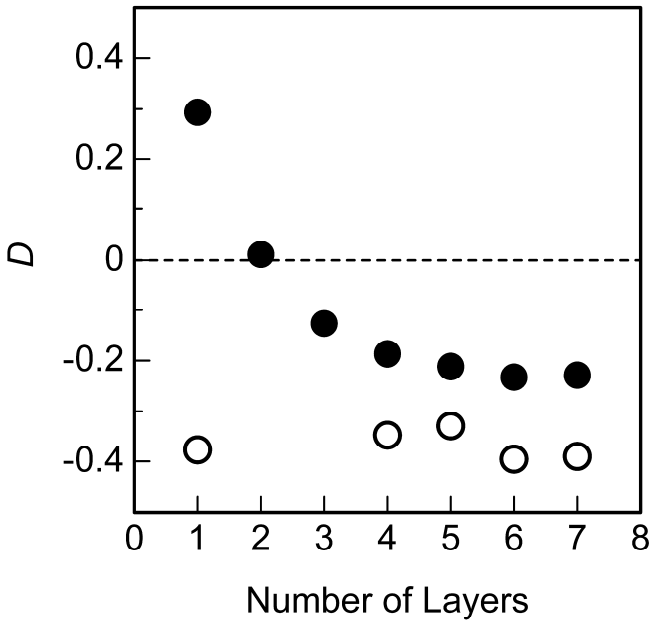

Figure 7.11. Dependence of *D* of PMPrS-*g*-MAH$_{0.15}$ multilayers dipped by the Y-type deposition on the number of layers. Solid and open circles indicate *D* values of the multilayers dipped by the arrangements $S_{\perp}$ and $S_{//}$, respectively.

7.4. Conclusion

The orientation of polysilane main chains in the PMPrS-*g*-MAH monolayers at the air/water interface was clarified by taking advantage of the strong UV absorption of the polysilane main chain. The R_A shows the inverted-V-shaped dependence on grafting yield due to the competition between the conformational constraint by the

compression and the structural disorder evoked by the grafted MAH units. The D has close relationship with R_A and exhibits a similar dependence on grafting yield. Thus, it is revealed that the orientation of monolayers is closely related to the conformation of polymers constituting the monolayers.

It was found that the orientation of PMPrS-*g*-MAH monolayers at the air/water interface is influenced by the subphase temperature. The D value increases with rising temperature to T_m of PMPrS due to the compression-induced orientation. However, the direction of the orientation abruptly changes around T_m because the flow-induced orientation exceeds the compression-induced one. And then the monolayers come to show no orientation above T_m. These results prove that the subphase temperature is a significant factor to obtain highly oriented monolayers.

Highly oriented LB films of PMPrS-*g*-MAH were obtained by the Y-type deposition. In case that the deposition is conducted with a substrate facing parallel to the compression direction, the compression-induced orientation and the flow-induced one cooperate, and the orientation keeps to upper layers. This fact demonstrates that the LB technique with PMPrS-*g*-MAH is a promising method to fabricate nanodevices in which polysilane chains highly align in the same direction.

References

1. Fujino, M. *Chem. Phys. Lett.* **1987,** *136,* 451.
2. Kepler, R. G.; Zeigler, J.M.; Harrah, L. A.; Kurtz, S. R. *Phys. Rev.* **1987,** *B35,* 2818.
3. Stolka, M.; Yuh, H. J.; McGrane, K.; Pai, D. M. *J. Polym. Sci., Polym. Chem.* **1987,** *25,* 823.
4. Abkowitz, M. A.; Knier, F. E.; Yuh, H. J.; Weagley, R.J.; Stolka, M. *Solid State Commun.* **1987,** *62,* 547.
5. Yuan, C. H.; Hoshino, S.; Toyoda, S.; Suzuki, H.; Fujiki, M.; Matsumoto, N. *Appl. Phys. Lett.* **1997,** *71,* 3326.
6. Suzuki, H.; Hoshino, S.; Furukawa, K.; Ebata, K.; Yuan, C. H.; Bleyl, I. *Polym. Adv. Technol.* **2000,** *11,* 460.
7. Samuel, L. M.; Sanda, P. N.; Miller, R. D. *Chem. Phys. Lett.* **1989,** *159,* 227.
8. Yokoyama, K.; Yokoyama, M. *Chem. Lett.* **1989,** 1005.
9. Mitter-Neher, S.; Neher, D.; Stegeman, G. I.; Embs, F. W.; Wegner, G. *Chem. Phys.* **1992,** *161,* 289.
10. Kajar, F.; Messier, J.; Rosilio, C. *J. Appl. Phys*. **1986,** *60,* 3040.
11. West, R. *J. Organomet. Chem.* **1986**, *300*, 327.
12. Miller, R. D.; Michl, J. *Chem. Rev.* **1989**, *89*, 1359.
13. West, R. Polysilanes and Related Polymers. In *Inorganic Polymers;* Mark, J. E., Allcock, H. R., West, R., Eds.; R. Prentice Hall, NJ, 1992.
14. Schwartz, D. K. *Surf. Sci. Rep.* **1997,** *27,* 241.
15. Embs, F. W.; Wegner, G.; Neher, D.; Albouy, P.; Miller, R. D.; Willson, C. G.; Schrepp, W. *Macromolecules* **1991**, *24*, 5068.

16. Yoshida, H.; Kani, R.; Hayase, S.; Horie, K. *J. Phys. Chem.* **1993**, *97*, 5370.

17. Kani, R.; Nakano, Y.; Majima, Y.; Hayase, S.; Yuan, C. H.; West, R. *Macromolecules* **1994**, *27*, 1911.

18. Kani, R.; Yoshida, H.; Nakano, Y.; Marui, S.; Mori, Y.; Kawata, Y.; Hayase, S. *Langmuir* **1993**, *9*, 3045.

19. Seki, T.; Tanigaki, N.; Yase, K.; Kaito, A.; Tamaki, T.; Ueno, K.; Tanaka, Y. *Macromolecules* **1995**, *28*, 5609.

20. Yoshida, M.; Nakanishi, F.; Seki, T.; Sakamoto, K.; Sakurai, H. *Macromolecules* **1997**, *30*, 1860.

21. Tachibana, H.; Kishida, H.; Tokura, Y. *Langmuir* **2001**, *17*, 437.

22. Tanaka, H.; Kunai, Y.; Sato, N.; Matsuyama, T. *J. Colloid Interface Sci.* **2011**, *363*, 440.

23. Tanaka, H.; Iwasaki, I.; Kunai, Y.; Sato, N.; Matsuyama, T. *Radiat. Phys. Chem.* **2011,** *80,* 884.

24. Chunwachirasiri, W.; Kanaglekar, I.; Winokur, M. J.; Koe, J. C.; West, R. *Macromolecules* **2001,** *34,* 6719.

25. Nagano, S.; Seki, T. *J. Am. Chem. Soc. Commun.* **2002,** *124,* 2704.

26. Jambe, B.; Jonas, A.; Deaux, J. *J. Polym. Sci. B. Polym. Phys.* **1997,** *35,* 1533.

Summary

This thesis includes studies on the conformational characteristics of radiation-modified polysilanes in their self-assemblies. The summary of each chapter is presented below.

In Chapter 1, the purpose of this thesis was described, and the key concepts of polysilane, radiation-induced graft polymerization, micelle formation and Langmuir-Blodgett (LB) films were explained.

In Chapter 2, the structures of poly(methyl-*n*-propylsilane) (PMPrS) amphiphilically modified through γ-ray-induced graft polymerization were investigated with ^{1}H NMR measurements. By use of methyl methacrylate (MMA) or diethyl fumarate (DEF) as monomers for the graft polymerization, grafting yield rose with increasing total absorption dose and monomer concentrations, but decreased with increasing dose rate. This result means that grafting yield of modified PMPrS can be controlled by changing irradiation conditions. However, the number of poly(methyl methacrylate) (PMMA) or poly(diethyl fumarate) (PDEF) graft chains per PMPrS chain was estimated to be less than 1.0 by analysis of ^{1}H NMR spectra. To improve graft density, maleic anhydride (MAH), which is known as a non-homopolymerizable monomer in radical polymerization, was used as a monomer for grafting. As a result, high density grafting, one MAH unit for 4.2 silicon atoms, was attained. It demonstrates that the structure of γ-ray-modified polysilane strongly depends on the polymerization characteristics of grafted monomers.

In Chapter 3, PMPrS's with polyelectrolyte side chains were synthesized by two

methods utilizing γ-ray-induced grafting and the pH responsiveness for one of those polymers was revealed mainly by investigating interfacial behavior of its monolayer at the air/water interface. In the first synthetic method, poly(methyl acrylate) (PMA) was grafted onto PMPrS through γ-ray-induced grafting, and then the PMA chains were hydrolyzed to poly(acrylic acid) (PAA) in the yield of ca. 97%. Thus PMPrS with polyelectrolyte side chains was successfully synthesized by the graft chain hydrolysis. The other method was the direct grafting of electrolyte monomers. Poly(methacrylic acid)-grafted PMPrS (PMPrS-*g*-PMAA) could be obtained through γ-ray-induced grafting of methacrylic acid (MAA) monomers onto PMPrS chains, which showed the effectiveness of radiation grafting for the synthesis of polyelectrolyte graft copolymers. PMPrS-*g*-PMAA exhibited pH responsive behavior. In addition to the pH-dependence of water solubility, interfacial behavior also depended on the pH. Langmuir monolayers of PMPrS-*g*-PMAA exhibited different surface pressure-area (π-A) isotherms according to the grafting yield and the pH of the subphase water. This result suggests that radiation modification is useful for fabricating polysilane-based ordered materials those are responsive to external stimuli.

In Chapter 4, PMA-grafted PMPrS (PMPrS-*g*-PMA) and PAA-grafted PMPrS (PMPrS-*g*-PAA) were synthesized by γ-ray-induced graft polymerization, and the association behavior of these graft copolymers was investigated in selective solvents composed of good and poor solvents for the PMPrS main chain. Fluorescence spectroscopy with perylene as a fluorescent probe revealed that PMPrS-*g*-PAA in a water/tetrahydrofuran (THF) mixed solvent self-assembles into micelles with a swollen core of PMPrS chains in the water content range of 50−95%. UV

spectroscopy demonstrated that a further increase of the water content gives rise to the conformational transition of the PMPrS chains in the micelle core from the random conformation to the conformation that corresponds to that in the solid state at a water content of ca. 95%, independent of the grafting yield. Similar behavior was also observed in dimethyl sulfoxide (DMSO)/THF solutions of PMPrS-*g*-PMA, for which the conformational transition occurred at the constant DMSO content of ca. 95%. These results indicate that solvatochromic behavior of polysilane, which is a characteristic feature of polysilane, proved to provide information on the inner structure of those micelles: PMPrS chains in the core undergo conformational transition as the content of the poor solvents for PMPrS increases, while maintaining the micelle structure.

In Chapter 5, changes in the micelle structure induced by a temperature change were revealed for the micelle of PMPrS-*g*-PAA synthesized through γ-ray-induced graft polymerization. This graft copolymer consisting of hydrophobic PMPrS and hydrophilic PAA forms micelles with different core states in water/THF mixed solvents depending on solvent compositions. The temperature effect on the micelles formed in the solvents with various solvent compositions was investigated by UV spectroscopy and light scattering measurements. In the case of a solid-core micelle formed at a water content of 99%, PMPrS-core chains changed from the quasi-all-trans conformation to the random conformation at 42 °C in the heating process, which was revealed from thermochromic behavior in the UV region. This result indicates that the PMPrS-core chains undergo phase transition from the solid state to the molten state. Also in the case of a swollen-core micelle formed at water contents from 89 to 95%, thermochromic behavior parallel to that of the solid-core

micelle appeared in UV absorption spectra. However, the transition temperature lowered as the water content of mixed solvent reduced. It was elucidated that this difference of the transition temperature is originated from the different local concentration of PMPrS chains within the core.

In Chapter 6, the variation in the morphology of monolayers at the air/water interface was investigated for two kinds of radiation-modified polysilanes with different structures: PDEF-grafted PMPrS (PMPrS-*g*-PDEF) and MAH-grafted PMPrS (PMPrS-*g*-MAH). PMPrS-*g*-PDEF has long but sparsely-attached PDEF graft chains, while PMPrS-*g*-MAH has short but densely-attached MAH graft units. The π-A measurements indicated that PMPrS-*g*-PDEF monolayers extensively spread at the air/water interface though PMPrS homopolymer hardly spreads. AFM observation revealed that PMPrS-*g*-PDEF monolayers have inhomogeneous structure containing string-like microstructures. This result suggests that PMPrS main chains are detached from the water surface to aggregate together and only PDEF chains spread over the water surface. In contrast, PMPrS-*g*-MAH formed uniform monolayers with a smooth surface. PMPrS main chains of PMPrS-*g*-MAH are anchored to the water surface by densely grafted MAH units. It was also demonstrated that only the PMPrS-*g*-MAH monolayers were successfully deposited layer-by-layer on a solid substrate by the Y-type deposition.

In Chapter 7, the orientation of PMPrS-*g*-MAH in monolayers at the air/water interface was investigated by polarized UV absorption spectroscopy. The absorbance ratio of the quasi-all-trans conformation of PMPrS to a random one showed inverted-V-shaped dependence on grafting yield. Dichroic ratio, which indicates the orientation of the monolayers, exhibited the similar dependence on

grafting yield. This fact indicates that the orientation is closely related to the conformation of polymers constituting monolayers. The orientation of PMPrS-*g*-MAH monolayers was influenced also by the subphase temperature. As the temperature increased to the melting point (T_m) of PMPrS, the dichroic ratio increased. However, the direction of the orientation abruptly changed around T_m, and then the monolayers came to show no orientation above T_m. This result demonstrates that the subphase temperature is a significant factor to obtain highly oriented monolayers. The orientation of PMPrS-*g*-MAH in LB films was also revealed, and highly oriented LB films were successfully obtained.

List of Publications

Chapter 2

Radiation-Induced Graft Polymerization of Amphiphilic Monomers with Different Polymerization Characteristics onto Hydrophobic Polysilane

Hidenori Tanaka, Isao Iwasaki, Yuichiro Kunai,

Nobuhiro Sato, and Tomochika Matsuyama

Radiation Physics and Chemistry **2011**, *80*, 884−889.

Chapter 3

Synthesis of pH-Responsive Polysilane with Polyelectrolyte Side Chains through γ-ray-Induced Graft Polymerization

Hidenori Tanaka, Yasushi Kawade, Nobuhiro Sato, and Tomochika Matsuyama

Radiation Physics and Chemistry **2012**, *81*, 185−189.

Chapter 4

Conformational Transition of the Core Chain in Radiation-Modified Polysilane Micelles Formed in Selective Solvents

Hidenori Tanaka, Nobuhiro Sato, and Tomochika Matsuyama

Langmuir **2005**, *21*, 7696−7701.

Chapter 5

Core Phase Transition of Radiation-Modified Polysilane Micelles As Revealed from Their Thermochromism

Hidenori Tanaka, Nobuhiro Sato, Tomochika Matsuyama

Rintaro Inoue, and Toshiji Kanaya

Polymer Journal **2007**, *39*, 874−877.

Chapter 6

Effect of the Graft Chain Length and Density on the Morphology of Radiation-Modified Polysilane Monolayers at the Air/Water Interface

Hidenori Tanaka, Yuichiro Kunai, Nobuhiro Sato, and Tomochika Matsuyama

Journal of Colloid and Interface Science **2011**, *363*, 440−445.

Chapter 7

Orientation of Radiation-Modified Polysilane in Monolayers at the Air/Water Interface As Revealed from Its Optical Property

Hidenori Tanaka, Yuichiro Kunai, Kenji Okayasu,

Nobuhiro Sato, and Tomochika Matsuyama

The Journal of Physical Chemistry C **2011**, *115*, 20242−20247.

Acknowledgements

The present thesis is based on the study carried out at the Department of Polymer Chemistry, Graduate School of Engineering, Kyoto University, from 2001 to 2005.

The author would like to express his most sincere thanks to Emeritus Professor Tomochika Matsuyama for his continuous guidance, valuable advices, discussion and collaborations through the course of the study.

The author is deeply grateful to Professor Toshiji Kanaya for his willing acceptance of the author's advisor and also for critically reading the drafts of this thesis and for the helpful suggestions.

Professor Fumihiko Tanaka, Professor Hiroo Iwata, Professor Takenao Yoshizaki and Professor Yoshinobu Tsujii are especially acknowledged for their critical review of this thesis.

The author is deeply indebted to Assistant Professor Nobuhiro Sato for his helpful guidance and advices.

The author is grateful to Assistant Professor Rintaro Inoue for the kind support in light scattering measurements and his helpful advices.

The author is indebted to Emeritus Professor Hitoshi Yamaoka for his kind guidance and encouragement.

The author wishes to express my sincere gratitude to Dr. Ryuji Fukuda and Dr. Shigeki Ohno at Kaneka Corporation for their support.

The author acknowledges the active collaboration and fruitful discussion with the colleagues of Matsuyama Laboratory: especially, Mr. Isao Iwasaki, Mr. Yasushi Kawade, Mr. Yuichiro Kunai, Mr. Hiroki Ogawa and Dr. Ryojun Sekine. Without

their collaboration and support, the author could not carry out his studies.

Finally, the author expresses his deep appreciation to his wife and daughter, Mayumi Tanaka and Ayana Tanaka, without their warm encouragement and understanding this thesis would not have been completed, and his parents, Kiyotsugu Tanaka and Chihoko Tanaka, for their support and encouragement.

January, 2012

Hidenori Tanaka